Metabolic impact of vitamin D on U937 cells during TLR2/1 activation with $Pam_3CysSerLys_4$, a bacterial lipoprotein mimic

By

Baloyi Ntsako Nhlanhla
(201403847)

MSc Dissertation

Submitted in fulfilment of the requirements
for the degree of

Magister Scientiae (MSc)

In

BIOCHEMISTRY

at the

FACULTY OF SCIENCE

DEPARTMENT OF BIOCHEMISTRY

UNIVERSITY OF JOHANNESBURG

SOUTH AFRICA

SUPERVISOR: Dr. Lungile Sitole

CO-SUPERVISOR: Dr. Fidele Tugizimana

July 2020

SUBMISSION DECLARATION

I, Ntsako Nhlanhla Baloyi, declare that the dissertation, which I hereby submit for the degree of *Magister Scientiae* in the Department of Biochemistry, at the University of Johannesburg, is my own work and has not previously been submitted by me for a degree at this university or any other tertiary institution.

SIGNATURE DATE

ACKNOWLEDGEMENTS

Without the following people, I would not have been able to carry out this research project:

- To my supervisor, **Dr Lungile Sitole,** words cannot express how grateful I am to have you as my supervisor. Thank you for the guidance and support you have shown me throughout the years. I highly appreciate what you have done for me ever since I met you. Thank you for all the wisdom you have shared with me.
- To my co-supervisor, **Dr Fidele Tugizimana**, thank you for your help and guidance. Thank you for the wisdom that you have shared with me. I appreciate what you have done for me. I salute you.
- To **Professor Liza Bornman**, thank you for all the contributions you have made to this project. You have always played an important role in my studies throughout the years. Without you, this study would not have been possible. I appreciate you.
- To **Dr Heather-Anne Byth-Illing**, thank you for all your assistance with the flow cytometry analysis. Your contribution to the project is highly appreciated.
- To **Mr Mutshinyalo Nwamadi**, thank you for assisting us with nuclear magnetic resonance spectroscopy analysis. You have always been there for us from the beginning of the study. Your support will never be forgotten.
- To **Dr Ilse du Preez**, your assistance with gas chromatography–mass spectrometry analysis is highly appreciated. It would not have been easy to perform this part of the study without your help. Thank you for all the contributions you have made in this study.
- To the **National Research Foundation (NRF)** and the **Faculty of Science at the University of Johannesburg**, thank you for your funds. This study was made possible because of you. To the Department of Biochemistry, thank you for giving me the opportunity to use your facilities for this research project.
- To my colleagues (**HIV/TB group**), thank you for the support you have shown me throughout the years. This study would not have been the same without you.
- To my **family**, thank you for believing in me. Your support is highly appreciated, and I shall not forget about it.
- And lastly, I would like to thank and give all the glory to **God almighty** ('Whatever you do, do it all for the glory of God', 1 Corinthians 10:31). Nothing would have been possible without God almighty. Thank you, Jesus.

ABSTRACT

Background: Bacterial infections remain one of the top causes of death worldwide despite the continuous development of conventional methods to eradicate this challenge. *Mycobacterium tuberculosis (M.tb*), a causative agent of tuberculosis (TB), is amongst the leading causes of mycobacterial mortality worldwide. Given the constant increase in TB incidence rates, there is a great need for better diagnostic and treatment methods for *M.tb*. Several studies have proposed the possible therapeutic role of vitamin D in antimycobacterial immunity. Vitamin D has been shown to boost the immune system against several ailments including TB, however, the exact mechanism through which vitamin D functions in antimycobacterial immunity remains elusive. In addition, the current conventional methods used to study the metabolism of vitamin D in the presence of mycobacteria are limited in terms of efficiency. As such, applying metabolomics to elucidate bacterial activity and vitamin D supplementation effects, at cellular level, could provide insight into the metabolic reprogramming associated with vitamin D during mycobacterial infection. Metabolomics is a multidisciplinary 'omics' science that deals with the identification and quantification of the metabolic changes in a biological system under specific conditions. This 'omics' field has shown promise in its ability to distinguish TB infected serum/plasma from uninfected serum/plasma. Metabolomics has been used to identify metabolic changes induced by *M.tb* infection; however, the metabolic reconfigurations induced by vitamin D in *M.tb* infection still need to be explored. Thus, the aim of this study was to evaluate the metabolic effects of 1,25-dihydroxyvitamin D_3 ($1,25(OH)_2D_3$), an active form of vitamin D, on the metabolome of U937 macrophages stimulated with Pam_3CSK_4 (a mycobacterial model). **Methods:** Cultured U937 monocytic cells were differentiated into macrophages using phorbol myristate acetate (PMA). Differentiation was confirmed by evaluating morphological changes of the cells and through flow cytometry evaluation of differentiation surface marker CD14. Following this, the cells were treated with Pam_3CSK_4 to stimulate bacterial infection and immunomodulatory effects towards bacterial lipoproteins. Furthermore, the cells were supplemented with vitamin D ($1,25(OH)_2D_3$). An untargeted NMR and GC-MS-based metabolomic approach where then conducted to characterise differential metabolic profiles of Pam_3CSK_4 stimulated cells,

$1,25(OH)_2D_3$ supplemented cells, a combination of Pam_3CSK_4 and $1,25(OH)_2D_3$ supplementation as well as the untreated cells. **Results:** Chemometric modelling and statistical analyses revealed a clear distinction between the metabolic profiles of Pam_3CSK_4 stimulated cells, $1.25(OH)_2D_3$ supplemented cells and cells supplemented with a combination of $Pam_3CSK_4/1.25(OH)_2D_3$ as compared to the control cells (untreated). Significant differences ($p<0.05$) were identified in 23 metabolites. These changes were detected in spectral regions related to methionine, galactose, myoinositol, threonine, glycine, beta-glucose, o-phosphocholine, valine, lactate, mannose, taurine, adenosine monophosphate, ornithine, glycerol, succinate, tyrosine, phenylalanine, glutamate, leucine, pyroglutamate, glutathione, beta-alanine and glutamine. Alterations in these metabolites have been linked to changes in bioenergy production (up-regulation of glycolysis – the Warburg effect), regulation of redox reaction, inflammation and protein synthesis. Likewise, the metabolic profile of Pam_3CSK_4 stimulated cells compared to $Pam_3CSK_4/1.25(OH)_2D_3$, showed significant differences in spectral regions of the aforementioned metabolites. These differences suggest that $1.25(OH)_2D_3$ induces metabolic reprogramming in Pam_3CSK_4 stimulated cells, by boasting macrophage immune response against mycobacteria. **Conclusion**: NMR- and GC-MS-based metabolomics successfully detected and identified metabolites discriminating a TLR2/1 stimulated response (Pam_3CSK_4 and $1.25(OH)_2D_3$ treatment). In addition, this multi-platform metabolite profiling allowed the characterisation of the metabolic alterations induced by Pam_3CSK_4 stimulation, $1.25(OH)_2D_3$ supplementation and a combination of $Pam_3CSK_4/1.25(OH)_2D_3$. Results obtained show that $1.25(OH)_2D_3$ promotes the elimination of bacterial infection by the macrophage and is therefore beneficial in the immune response against mycobacterial infection. Perspective studies will include quantitative analysis of metabolites implicated and the use of additional analytical techniques such as liquid chromatography-–mass spectrometry (LC-MS) to detect as many metabolites as possible.

TABLE OF CONTENT

LIST OF FIGURES

Chapter 2

Chapter 3

Chapter 4

Appendix

LIST OF TABLES

LIST OF ABBREVIATIONS

^{1}H-NMR	Proton Nuclear Magnetic Resonance
^{13}C-NMR	Carbon Nuclear Magnetic Resonance
^{31}P-NMR	Phosphorus NMR
1D	One Dimensional
1,25$(OH)_2D_3$	1,25-dihydroxyvitamin D_3
25(OH)D	25-hydroxyvitamin D
α	Alpha
α1β1	Alpha-1 beta-1 integrin
β	Beta
β0	External electromagnetic field
dB	Decibel
eV	Electron Volt
hrs	Hours
Hz	Hertz
ɣ	Gamma
°C	Degrees Celsius
IU/mL	International units per millilitre
m	Metre
ml	Millilitre
mm	Millimetre
mM	Millimolar
m/z	Mass to charge ratio
ng/mL	Nanograms per millilitre.
s	second
V	Volt
w/v	Weight per volume
µg	Microgram
µl	Microlitre
µm	Micrometre

%	Percentage
ΔE	Change in energy
AMP	Adenosine Monophosphate
ANOVA	Analysis of Variance
APCs	Antigen-Presenting Cells
ATCC	American Type Culture Collection
ATP	Adenosine Triphosphate
AUROC	Area Under Receiver Operating Characteristic Curve
BBI	Double resonance broadband
BCAAs	Branched-Chain Amino Acids
BCAT	Branched-chain aminotransferase
BCKAs	Branched-Chain Keto acids
BCKDC	Branched-Chain Keto acid Dehydrogenase Complex
BMRB	Biological Magnetic Resonance Data Bank
BSA	Bovine Serum Albumin
BSTFA	N,O-Bis(trimethylsilyl)trifluoroacetamide
C1	Carbon 1
C4	Carbon 4
CAMP	Cathelicidin Antimicrobial Peptide
CD	Cluster of Differentiation
CE	Capillary Electrophoresis
CO_2	Carbon Dioxide
CV	Cross-Validation
CV-ANOVA	Cross Validated-Analysis of Variance
CYP24A1	24-hydroxylase
CYP27B1	1-α-hydroxylase
DBP	Vitamin D binding protein
DCs	Dendritic cells
DEFB4	β-defensin 4
DModX	Distance to Model
DMSO	Dimethyl Sulfoxide

DNA	Deoxyribonucleic Acid
FBS	Fetal Bovine Serum
Fc	Fragment Crystallizable
Fe	Iron
FGF23	Fibroblast Growth Factor 23
FID	Free Induction Decay
FITC	Fluorescein Isothiocyanate
FSC	Forward Scatter
FT-IR	Fourier-Transform Infrared
G1P	Glucose-1-Phosphate
G6P	Glucose-6-Phosphate
Gal1P	Galactose-1-Phosphate
GC	Gas Chromatography
GCL	Glutamate-Cysteine Ligase
GC-MS	Gas Chromatography Mass Spectrometry
GCxGC–TOFMS	Two-Dimensional Gas Chromatography– Time-Of-Flight Mass Spectrometry
GS	Glutathione Synthetase
GSH	Glutathione
GSNO	S-nitrosoglutathione
H_2O	Water
HAMP	Hepcidin Antimicrobial Peptide
He	Helium
HEK293T	Human Embryonic Kidney 293T
HIV	Human Immunodeficiency Virus
HMDB	Human Metabolome Database
HPLC	High Performance Liquid Chromatography
IFN-γ	Interferon gamma
Ig	Immunoglobulin
IgG2a	Immunoglobulin G2a
KDa	Kilo Dalton

KEGG	Kyoto Encyclopedia of Genes and Genomes
IL-6	Interleukin 6
LC	Liquid Chromatography
LC-MS	Liquid Chromatography-Mass Spectrometry
LDA	Linear Discriminant Analysis
LG	L-glutamine
LTB	Latent Tuberculosis
MDP	Muramyl dipeptide
Min	Minute
MMP-9	Matrix Metalloproteinase
MPS	Multi-Purpose Sampler
MS	Mass Spectrometry
MSI	Metabolomics Standard Initiative
M.tb	*Mycobacterium tuberculosis*
MVDA	Multivariate Data Analysis
NaCl	Sodium Chloride
NF-κB	Nuclear Factor Kappa Beta
NIST	National Institute of Standards and Technology
NK	Natural Killer
nmol/L	Nanomoles Per Liter
NMR	Nuclear Magnetic Resonance
NO	Nitric Oxide
NOD2	Nuclear-binding Oligomerization Domain-containing protein 2
NOESY	Nuclear Overhauser Effect Spectroscopy
NOS2	*Nitric Oxide Synthase 2*
NTM	Nontuberculous mycobacteria
OH	Hydroxyl
OPLS-DA	Orthogonal Partial Least Square Discriminant Analysis
OS	Oxidative Stress
Pam_3CSK_4	Tripalmitoyl-S-glyceryl-L-Cys-Ser-(Lys)4
Pam	Tripalmitoyl-S-glyceryl-L-Cys-Ser-(Lys)4

PAMPs	Pathogen–Associated Molecular Patterns
PBS	Phosphate-Buffered Saline
PBMCs	Peripheral Blood Mononuclear Cells
PCA	Principal Component Analysis
PCa	Prostate cancer
PKC	Protein Kinase C
PD	Tripalmitoyl-S-glyceryl-L-Cys-Ser-(Lys)4/1,25-dihydroxyvitamin D_3
Pen-Strep	Penicillin-Streptomycin
PLOT	Porous Layer Open Tubular
PLS	Partial Least Squares
PLS-DA	Partial Least Squares Discriminant Analysis
PMA	Phorbol Myristate Acetate
PMTs	Photomultiplier Tubes
ppm	Parts Per Million
PRRs	Pattern-Recognition Receptors
p-value	Probability value
QC	Quality Control
RA	Retinoic Acid
Redox	Oxidation-Reduction
RF	Radio Frequency
RNA	Ribonucleic Acid
RNS	Reactive Nitrogen Species
ROC	Receiver Operating Characteristic
ROS	Reactive Oxygen Species
RPMI	Roswell Park Memorial Institute
RXR	Retinoid X Receptor
S/N	Signal to noise ratio
SCOT	Support-Coated Open Tubular
SIMCA	Soft-Independent modelling of Class Analogy
SSC	Side Scatter

TB	Tuberculosis
TBSA	Tuberculostearic Acid
TCA	Tricarboxylic Acid Cycle
Th	T helper cell
TLR	Toll-Like Receptor
TMCS	Trimethylchlorosilane
TNF-α	Tumor Necrosis Factor Alpha
TPA	Tetradecanoil-13-phorbol acetate
tRNA	Transfer Ribonucleic Acid
UDP	Uridine Diphosphate
UVB	Ultraviolet B
VDB	Vitamin D Binding protein
VDR	Vitamin D Receptor
VDRE	Vitamin D Response Element
VitD	1,25-dihydroxyvitamin D_3
VIP	Variable Importance Plot
WCOT	Wall-Coated Open Tubular
WHO	World Health Organization
Zn^{2+}	Zinc

CHAPTER 1

INTRODUCTION

Tuberculosis (TB), a contagious disease that is airborne and caused by *Mycobacterium tuberculosis* (*M.tb*), remains a major threat worldwide as it is an ancient disease that has caused millions of deaths (Soto-Ramirez *et al.,* 2016; Zumla *et al*., 2013). According to the World Health Organisation (WHO), at least 10 million people, globally, are diagnosed with TB each year. TB is also a poverty-related disease with 95% incidence rates reported in developing countries (Barter *et al.,* 2012; Okhovat-Isfahani *et al*., 2019). Africa alone accounts for 24% of all TB cases, which makes it the second-highest after South-East Asia (44%) (WHO, 2019). Given the constant increase in TB incidence rates, there remains a great need for better diagnostic methods and treatments for TB. The diagnosis and treatment of TB are currently very challenging for two key reasons. Firstly, resistance in *M.tb* is a common occurrence; for instance, in 2018 it was estimated that there were already over half a million new multidrug-resistant cases (WHO, 2019). Secondly, co-infection with Human Immunodeficiency Virus (HIV) is also very common and poses a greater challenge in diagnosis and treatment interventions. In South Africa, more than 60% of individuals infected with TB also test HIV positive, thus making South Africa the epicentre of HIV/TB co-infection (WHO, 2018).

In the pre-antibiotics era, natural remedies such as the use of cod liver oil and sunlight exposure were used as a form of TB therapeutics. Most recently, several studies have suggested the possible therapeutic role of Vitamin D in antimycobacterial immunity (Dini and Bianchi, 2012; Salahuddin *et al.,* 2013). Vitamin D has been shown to boost the immune system against several ailments including TB (Marques *et al.,* 2010; Thacher and Clarcke 2011). When supplemented with vitamin D, TB patients show an accelerated clinical recovery rate (Salahuddin *et al*., 2013). Furthermore, vitamin D supplementation decreases the activation and the progression of latent TB (LTB) to active TB (Arnedo-Pena *et al.,* 2015). The exact mechanisms through which vitamin D functions in antimycobacterial immunity, however, remains elusive. Additionally, there is limited knowledge of the metabolic effect of vitamin D during mycobacterial infection. For this reason, the role of vitamin D during mycobacterial infection needs to be explored so as to understand how vitamin D affects the metabolic pathways involved in mycobacterial infection.

The emerging latest cardinal omics approach, metabolomics, has provided new possibilities of understanding the metabolic reprogramming of a biological system associated with a stimulus. Recently, high throughput and high sensitivity techniques such as nuclear magnetic resonance (NMR) spectroscopy, mass spectrometry (MS)-based platforms (such as gas

chromatography-–mass spectrometry spectrometry, GC-MS), infrared spectroscopy and Raman spectroscopy have found use in metabolomics. Nicholson *et al*. (1999) defined metabolomics as a multidisciplinary 'omics' science that evaluates the metabolic changes of a biological system by identifying and quantifying the small molecular weight molecules (metabolites), components of metabolism, under specific conditions. Metabolomics has been successfully used to determine the efficacy of pharmaceutical drugs, assessment of drug toxicity, identification of disease biomarkers, enzyme discovery, determining the quality and safety of food, and exploration of metabolic networks in systems biology (Clayton *et al*., 2006; Gomez-Casati *et al.,* 2013; Liu *et al.,* 2018). Available metabolomics software and databases allow for the identification of the metabolic pathways associated with the altered metabolites under specific conditions. Ultimately, metabolomics can identify metabolites associated with a perturbation, therefore, providing reliable biomarkers for a disease. Hence, metabolomics is used in diagnostic test development (German *et al.,* 2005).

Metabolomics investigations of TB infected biofluids have been extensively performed (as reviewed by Mirsaeidi *et al*., 2015). Using ^{1}H NMR, Vrieling *et al.* (2018) and Zhou *et al*. (2013) identified plasma-based and serum biomarkers in TB patients. Furthermore, Dang *et al.* (2013) used GC-MS to identify *M.tb* infection biomarkers in culture, serum and urine. In other studies, Du Preez and Loots (2013) and Loots (2014) used two-dimensional gas chromatography coupled with time-of-flight mass spectrometry (GCxGC–TOFMS) to detect *M.tb* associated metabolites in sputum and mycobacterial cultures, respectively. Currently, no study has investigated the metabolic effect of vitamin D supplementation in TB infected cells using a metabolomics approach. As such, the main aim of this study was to make use of an NMR and GC-MS-based metabolomics approach to measure the metabolic reprogramming induced by vitamin D supplementation, in the presence of mycobacterial elicitor to mimic infection, in macrophages. This is aimed at identifying metabolites markers associated with mycobacterial infected cells in response to vitamin D in order to identify the specific metabolic pathways targeted by vitamin D. Taken together, this information can be used to determine the effectiveness of vitamin D in the immune response against mycobacterial infection.

In the present study, tripalmitoyl-S-glyceryl-L-Cys-Ser-(Lys)4 (Pam_3CSK_4), a synthetic mycobacterium that elicits toll-like receptor (TLR) 2/1, was used to stimulate U937 macrophages *in vitro*. The stimulated macrophages were supplemented with 1,25-dihydroxycholecalciferol ($1,25(OH)_2D_3$), an active form of vitamin D to evaluate its metabolic effect using NMR and GC-MS–based metabolomics.

The following chapter (**Chapter 2**) gives a detailed review of topics related to this study. This is followed by the hypothesis, aim, objectives, and study workflow. The succeeding chapter (**Chapter 3**) gives detailed materials and methods used to achieve the aim of the study. **Chapter 4** provides the generated results. The detailed discussion of each set of results is given in **Chapter 5**. The overall conclusion and future perspective are given in **Chapter 6**. **Chapter 7** provides the comprehensive list of references used in this study**,** followed by the

appendix. The appendix at the end of the dissertation consists of all additional and complimentary data that are not included in the results chapter.

CHAPTER 2

LITERATURE REVIEW

2.1. Mycobacteria

Bacterial infections are among the top causes of disease-related deaths worldwide (Raoult *et al.,* 2019) with mycobacteria being the main contributor. *Mycobacterium* is a member of the genus actinobacteria with several species classified into tuberculous or nontuberculous mycobacteria (NTM). Whilst tuberculous bacteria are disease-causing (e.g. TB), NTM are less pathogenic in humans. The latter mainly cause opportunistic infections in immunocompromised individuals (Tortoli, 2009). *Mycobacterium* of TB in humans. TB is the leading cause of infectious disease-related deaths worldwide. Moreover, one-third of the world's population is latently infected with *M.tb*. (Osman *et al*., 2017; Soto-Ramirez *et al*., 2017; Zumla *et al*., 2013). Thus, TB remains a worldwide threat. The prevalence of *M.tb* infection is also accelerated by the development of new strains of *M.tb,* some of which are resistant to the available anti-TB drugs (Chandra *et al*., 2016). Hence, there is a great need for a better understanding of the biochemistry, metabolism, and pathogenesis of mycobacteria as this is crucial for controlling mycobacterial infections. Therefore, timely, accurate and easy-to-use detection methods for mycobacteria are required (Palomino, 2005). In an attempt to study exposure to *M.tb, in vitro* models for immune cell stimulation have been developed. Tripalmitoyl-S-glyceryl-L-Cys-Ser-(Lys)4, commonly known as Pam_3CSK_4, is an *M.tb* lipoprotein mimic used to stimulate immune cells in *in vitro* models (Akira *et al*., 2006).

2.2. Pam_3CSK_4

Pam_3CSK_4 is a synthetic molecule that mimics bacterial triacylated lipoprotein of a wide range of bacteria (**Figure 2.1**), including *M.tb*, *Neisseria meningitidis*, *Trypanosoma cruzi* and zymosan of yeast cell wall (Nyirenda *et al.,* 2013). Pam_3CSK_4 stimulates immunomodulatory effects similar to those observed against lipoproteins from these bacteria (Akira *et al.*, 2006; Aliprantis *et al.,* 1999). Pam_3CSK_4 consists of carboxy terminal amino acids and N-acyl-S-diacylglyceryl cysteine and can therefore mimic the acylated amino terminus of bacterial lipopeptides. As such, Pam_3CSK_4 has captured the interest of many researchers working on *in vitro* based bacterial research, particularly those concerned with the study of Toll-like receptors (TLRs), especially TLR 2 and 1 (Du *et al*., 2011; Zhang *et al.,* 2016; Zhu *et al*., 2018; Zom *et al.,* 2018). Both Pam_3CSK_4 and bacterial triacylated lipoprotein stimulate the immunomodulatory effect towards bacteria with the acylated N-terminal cysteine (Kang *et al*., 2009).

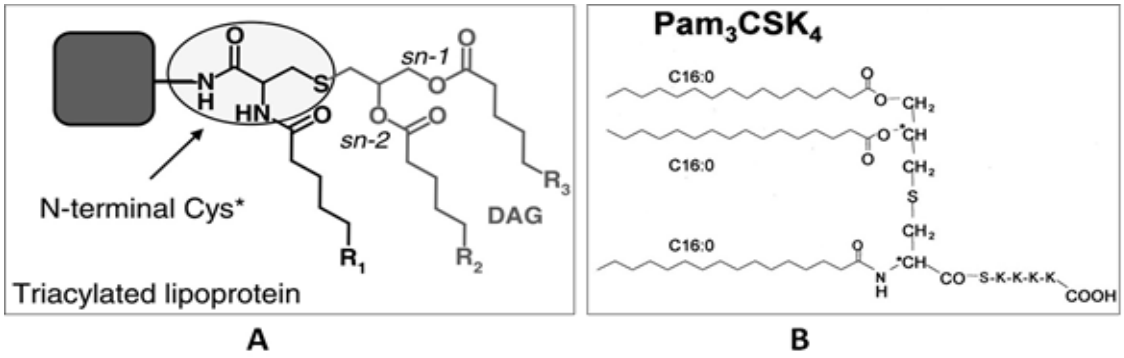

Figure 2.1: Structural representation of a bacterial triacylated lipoprotein (A) and Pam_3CSK_4 (B). Both have three lipid chains with one lipid chain attached to the N-terminal of cysteine. Both molecules induce an immunomodulatory effect through the acylated N-terminal cysteine. Adapted from Schromm, 2007; Wiktor *et al.*, 2017.

Pam_3CSK_4 is recognised by the Toll-like receptor 2/1 (TLR 2/1) protein, a membrane-bound dimer TLR receptor on the cell surface. TLRs form a major part of the innate immune response as they recognise pathogens and transduce a signal to activate downstream pathways that initiate the mechanisms responsible for the elimination of the pathogen. The downstream pathways stimulated by the activation of TLR2/1 by Pam_3CSK_4 are summarised in **Figure 2.2.**

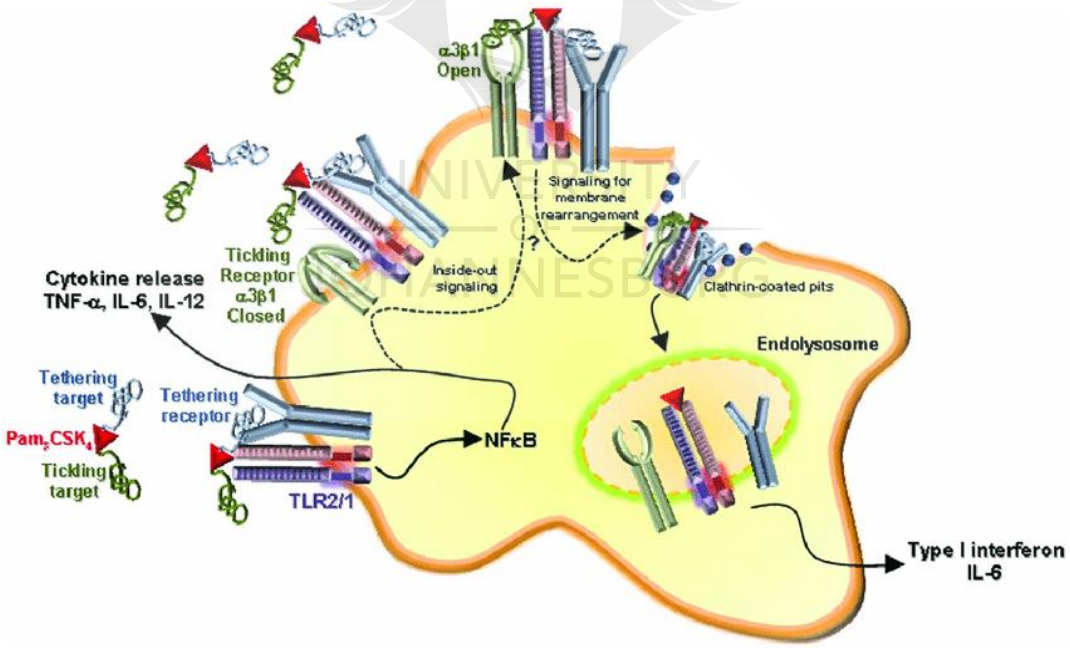

Figure 2.2: Pam_3CSK_4-induced stimulation of heterodimer TLR 2/1.TLR2/1 activation by Pam_3CSK_4 is associated with elevated expression of NF-kB, which stimulates the production and release of cytokines such as TNF-α, IL-6 and IL-12. TLR2/1 activation is also associated with the activation (opening) of α1β1 integrin receptor to initiate the endocytosis of the Pam_3CSK_4-TLR 2/1 complex. The resulting endolysosome further secretes type 1 interferon and IL-6 to signal neighbouring cells about the infection. Abbreviations: α1β1: alpha-1 beta-1 integrin; TLR2/1: Toll-like receptor 2/1; Pam_3CSK_4: Tripalmitoyl-S-glyceryl-L-Cys-Ser-(Lys)4; NF-kB: Nuclear Factor kappa beta; TNF-α: Tumour necrosis factor- alpha; IL-6: Interleukin 6; IL-12: Interleukin 6. Adapted from Marre *et al.,* 2010.

The focus of this study was on *M.tb* and as such, Pam_3CSK_4 was used to mimic for mycobacteria. Pam_3CSK_4 can provide a good starting point for understanding common, underlying mechanisms of *M.tb* pathogenesis. In addition, Pam_3CSK_4 provides a good tool to study mechanisms associated with TLR2 activation, the main TLR that initiates host immune response towards *M.tb* infection (Xue *et al*., 2008). Pam_3CSK_4 may thus shed light on the disease mechanisms associated with *M.tb*. Both *M.tb* infection and Pam_3CSK_4 share common biological effects such as the secretion of pro-inflammatory cytokines including IL-1, IL-6, IL-23 and TNF-α. The production of reactive oxygen species (ROS) is also observed in both cases (Bardoel *et al*., 2014; Yang *et al*., 2012).

2.3. Vitamin D

Prior to the antibiotic era, vitamin D was used to boost the immune system against several diseases including infectious diseases, inflammatory diseases, hypertension, diabetes mellitus and auto-immune diseases (Marques *et al.,* 2010; Thacher and Clarcke, 2011). Vitamin D deficiency has been associated with immune response disorders. Interestingly, vitamin D was used for TB treatment (Wejse *et al*., 2009; Wu *et al*., 2018). Findings have shown that individuals with TB have less vitamin D than healthy individuals (Gao *et al*., 2014). When supplemented with vitamin D, TB patients show ease in the disease symptoms. Furthermore, vitamin D supplementation decreases the activation and the progression of latent TB (LTB) to active TB (Arnedo-Pena *et al.*, 2015). In their study, Talat *et al*. (2010) reported that individuals with vitamin D deficiency are five times more likely to develop active TB compared to those with sufficient vitamin D. People of African descent are commonly known to have low vitamin D levels and are more likely to get TB than individuals from European descent (Green *et al*., 2015). Accordingly, TB is more common in African countries (Barter *et al.,* 2012).

2.3.1. Vitamin D and its metabolism

Vitamin D is an essential steroid hormone acquired from vitamin D rich nutritional sources, vitamin D supplements and through ultraviolet B (UVB) radiation-dependent synthesis (Prietl *et al*., 2013). Vitamin D_2 (ergocalciferol) and vitamin D_3 (cholecalciferol) are two well-known forms of the hormone vitamin D. Whilst vitamin D_2 originates from ergosterol UV radiation in fungi and some plants, vitamin D_3 originates from the UV radiation of 7-dehydrocholesterol to form previtamin D_3 in animals' skin (Tripkovic *et al*., 2012). Humans self-synthesize cholecalciferol and acquire ergocalciferol from vitamin D supplements and dietary sources such as fish, eggs and cheese (Kulie *et al*., 2009). $1,25(OH)_2D_3$ is an active form of vitamin D with various biological effects. The classical biological functions of this hormone include the regulation of minerals such as calcium and phosphate homeostasis to promote bone health (Prietl *et al.,* 2013). $1,25(OH)_2D_3$ further promotes the proliferation and differentiation of cells

such as osteoclast, endothelial cells, lymphocytes and keratinocytes (Khammissa *et al*., 2018). $1,25(OH)_2D_3$ has been shown to also regulate the innate and adaptive immune response (Chun *et al*., 2014).

UVB radiation-dependent synthesis of vitamin D involves the photolytic conversion of 7-dehydrocholesterol—a precursor of vitamin D—to pre-vitamin D_3 in the lower epidermis of the skin. Pre-vitamin D_3 is then converted to vitamin D_3 (cholecalciferol), similar to that obtained in dietary sources and supplements. Vitamin D_3 binds to vitamin D binding protein (DBP), which transports vitamin D_3 to the liver to be enzymatically converted to 25-hydroxyvitamin D (25(OH)D), the main circulating inactive form of vitamin D through hydroxylation by 25-hydroxylase. 25(OH)D has the longest half-life and hence it is used to determine vitamin D status (Zhang and Naughton, 2010). 25(OH)D circulates to the kidneys or any tissue that express 1α-hydroxylase (CYP27B1) such as the cerebellum, osteoblasts, pancreatic islets, placenta, monocytes, macrophages and dendritic cells (Hewison, 2012; Owens *et al*., 2018;), where it is hydroxylated to the circulating active metabolites of vitamin D. Although the conversion of 25(OH)D to $1,25(OH)_2D_3$ can also occur under normal, healthy conditions, monocytes and macrophages, among other immune cells produce high levels of $1,25(OH)_2D_3$ through CYP27B1 following the activation of these cells by the pathogen. Pathogen-dependent activation of immune cells is associated with an increased expression of vitamin D receptor (VDR) and 1α-hydroxylase, CYP27B1 (**Figure 2.3**). In addition to $1,25(OH)_2D_3$ production in the kidney, enzyme 24-hydroxylase (CYP24A1) hydroxylates C-24 of $25(OH)D_3$ to yield $24,25(OH)_2D_3$, a less active vitamin D hormone as compared to $1,25(OH)_2D_3$ (Jones *et al*., 2012).

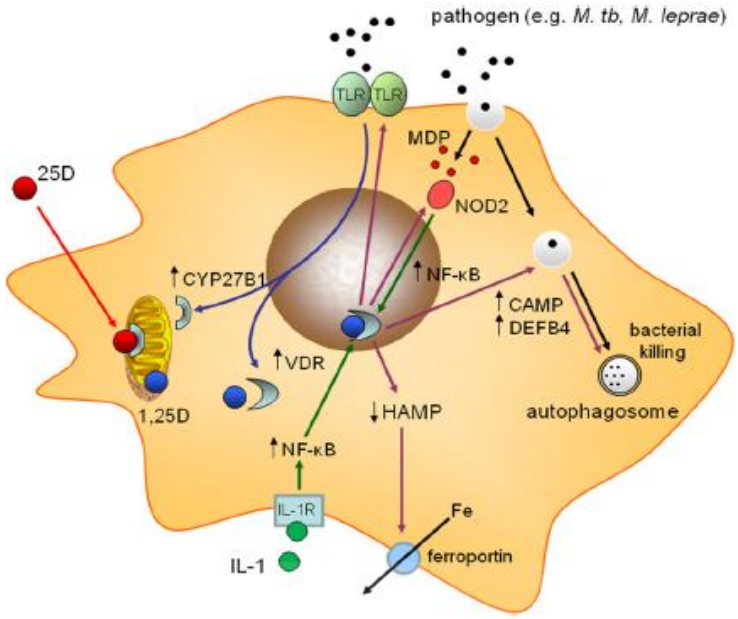

Figure 2.3: Vitamin D-mediated innate immune response following activation of TLR2/1 by a bacterial pathogen. The activation of TLR2/1 is linked with the conversion of 25D to 1,25D by enzyme CYP27B1. Subsequently, VDR binds 1,25D and stimulates the expression of CAMP and DEFB4. Bacterial killing is also achieved through autophagy and formation of autophagosomes. The suppression of HAMP regulates ferroportin, which promotes the extracellular transportation of Fe to facilitate bacterial elimination. IL-1R is stimulated to bind IL-1, which promotes the synthesis of NF-κB. Together with MDP binding to NOD2, NF-κB provides an additional response to facilitate the interaction of VDR with 1,25D, therefore facilitating the bacterial elimination. Abbreviations: 1,25D: 1,25-dihydroxy vitamin D; 25D: 25-hydroxyvitamin D; CAMP: Cathelicidin antimicrobial peptide; CYP27B1: 1α-hydroxylase; DEFB4: β-defensin 4; Fe: Iron; HAMP: Hepcidin antimicrobial peptide; IL-1: interleukin 1; IL-1R: Interleukin 1 receptor; MDP: muramyl dipeptide; NF-κB: Necrosis factor-kappa beta; NOD2: Nuclear-binding oligomerization domain-containing protein 2; TLR2/1: Toll-like receptor 2/1; VDR: Vitamin D receptor. Adapted from Chun *et al*., 2014.

2.3.2. Regulation of vitamin D metabolism

The regulation of vitamin D metabolism is achieved through the regulation of enzymes CYP27B1 in the kidney and 25-hydroxylase in the liver. 1α-Hydroxylase is more tightly regulated as compared to 25-hydroxylase since it controls $1,25(OH)_2D_3$ synthesis (Kochupillai, 2008). At low concentrations of $1,25(OH)_2D_3$, parathyroid hormone induces 1α-hydroxylase to favour $1,25(OH)_2D_3$ synthesis (Christakos, 2017). The increase in the levels of $1,25(OH)_2D_3$ eventually results in a feedback mechanism that triggers an increase in the level of bone fibroblast growth factor 23 (FGF23). FGF23 is a phosphaturic hormone produced by osteocytes and osteoblasts. This hormone inhibits 1α-hydroxylase expression to decrease $1,25(OH)_2D_3$ synthesis (Khammissa *et al*., 2018). Simultaneously, increasing levels of FGF23 induces the expression of 24-hydroxylase, an enzyme that catalyses the conversion of $25(OH)D_3$ to a less active vitamin D metabolite, $24,25(OH)_2D_3$ in the kidneys (Perwad and Portale, 2011).

2.3.3. Role of 1,25(OH)$_2$D$_3$ in innate immunity

TLR2/1-pathogen interaction activates an innate immune defence mechanism strengthened by 1,25(OH)$_2$D$_3$. This form of immunity comprises chemotactic and phagocytic processes of monocytes and macrophages (Purnamasari *et al.,* 2014). The activation of vitamin D-–mediated innate immunity depends on the recognition of pathogen-–associated molecular patterns (PAMPs) by pattern-recognition receptors (PRRs) such as TLR2/1. Upon pathogen perception by TLR2/1, liganded VDR binds the retinoid X receptor (RXR) to form a heterodimer that binds a specific gene sequence called a vitamin D response element (VDRE). Liganded VDR–RXR heterodimer is responsible for the activation of hundreds of target genes or repression by recruiting coactivators or coreceptors, respectively, to a particular target gene (Christakos *et al*., 2016; Rosen *et al.,* 2012). These mechanisms result in the expression or suppression of target genes with biological effects that will favour the elimination of the pathogen. β-Defensin 4 (*DEFB4*) and cathelicidin antimicrobial peptide (*CAMP*) are well known genes that encode antibacterial proteins β-defensin 2 and cathelicidin antimicrobial peptide, respectively. Collectively, these antibacterial proteins facilitate the elimination of the bacterial pathogen, **Figure 2.3** (Baeke *et al.,* 2010; Liu *et al.,* 2006).

In addition to the elimination of the bacteria by antibacterial proteins, autophagy and formation of autophagosomes following the activation of TLR2/1 also play a major role in pathogen elimination. Furthermore, accessory immune response mechanisms (shown in green in **Figure 2.3**) are also activated in response to increasing 1,25(OH)$_2$D$_3$. For instance, the expression of interleukin–1 receptor (IL-1R) and muramyl dipeptide is induced following the activation of TLR2/1 and production of 1,25(OH)$_2$D$_3$. IL-1R facilitates the binding and the entry of cytokine IL-1, which in turn, induces the expression of Necrosis factor-kappa beta (NF-κB) to facilitate pathogen elimination. In addition to these direct mechanisms of bacterial elimination, hepcidin antimicrobial peptide (HAMP) indirectly kills the pathogen by decreasing intracellular iron (Fe), which is needed to maintain bacterial growth and survival. HAMP primarily regulates ferroportin, the iron exporter located on the cell membrane (Ganz, 2011).

2.3.4. Role of 1,25(OH)$_2$D$_3$ in adaptive immunity

The adaptive immune response also plays a crucial role as a second defence mechanism against pathogenic infection. The major key players in adaptive immunity include dendritic cells (CDs), B -cells and T -cells, including effector T -cells and regulatory T -cells due to their ability to express VDR in response to antigenic activation. 1,25(OH)$_2$D$_3$ has different biological effects in adaptive immunity *in vitro* and *in vivo* (Hewison, 2012). Briefly, dendritic cells—also known as antigen-presenting cells (APCs)—are the first immune cells of the adaptive immune response triggered by 1,25(OH)$_2$D$_3$ signalling. DCs capture the antigen for processing and presentation to the T cells (Purnamasari *et al*., 2014). It was first thought that 1,25(OH)$_2$D$_3$

suppresses T cell proliferation; however, subsequent studies revealed that the effects of 1,25 $(OH)_2D_3$ are dependent on the phenotype of the T cell. Thus, high levels of 1,25$(OH)_2D_3$ are associated with down-regulation of T helper cell 1 (Th1) and T helper cell 17 (Th17), causing inhibition of proinflammatory cytokines associated with these T helper cells such as interferon- gamma (IFN-γ), IL-2, IL-17 and IL-21. On the other hand, T helper cell 2 (Th2) and Treg are up-regulated, resulting in an increase in IL-4 and IL-10 (Hewison, 2012). The biological significance of switching from Th1 to Th2 phenotype is to limit the tissue damage resulting from excessive Th1. Th17, on the other hand, has been linked not only with promoting immune response but also with promoting inflammatory tissue damage, hence it is down-regulated by 1,25$(OH)_2D_3$ (Korn *et al*., 2007).

Activated T cells indirectly stimulate B cell activation through mechanisms including the suppression of immunoglobulin (Ig) secretion, inhibition of proliferation and differentiation of plasma cells as well as the stimulation of B cell apoptosis (Purnamasari *et al*., 2014). B cells use autocrine mechanisms to produce their own 1,25$(OH)_2D_3$ that regulates immunity. In addition, B cells stimulate increased expression of IL-10, a cytokine that inhibits the presentation of the antigen by DCs and macrophages as well as the inhibition of T cell activation (Heine *et al.,* 2008). The biological significance of 1,25$(OH)_2D_3$ mediated adaptive immune response is to balance the activity of the immune response, therefore preventing the tissue damage resulting from excessive cytokines and anti-microbial proteins (Handono *et al.,* 2012).

2.3.5. Vitamin D status and deficiency: why it happens, prevalence and consequences

Vitamin D deficiency is one of the major health problems worldwide across all age groups (Regmi *et al*., 2017). Vitamin D status is determined using 25(OH)Dlevels since it is the main circulating form of vitamin D and has a long half-life during circulation (Zhang and Naughton, 2010). The concentration of 25(OH)D used to determine whether this hormone is deficient or not remains unclear. The United States Institute of Medicine, however, defined a concentration of <30 nmol/L 25(OH)D as deficient, 30–49 nmol/L as insufficient and 50–125 nmol/L as sufficient (Looker *et a*l., 2011). Vitamin D deficiency occurs when the serum level of vitamin D is extremely low which could be alluded to inadequate dietary uptake or reduced vitamin D synthesis, most probably from decreased sunlight exposure (Nighat *et al*., 2010). Additionally, obesity, age, race, dark skin pigmentation, season, latitude and the use of sunscreen also contribute towards vitamin D deficiency (Souberbielle, 2016; Zhang and Naughton, 2010). This health problem is also associated with an increased risk of neoplastic, immune and metabolic disorders (Holick, 2007). In children, vitamin D deficiency is associated with rickets whereas in adults it is associated with osteomalacia, multiple sclerosis, cardiovascular diseases and chronic diseases (Cantorna *et al*., 2004; Holick, 2007; Wu *et al.,* 2007). Moreover, individuals with vitamin D deficiency are more susceptible to infectious

diseases as opposed to healthy individuals (Garg *et al*., 2016). The levels of serum vitamin D can be improved by the intake of vitamin D dietary products and vitamin D supplements (Kennel *et al*., 2010). Although vitamin D supplementation has been shown to decrease the activation and the progression of latent TB (LTB) to active TB, the molecular mechanism of vitamin D in the presence of mycobacteria remains elusive. As such, the aim of this study was to make use of metabolomics in order to explore the role of vitamin D in immune response to TLR2/1 elicitation by a mycobacterial elicitor.

2.4. Metabolomics

2.4.1. The origin of metabolomics

The use of metabolic profiling dates back as early as the 1950s (Williams, 1956) where it was used to understand complex biological systems before the term metabolome was even introduced to literature in September 1998 (Oliver *et al*., 1998). Subsequently, the term metabolomics and its equivalent term metabonomics were formulated at the end of the 1990s (Oliver *et al*., 1998; Nicholson *et al*., 1999). The two terminologies, metabolomics and metabonomics, are often used interchangeably in the literature. The current study, however, uses the term metabolomics, as it describes a comprehensive analysis of as many metabolites as possible in a biological system (Clish, 2015). Metabolomics can thus be described as the detection and quantitative measurements of the metabolites in a biological system under specific conditions or perturbation. On the other hand, metabonomics is defined as the quantitative measurement of the metabolic changes of a living system in response to genetic modification or any pathophysiological stimulus (Nicholson *et al*., 1999). Thus, metabonomics emphasizes on the characterisation of the differences in metabolites due to genetic modification, disease, environmental stress or any other stimulus that perturbs the metabolism of the given organism (Ramsden, 2009).

Metabolites are low molecular-mass compounds (<1.5 kDa) involved in metabolic processes of an organism and they are the endmost products of gene expression. The total number of metabolites of an organism—the metabolome—comprise amino acids, esters, lipids, steroids, carbohydrates, organic acids, oligopeptides, bile acids, nucleosides and nucleotides (Clarke and Haselden, 2008; Mirsaeidi *et al*., 2015). These are small molecules that are biologically essential for energy production and storage, signal transduction and apoptosis among other biological roles (Johnson *et al.*, 2016). Despite being the youngest omics in the omics cascade, the use of metabolomics has grown quite rapidly over the past years, particularly in the medical field and in basic research. This is due to its promising ability in providing early clinical diagnostics, drug refinement, and personalised medicine (Riekeberg and Powers, 2017). The planning of a metabolomics experiment is determined by the aim of a study, however, a typical workflow is shown in **Figure 2.4.**

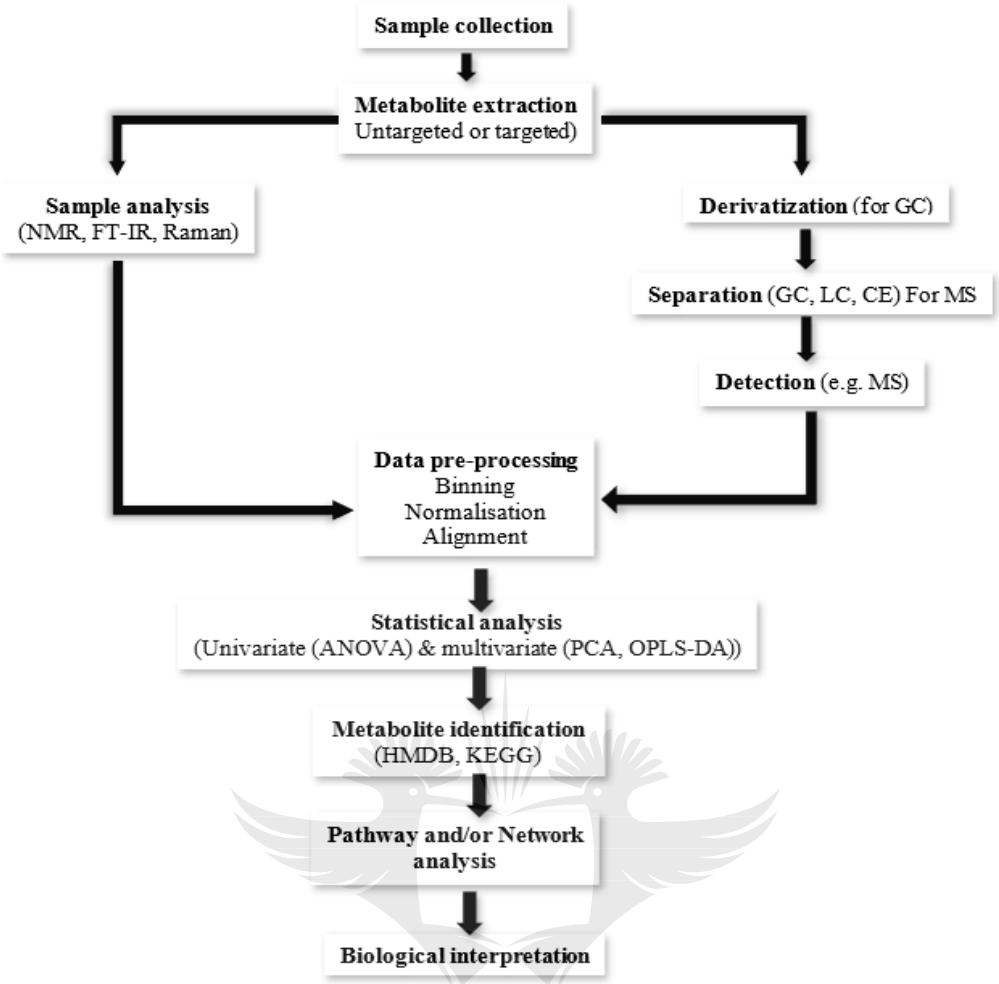

Figure 2.4: A typical metabolomics workflow. The diagram illustrates the common steps followed in a metabolomics experiment. It also highlights techniques used at different stages of metabolomics depending on the type of sample specimen being analysed and the aim(s) of the experiment. Abbreviations: ANOVA: Analysis of variance; CE: Capillary electrophoresis; FT-IR: Fourier-transform infrared; GC: Gas chromatography; HMDB: Human Metabolome Database; KEGG: Kyoto Encyclopedia of Genes and Genomes; LC: Liquid chromatography; MS: Mass spectrometry; NMR: Nuclear magnetic resonance; OPLS-DA: Orthogonal projections to latent structures–discriminant analysis; PCA: Principal component analysis.

2.4.2. Metabolomics approaches

Metabolomics studies take one of two approaches, namely the targeted or untargeted approach. The untargeted approach is a starting point for any metabolomics study as it focuses on the global profiling of as many metabolites as possible in a given biological system. More than one analytical platform is normally used in the untargeted approach to profile as many metabolites as possible. A new hypothesis is usually derived from the initial findings of the untargeted approach. In contrast, a targeted approach is a hypothesis-driven approach that focuses on profiling a group of predefined metabolites, usually with similar biological properties. It is therefore common in this approach that the physio-chemical properties and

structures of the metabolites of interest are known beforehand (Schrimpe-Rutledge *et al*., 2016; Tzoulaki *et al*., 2014). The benefits of using a targeted over an untargeted approach include high sensitivity and increased maximum analytical throughput. Untargeted metabolomics is, however, more comprehensive and unbiased. The largest number of metabolites are therefore detected using the latter approach. Untargeted metabolomics is widely used for the discovery of novel metabolites and biomarkers. Despite these strengths, untargeted metabolomics remains less sensitive compared to the targeted approach (Kirkwood *et al*., 2013). Whilst the untargeted approach is crucial for metabolite discovery and relative quantification, the targeted approach is useful for validation and absolute quantification of the already known metabolites (Schrimpe-Rutledge *et al.,* 2016).

2.4.3. Why metabolomics over other omics technologies

Metabolites are influenced by genetic and epigenetic processes, post-translational modifications, protein transport and signal transduction (Kell and Oliver, 2016; Likic *et al*., 2010). Metabolomics can therefore provide comprehensive information from different molecular stages (**Figure 2.5**). Metabolomic analysis, in comparison to other omics, can also provide phenotypic information of an organism induced by various stimuli such as diseases and medication (Wishart *et al*., 2007). Understanding the changes in the metabolome resulting from a disease could play a crucial role in the development of better disease characterisation methods, diagnostics and treatment (Du Preez *et al*., 2019). Despite the change in the metabolome under various conditions, the basic chemical structure of a metabolite is similar throughout different species (Duft *et al*., 2017). As such, metabolites can provide more reliable and robust biomarkers for a perturbation (German *et al*., 2005). Another strength of metabolomics includes the ability to profile changes due to 'silent mutation' (Raamsdonk *et al.,* 2001). Hence, metabolomics has the potential to provide useful disease biomarkers that give a better understanding of the underlying disease mechanisms. Biomarkers can be used to monitor disease at different stages such as early, latent or late stages (Atan *et al*., 2018; Du Preez *et al*., 2017). The advantages and disadvantages of the different omics platforms have been summarised in **Table 2.1**.

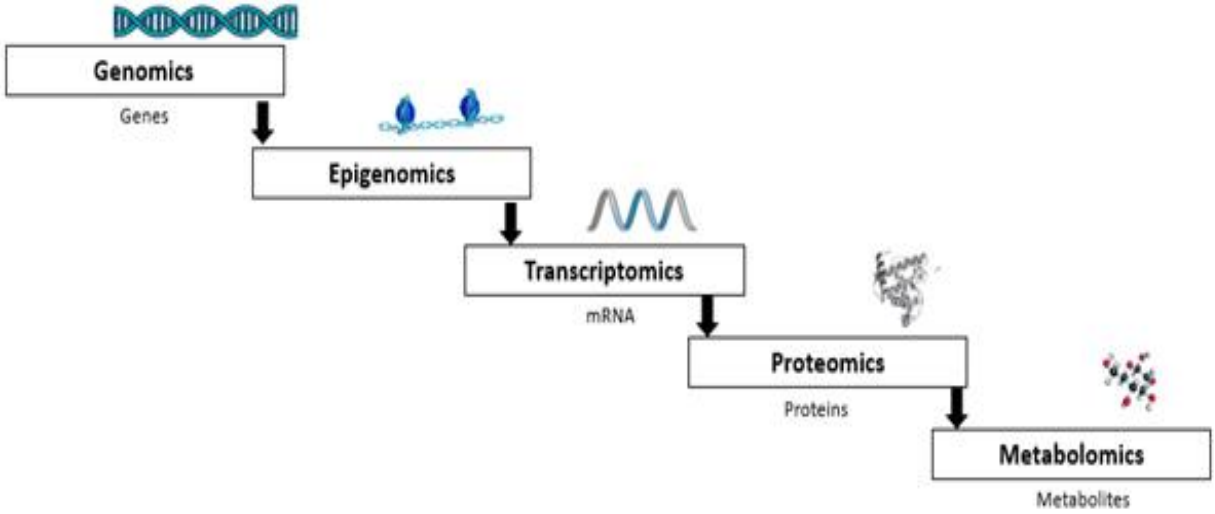

Figure 2.5: The omics cascade. The omics cascade showing the flow of molecular information from the genome, to epigenome, transcriptome, proteome and metabolome. Metabolomics is at the end of the cascade. Hence metabolites correlate to the phenotype of a biological system.

Table 2.1: Comparison of main omics technologies, adapted from Diamandis *et al*., 2010; Draghici *et al*., 2006; Fliser *et al*., 2007; Jax *et al*., 2018; Johnson and Gonzalez, 2012; Kinoshita *et al*., 2006; Kuehnbaum and Britz-McKibbin, 2013; Kalantari *et al*., 2015; Lorincz, 2011; Mesri, 2014; Roberts and Middleton 2017; Serkova *et al*., 2011; Zhan, 2015; Zhao *et al*., 2014.

Omics	Description	Strengths	Weaknesses
Genomics	Concerned with the study of the whole genome. The complete set of all genes in an organism.	• The available knowledge is substantial. • Genomics can be used to develop diagnostic, prognostic and treatment for patients. • Multiple genes can be identified simultaneously, allowing the detection of, e.g. altered gene(s) associated with a disease.	• Unintended Identification of gene mutations not associated with the condition of interest may complicate result interpretation and lead to false conclusions. • Genes are sensitive to various stimuli such as disease and environmental factors.
Epigenomics	The study of the epigenome includes studies on DNA methylation, histone modification and RNA regulation.	• Genetic information missed in gene expression profiles can be recovered in the epigenome. • Epigenetic profiles are highly stable. • Provides epigenetic biomarkers for diseases.	• Diversity in epigenetic changes across tissue types. • Diagnosis of epigenetic changes may require several assays. • Susceptible to false discovery of new biomarkers.
Transcriptomics	The study of the transcriptome, the entire set of RNA molecules of an organism or a cell.	• Gives a better understanding of gene expression and gives the possible functions, which would reflect the phenotype.	• Many transcriptome studies use microarrays approach, which suffers from detecting very lowly expressed and novel transcripts • Difficulty in detecting splice variants.

Proteomics	The study of proteins including their folding, localization, expression, function and interaction	• Understanding of genomic information in terms of protein structures and functions. • The proteome is close to the biological function (phenotype).	• Challenges in linking the proteome and the genome. • Lack of stability in the proteome during sample preparation may lead to false representation of the original proteome of an organism.
Metabolomics	The detection and quantitative measurements of the metabolites in a biological system under specific conditions or perturbation.	• High throughput, sensitivity, and accuracy. • Qualitative and quantitative. • The ability to study a specific phenotype at a molecular level. • Metabolites correlate with the phenotype of an individual. • Availability of advanced analytical techniques. • Disease biomarker discovery.	• Difficulties in metabolite identification and interpretation. • Many knowledge gaps in human metabolomics. • Data handling and processing can be challenging. • Metabolome can be altered by various genetic and environmental stimuli other than those of interest. • Variations between individuals in human metabolomics. • Metabolome complexity and variations. • Difficulties in translation of metabolites into metabolic pathways and biological interpretation.

2.4.4. Metabolomics analytical platforms

The high reproducibility and high throughput provided by metabolomics are made possible by the availability of advanced sensitive and selective spectroscopy and spectrometry-based analytical techniques. These techniques make use of the emission, absorption or scattering of electromagnetic radiation by matter (atoms, molecules, ions or solids) for qualitative and quantitative analysis (Kalantri *et al*., 2010). Fourier transformation-infrared (FT-IR) spectroscopy, Raman spectroscopy, nuclear magnetic resonance (NMR) spectroscopy and mass spectrometry (MS) are the well-known metabolomics analytical techniques, however, NMR and MS are the most widely used techniques due to their high sensitivity and selectivity (Dunn and Ellis, 2005). Despite being the preferred techniques, NMR and MS also come with their own weaknesses (**Table 2.2**). Combining the two usually gives complementary information (Bingol and Brüschweiler, 2015). The choice of the analytical technique to use in a metabolomics experiment is influenced by the type of the biological system to be analysed as well as the aim of the experiment or question to be answered (Trygg *et al.,* 2007). Despite the strength provided by each analytical platform, there is no single analytical platform that can detect the entire metabolome within a biological systemdue to the metabolite heterogeneity (Booth *et al.,* 2013).

Table 2.2: Comparisons of NMR and MS analytical platforms. Adapted from Carlos *et al*., 2011; Davis and Mauer, 2010; De Villiers and Loots, 2013; Faghihzadeh *et al*., 2016; Kalantri *et al*., 2010; Mogilevsky *et al*., 2012.

Technique	Description	Advantages	Disadvantages
NMR spectroscopy	Involves the analysis of the magnetic properties of the atomic nuclei of a molecule under a magnetic field.	• Non-destructive and therefore samples can be recovered. • Requires a minimal sample preparation. • Can simultaneously measure all kinds of metabolites. • Can be used for *in vivo* studies.	• Less sensitive (as compared to mass spectroscopy). • Does not always accurately detect fats and lipids. • NMR spectra of biological samples are complex and hence large peaks may mask small peaks.
Mass spectrometry	Involves the ionization of molecules of interest followed by the measurement of their mass-to-	• High sensitivity and specificity. • Requires small sample size for analysis. • Qualitative and quantitative technique.	• Extensive sample preparation is required. • Inability to measure many large biological molecules. • Destructive and hence samples cannot be recovered. • Time consuming.

	charge (m/z) ratio.	• Can detect a wide dynamic range of metabolites.

2.4.5. The basic principle of NMR spectroscopy

Atomic nuclei of some atoms such as that of ^{1}H, ^{13}C and ^{31}P consist of a spin, which is a property similar to atomic mass and charge (Demarest, 2015; Yabsley *et al*., 2012). The spin generates the magnetic field in the nucleus. This causes the random orientation of the spins, however when the atomic nuclei are subjected to the external magnetic field generated by the NMR spectrometer, two spin states are produced, one aligned with the external magnetic field and the other against the external magnetic field. The spin aligned with the external magnetic field is called the alpha (α) spin and has a lower energy state. The spin against the external magnetic, called the beta (β) spin, has a higher energy state (Antcliffe and Gordon, 2016; Boyer, 2012; Zia *et al*., 2019). When the nuclei are subjected to the radiofrequency energy, α spin is excited to a higher energy state. The higher energy state is less stable and therefore the α spin will return to the lower energy state in a process known as relaxation. The α spin emits the absorbed radiofrequency energy as it returns to the lower energy state. The emitted radiofrequency energy is converted into a signal which is represented on the NMR spectrum (**Figure 2.6**). The horizontal x-axis of the NMR spectrum represents the resonant frequency as the chemical shift in parts per million (ppm). Nuclei of different chemical groups resonate at different frequencies and hence will have different chemical shifts. The vertical y-axis of the NMR spectrum gives the intensity of the resonance signal, proportional to the concentration of the sample analysed (Antcliffe and Gordon, 2016; Chatham and Blackban 2001; Wilson and Walker, 2010). Several types of NMR experiments have been developed to study various molecules. These include proton NMR (^{1}H-NMR), carbon NMR (^{13}C-NMR) and phosphorus NMR (^{31}P-NMR). In a biological context, the basic applications of ^{1}H-NMR, ^{13}C-NMR and ^{31}P-NMR are to detect groups of metabolites, identify bio-molecular structures (such as fatty acids carbohydrates and amino acids) and to analyse the biochemical processes that involve adenosine triphosphate (ATP) (Beckonert *et al*., 2007; Boyer, 2012). The use of NMR spectroscopy has grown tremendously over the years both *in vitro* and *in vivo*. NMR spectroscopy is widely applied in biological sciences (biomolecular structure determination, protein functions and interactions), metabolomics, pharmaceutical research (drug screening), medical sciences, food sciences and forensics (Hatzakis, 2019; Lu, 2013; Marion, 2013; Santos *et al*., 2018).

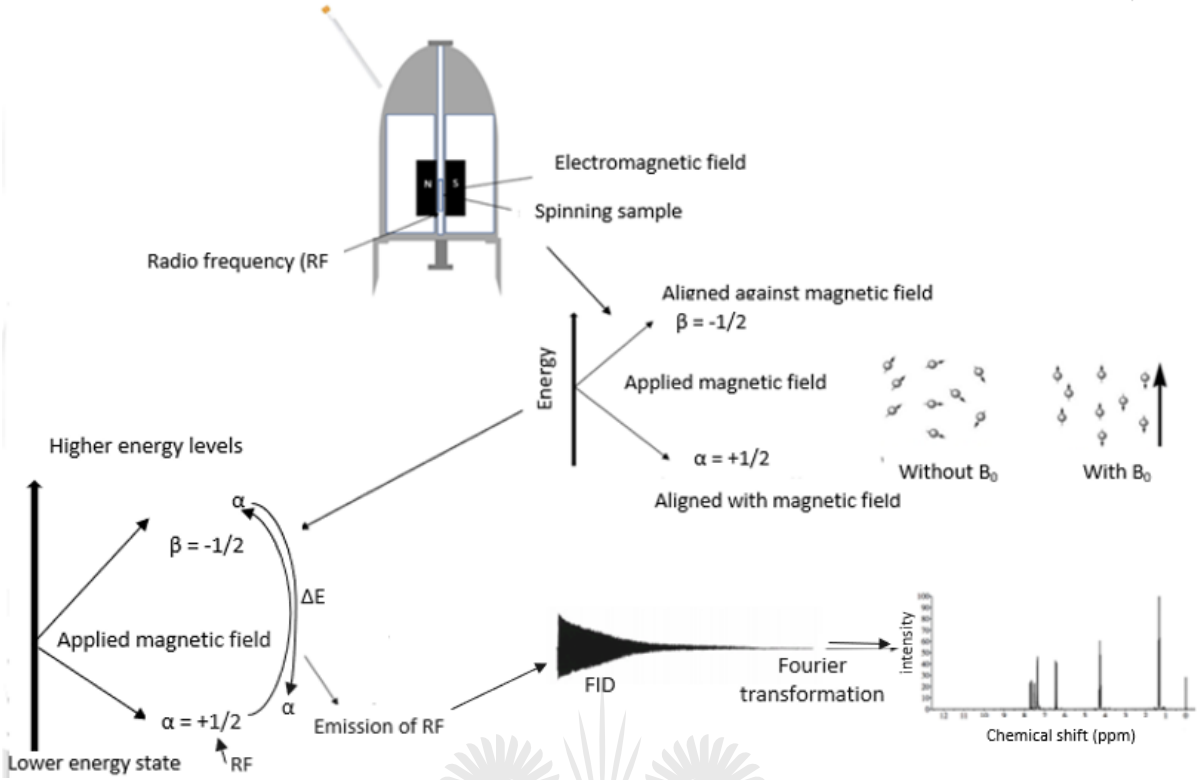

Figure 2.6: A diagram representing the basic principles of NMR spectroscopy. When the sample is placed under the magnetic field in the NMR spectrometer, the spins in the protons of each molecule are either aligned with or against the direction of the external electromagnetic field (β_0). Spin aligned with the magnetic field (α) has a lower energy state and are more stable than the spin aligned against the magnetic field (β). As the radio frequency energy is applied to the nuclei at lower energy state (α), the α spins are excited to higher (β) energy state. This excitation is short-lived and therefore the α spins return to a lower energy state after a very short period. The α spins emit radio frequency energy as they return to the lower energy state at different times. The emitted radio frequency energy is converted into free induction decay (FID), which is a time-domain signal. FIDs are processed and converted into a frequency domain spectrum by Fourier transformation and represented on the NMR spectrum as intensity *vs*. chemical shift (ppm) on the y-axis and x-axis, respectively. Abbreviations: ΔE: Change in energy; α: alpha; β: Beta; β0: External electromagnetic field; FID: Free induction decay; RF: Radio frequency

2.4.6. The basic principle of mass spectrometry

Despite the analytical strengths offered by NMR spectroscopy, MS has become a popular analytical platform in metabolomics due to its high sensitivity (Markley *et al*., 2017). The basis of MS involves ionisation of the molecules with subsequent measurement of mass to charge ratio (m/z) of the formed ions. This provides both qualitative and quantitative information concerning each molecule in a mixture (Urban, 2016). Mass spectrometers (the instruments used in mass spectrometry) consist of different components, each with a distinct function. The main components include the ion source, mass analyser, and a detector (**Figure 2.7**). Following the introduction of a sample mixture, containing the molecules of interest, in the ion source, the molecules are ionised to produce gaseous ions, which are transferred to a

mass analyser. The mass analyser sorts the ions based on their mass to charge ratio under the electric or magnetic field. These ions are then detected by an ion detector which determines the abundance of each ion. Subsequently, the ion detector produces electric signals which are processed and presented in a histogram called a mass spectrum; a function of m/z and relative abundance, on the x-axis and y-axis, respectively (Murayama *et al.*, 2009; Patel *et al*., 2012). Collectively, a mass spectrum represents the structure of the original molecules, the resulting fragments and any other species that may be formed during ionization (Urban, 2016).

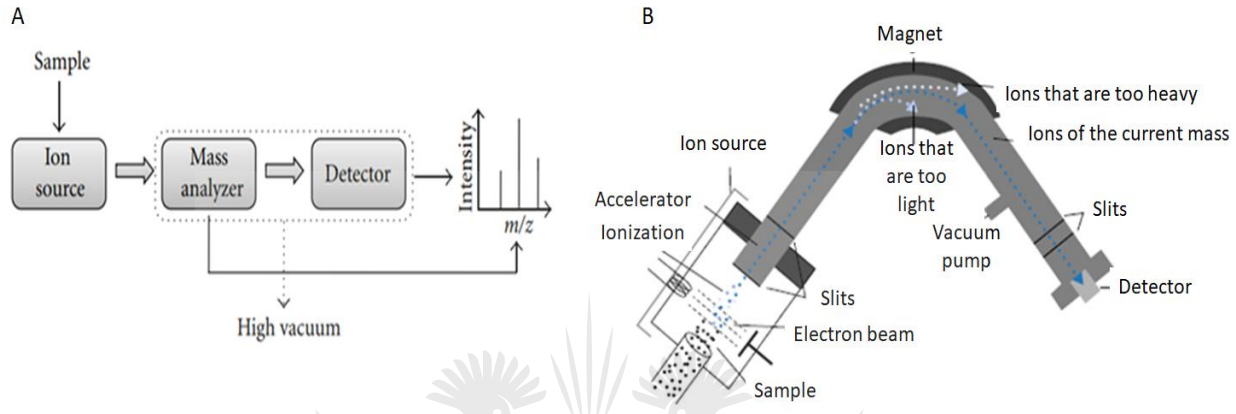

Figure 2.7: Simplified (A) and detailed (B) schematic representations of the components of the mass spectrometer. Sample in the injector is delivered to the ion source where it is ionized into gaseous ions. The formed ions are sorted according to their m/z ratio in the mass analyser. The detector detects the electrical signal of each ion generated to give a mass spectrum. Adapted from Banerjee and Mazumdar, 2012 (A) and Antcliffe and Gordon, 2016 (B).

Mass spectrometers are used as detectors hyphenated to chromatographic techniques such as gas chromatography (GC), and liquid chromatography (LC). Briefly, GC-MS deals with the separation of volatile and semi-volatile compounds using a high temperature and subsequent detection with MS (Sneddon *et al*., 2007). LC-MS, on the other hand, uses a liquid-based mobile phase, usually made of organic solvents and water, to separate different compounds in a mixture prior to ionisation and detection by MS. The coupling of MS with other techniques, particularly chromatographic techniques, enables the analysis of a wide range of molecules. MS has a wide range of applications in several fields including clinical studies, protein characterisation, drug discovery, quality control, food safety protocols, space exploration, pharmacokinetics and metabolomics (as reviewed by Patel *et al*., 2012; Urban, 2016).

2.4.7. Gas chromatography –mass spectrometry (GC-MS)

The basis of GC-MS (**Figure 2.8**) is that volatile and semi-volatile compounds in a mixture are separated by GC and detected by MS. Separation of the compounds with GC is based on the partition of compounds in a mixture between the mobile phase and the stationary phase as the compounds pass through the column by the carrier gas (AL-Bukhaiti *et al*., 2017; Sneddon *et al*., 2007). Prior to GC-MS analysis, a sample containing a mixture of compounds is dissolved in a solvent such as methanol, acetone or heptane. The sample mixture is then delivered into the sample injector. The sample injector is placed in an oven to vaporise the sample upon injection (AL-Bukhaiti *et al*., 2017; Klee and Blumberg, 2002; Kupiec, 2004). The mobile phase carrier gas, as the name implies, carries the vaporised sample mixture through the column equipped with the stationary phase. The carrier gas is inert so that it does not react with the samples. Helium, nitrogen, argon or hydrogen are the most commonly used carrier gases, depending on the type of detector used (Hussain and Maqbool, 2014).

A GC stationary phase comes in one of two available columns, namely, packed column or capillary (open tubular) column. In the former, the spherical stationary phase material is packed across the column tubing forming small sieves to allow the mobile phase to pass through. Some of the stationary phase materials used for packed columns include polyethylene glycols, methylphenyl- and methylvinylsilicone gums, apiezon L, succinic, phthalic acids and b-cyclodextrin-based phases for chiral separations (Wilson and Walker, 2010). In capillary columns, the stationary phase is either a direct or indirect coat attached to the wall of the column, leaving an opening at the centre of the column. Hence, it is also called an open tubular column (Skoog *et al*., 2018). The capillary (open tubular) column functions on the principle of adsorption (Ye *et al*., 2000). Capillary columns are of two types, namely, wall-coated open tubular (WCOT) and support-coated open tubular (SCOT), also called porous layer open tubular (PLOT). WCOT differs from SCOT/ PLOT in that the stationary phase in WCOT is coated to the wall of the column whereas in SCOT/PLOT, the stationary phase is coated to a support (Skoog *et al*., 2018).

As a mixture of compounds passes through the stationary phase, some compounds interact weakly with the stationary phase and elute from the column first. On the contrary, molecules that interact strongly with the stationary phase spend a longer time in the column and they have longer elution time (AL-Bukhaiti *et al*., 2017; Hussain and Maqbool 2014). In addition to these polarity-dependent interactions of the compounds and the stationary phase, temperature also determines the time spent by the compounds in the column. Thus, compounds with low boiling points elute first as compared to those with high boiling points (Oña-Ruales *et al*., 2016). Due to the crucial role that temperature plays in compound separation in a mixture, the column is placed in an oven so that the temperature can be controlled. The oven can be set to maintain a constant or gradually increasing temperature, known as ramping (Wilson *et al*., 2014). Ultimately, each compound in a mixture is eluted from the column at different elution times to be detected by the MS as described in **Section**

2.4.6. The GC-MS results are represented on a mass spectrum; a plot of m/z ratio and intensity on the x-axis and y-axis (Murayama *et al.*, 2009; Patel *et al*., 2012).

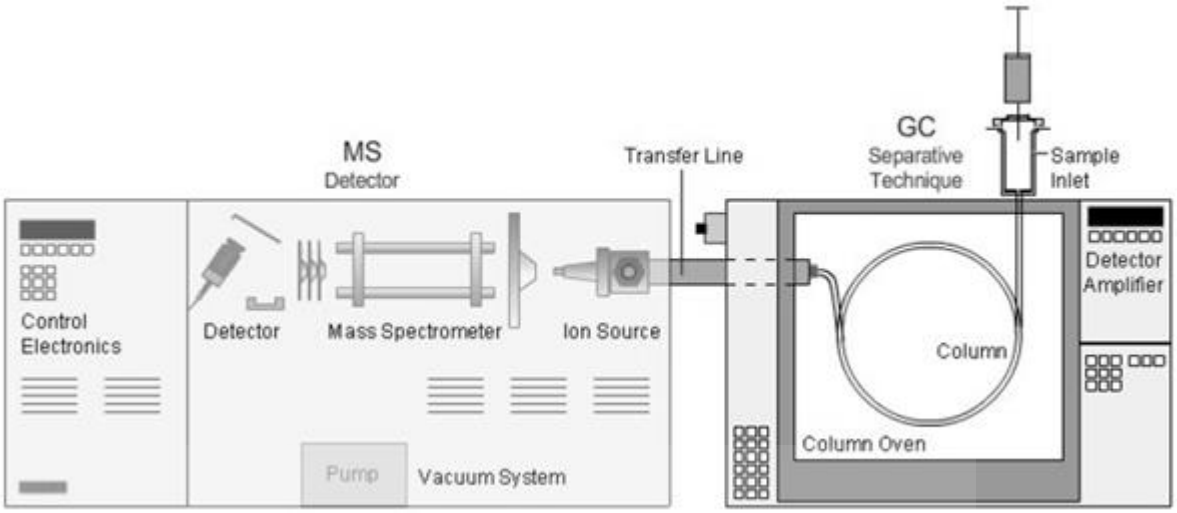

Figure 2.8: A diagram of GC-MS. From right to left, a mixture of compounds is injected into the GC through the sample inlet port. The mixture is vaporized prior to separation in the column, positioned in an oven. The mixture is separated based on the affinity of each compound to the stationary as well as the boiling point of each compound in a mixture. The separated compounds pass through the transfer line to the MS, where they are ionised for detection. The detected ions are represented on the mass spectrum.

2.4.8. Two-dimensional gas chromatography (GC×GC) coupled with time-of-flight mass spectrometry (TOFMS)

Although conventional GC provides a powerful separation technique, the complexity of many compounds exceeds the capacity of one-dimensional GC. To overcome this challenge, comprehensive two-dimensional gas chromatography (GC×GC) has been developed (Rocha *et al*., 2007; Tranchida *et al*., 2004). In GCxGC, sample separation is carried out using two separate columns with different polarities of the stationary phase (Kalinova *et al*., 2006; Spanik *et al.,* 2012). The interface connecting the two columns, the modulator, is a cryogenic trap that condenses compounds as they elute from the primary column to the secondary column (Kalinova *et al*., 2006). The modulation process is essential as it increases the separation power and sensitivity (Dekeirsschieter *et al*., 2012; Patterson *et al*., 2011). Both separation potential and sensitivity are enhanced in two-dimensional GC×GC as compared to one dimensional GC (Zrostlıkova *et al*., 2003). The second column of the GCxGC is very short and can produce peaks as narrow as 0.1 s. This requires a detection system with high acquisition rates to properly describe each peak. Conventional MS can only acquire up to 50 spectra s^{-1} and therefore it cannot properly detect all the peaks generated in GCxGC. As a result, the high-speed time-of-flight mass spectrometry (ToF-MS) has been developed with the capability to acquire up to 500 spectra s^{-1} (Kalinova *et al*., 2006; Rocha *et al*., 2007). ToF-MS can detect a larger number of compounds in extreme complex mixtures, making ToF-MS the most effective GCxGC detector (Mohler *et al*., 2006). In general, GC×GC–ToF-MS provides

a powerful, sensitive and selective analytical technique for compound separation, detection and identification (Snow *et al*., 2010).

Although the application of GC-MS is only limited to volatile and semi-volatile compounds, GC-MS is used in several fields. GC-MS has been shown to be capable of precise identification and quantification of an individual compound from a mixture. Secondly, GC-MS is capable of identifying traces of contaminants in research concerned with compound purification (Tumuluru *et al*., 2012). Hence GC-MS has gained popularity in fields such as food sciences (Hussain and Maqbool, 2014), forensics, environmental studies, beverage, geo-chemical and astro-chemistry research, medicine and pharmaceutical research, biological and pesticides detections, energy and fuel applications, industrial and academic research (as reviewed by Al-Rubaye *et al*., 2017).

2.4.9. Metabolomics statistical analysis

Metabolomics analytical techniques generate high dimensional complex data, making it difficult to process and analyse the acquired data. The complexity of the data generated in metabolomics prompts the need for statistical methods that will be able to handle such data. Multivariate data analysis (MVDA) is used to statistically make sense of the generated data. MVDA is categorised into unsupervised and supervised methods. The unsupervised methods are usually the first statistical methods applied. These methods are called unsupervised simply because the data analysed are not assigned to class membership. Thus, prior knowledge about the data membership is not required (Ren *et al.,* 2015). Unsupervised methods can be categorised further into dimension reduction methods and cluster analysis methods.

2.4.9.1. Unsupervised statistical methods

Principal component analysis (PCA) remains the most commonly used dimension reduction method. This is an exploratory analysis method that reduces the complexity of high dimensional data by capturing the information that contributes to the observed variation. PCA reduces the dimensionality of the data set without the loss of core information (Gromski *et al*., 2015; Saccenti *et al*., 2014). Ultimately, PCA gives a summary of the data set, showing the within-group and between-groups variation in the given data set. The trend, grouping and outliers in the data set can also be seen in PCA modelling (Trygg *et al*., 2007). Cluster analysis methods, such as hierarchical cluster, seek to find a cluster of samples in multidimensional space with similar characteristics. The clustering of samples forms a tree-like structure called a dendrogram (Goodacre *et al*., 2007; Chen *et al*., 2009).

2.4.9.2. Supervised statistical methods

In addition to unsupervised methods, supervised methods are used in metabolomics data analysis mainly for prediction, classification and biomarker discovery. Unlike unsupervised methods, supervised methods determine and explain the association between the predictors (X-data) and the categorical (e.g. disease vs. healthy) or quantitative (age, body mass index, sex, blood glucose) response variable (Y-data) in the data set (Ren *et al.,* 2015). Commonly used supervised methods are based on partial least squares (PLS), which include projections to latent structures-discriminant analysis (PLS-DA) and orthogonal projections to latent structures–discriminant analysis (OPLS-DA). Whilst PLS-DA is widely used for the differentiation of classes in the data-set (Worley and Powers, 2013); its extension, OPLS-DA aims to maximize the differentiation of groups and identification of marker metabolites. These are metabolites responsible for differentiating the different groups in a data-set (Shin *et al*., 2011; Trygg *et al*., 2007). Another classic example of a supervised method, linear discriminant analysis (LDA), functions similarly to PCA in the manner that it projects a high dimensional dataset onto a lower dimensionality subspace (Kim and Yeom, 2017). LDA extracts, separates and classifies dataset, into groups with similar features, maximizing separation between-–groups covariance and minimizing separation within-–group covariance (Giraldi *et al*., 2008; Yeom *et al*., 2007).

Although multivariate data analysis is the most important component in handling complex metabolomics data, univariate statistical methods are just as important since they allow metabolomics data features to be analysed independently. However, univariate methods do not account for interacting metabolomic features as opposed to multivariate data analysis and this is the main disadvantage of univariate statistical methods in metabolomics (Lazar *et al*., 2015). Univariate statistical methods are used for the reduction of a large number of measured features to those that only show the maximum variations between study groups in response to the investigated perturbation (Bartel *et al*., 2013). Among several univariate methods available, parametric tests, Student's *t*-test and analysis of variance (ANOVA) are commonly used to analyse metabolomics features independently in a data-set (Alonso *et al*., 2015). A probability value (*p*-value) is widely used to determine the statistical significance of the difference between two variables measured in, for example, cases and controls. By using a *p*-value, one can easily accept or reject the null hypothesis or alternative hypothesis (Vinaixa *et al*., 2012).

2.4.10. Statistical validation

Statistical data generated in MVDA require validation, mainly to assess their significance and reliability (Worley and Powers, 2013). In supervised methods, for instance, detection of many variables (metabolites) from a small sample size comes with the danger of model overfitting. Although an over-fitted model can show a very good performance, such a model might not

accurately predict a new set of data. As a result, such a model cannot be duplicated (Xi *et al*., 2014). Two main approaches, test-set validation and cross-validation (CV), have been developed for multivariate model validation. The former uses a new separate dataset to validate the developed model whereas, in the latter, model validation is performed using the same dataset used to generate the original model (Trivedi and Iles, 2012). The cross-validation method can cope with a low sample number; hence it is usually the method of choice (Westerhuis *et al*., 2008). In cross-validation, the experimental dataset is separated into different groups, which are randomly used in different combinations to build a permuted model. The original model is then validated by comparing it to the permuted model to determine the predictive accuracy (Trivedi and Iles, 2012).

Cross-validation is subdivided into two categories, namely internal and external cross-validation. Whilst internal cross-validation deals with the selection of the number of latent variables and finds an optimal PLS-DA model, external cross-validation focuses on the measurement of the performance of the model (Xi *et al.,* 2014). A matric Q^2 is used to measure the predictive ability of the developed model, which is the ability of the model to accurately predict new data when applied to the model. Furthermore, parameter R^2 (the goodness of fit) explains the amount of variation between groups explained by the model. Therefore, Q^2 and R^2 describe the quality of the model and their values range between 0 and 1 (Shin *et al.*, 2011). A model with good predictive ability is indicated by $Q^2 \geq 0.5$ (Lauri *et al*., 2016), however, a model with $Q^2 \geq 0.4$ is also acceptable for biological studies (Westerhuis *et al*., 2008). The R^2 value is always higher than the Q^2 value for a good model (Sedghipour and Sadeghi-Bazargani, 2012). In addition to Q^2 and R^2, cross validated-analysis of variance (CV-ANOVA) and area under the receiver operating characteristic (ROC) curve (AUROC) are used to validate the OPLS-DA models. CV-ANOVA assesses the significance (reliability) of the PLS-DA and OPLS-DA models whereas the ROC curve validates the robustness and predictive performance of a model (Subramani *et al.,* 2016).

2.4.11. Metabolites annotation, pathways and network analysis

Statistical analysis is followed by metabolite annotation, pathways and network analysis as well as the biological interpretation of the generated results. These are performed using a combination of available metabolomics software and databases. Identification of metabolites in human-based metabolomics can be done through various metabolomics databases such as Human Metabolome Database (HMBD), Biological Magnetic Resonance Data Bank (BMRB), Madison Metabolomics Consortium Database, Bayesil NMR Web App, MetaboMiner NMR command line Interface and SpinAssign. Amongst these databases, HMDB is the commonly used database for human-based metabolites identification as it has more than 8000 verified entries (Aretz and Meierhofer, 2016). The identified metabolites are used to construct or identify relevant biological pathways to extract more useful biological information from the acquired data. Pathway analysis gives an overview and understanding of enzyme regulation

as well as post-translational modification of enzymes or proteins involved in metabolite synthesis (Nägele, 2014). The metabolism of an organism can further be explained by an alternative method, namely network analysis. A metabolic network gives information about the association and the interaction of genes, proteins and metabolites or small molecules (Kuhn *et al.*, 2008). Kyoto Encyclopedia of Genes and Genomes (KEGG), which is a popular choice for pathway and network analysis, houses most biological pathways and networks that have been identified to date. KEGG biological pathways and networks are constructed on the basis of linking a set of genes with their interacting molecules to produce a network (Kanehisa and Goto, 2000).

2.4.12. Biological interpretation of metabolomics data

The major goal of any metabolomics experiment is to identify and understand the biological events that take place in a biological system under specific conditions. Accordingly, data acquired from a metabolomics experiment should correspond to the phenotype of the biological system of interest. There remains, however, a large knowledge gap in the translation of metabolomic data to biological interpretation (Scalbert *et al.,* 2009). A single metabolite can participate in several metabolic processes, making it difficult to assign a metabolite detected in a metabolomics experiment to a single biological pathway. Nonetheless, the use of metabolomics tools/databases can provide sufficient information that could eventually lead to a true representation of the physiology of an organism or the biological question being investigated (Aretz and Meierhofer, 2016). Understanding metabolite up-regulation or down-regulation does not only provide insight into the biological pathways involved but also contains the information regarding the enzymes or other molecules involved in a metabolic pathway. Such information can be useful in determining the health status of an organism as well as the pharmacological action of a given treatment (Chagoyen and Pazos, 2012).

2.4.13. Challenges in metabolomics

Metabolomics has its challenges despite the advancement made over the past years. Firstly, various genetic and environmental stimuli can alter the metabolome of an organism. Care should therefore be taken during sample handling to obtain data that represent the true physiology of an organism (Johnson and Gonzalez, 2012). Secondly, some metabolites are identical across different species, which makes it difficult to study the metabolism of two interacting organisms (e.g. the interaction between the host and the pathogen). Thus, the host metabolome might not be differentiated from the pathogen's metabolome (Schrimpe-Rutledge *et al*., 2016). Experimentally, metabolite extraction and data acquisition can also be challenging. In addition to biological and experimental related challenges, major challenges

are usually encountered in data processing, data visualisation, metabolite identification and validation (Bowler *et al.,* 2017). Over the years, an effort has been made to overcome these challenges through the improvement of both analytical techniques as well as the statistical methods and software used in data handling (Steuer *et al*., 2019).

2.4.14. Exploring 1,25(OH)$_2$D$_3$ metabolic impact through NMR and MS-based metabolomics

Metabolomics has previously been applied in *M.tb*-related research, leading to the identification of TB biomarkers from various sample matrices (including *M.tb* culture, serum, plasma, lung tissue, spleen tissue) (Behrends *et al*., 2012; Dang *et al*., 2013; De Buck *et al*, 2014; Feng *et al*., 2015; Frediani *et al*., 2014; Halouska *et al*., 2014 and Mahapatra *et al*., 2014). Tuberculostearic acid (TBSA), for example, is one of the most reliable TB biomarkers identified in metabolomics across various sample specimens (Du Preez *et al*., 2017). Through metabolomics, new metabolic processes, gene function, virulence factors and enzyme activity can be described to better understand the mechanism of the pathogen (Du Preez *et al*., 2019).

Vitamin D has been closely related to improving the outcome of TB, however, a very limited amount of research has been conducted on understanding the metabolic effect of vitamin D during *M.tb* infection. Nonetheless, the association between vitamin D and *M.tb* infection has been described (Gibney *et al.,* 2008). In their study, Gibney *et al*. (2008) reported that higher levels of vitamin D are associated with lower probability of *M.tb* infection and vice versa. Although vitamin D alone has not been clinically evaluated as a treatment for TB (Kearns, 2014), the use of vitamin D with anti-TB drugs has been shown to accelerate the improvement of clinical outcomes of *M.tb* infection (Hassanein *et al*., 2016). This association has been less studied through metabolomics. As such, investigations are needed to understand the metabolic effect of vitamin D during mycobacterial infection.

The metabolic effects of supplementary 1,25(OH)$_2$D$_3$ *in vitro* have been investigated in previous studies. A study by Santos *et al*. (2017) revealed that *in vitro* 1,25(OH)$_2$D$_3$ supplementation in human embryonic kidney 293T (HEK293T) cells alters the cellular metabolic profile of the cells. Using NMR spectroscopy, Santos *et al*. (2017) found a slight increase in intracellular lactate concentration in HEK293T cells treated with 1,25(OH)$_2$D$_3$. An increase in lactate concentration is associated with up-regulation of glycolysis. Other metabolic pathways including the polyol pathway and Krebs cycle were down-regulated whereas phosphocholine pathway was up-regulated in the presence of 1,25(OH)$_2$D$_3$. In another *in vitro* study, Abu El Maaty *et al*. (2017) reported metabolic changes associated with *in vitro* 1,25(OH)$_2$D$_3$ supplementation. In their study, Abu El Maaty *et al.* (2017) supplemented different human prostate cancer (PCa) cell lines (LNCaP, VCaP, DU145 and PC3) with 1,25(OH)$_2$D$_3$ prior to MS-based (GC-MS) metabolic profiling. The authors reported that the responsiveness of these cell lines to 1,25(OH)$_2$D$_3$ differs with LNCaP being the most responsive

cell line. In LNCaP cells, supplementary $1,25(OH)_2D_3$ induced metabolic reprogramming of glucose metabolism, fatty acid metabolism, glutamine metabolism and tricarboxylic acid (TCA) cycle. Their study showed that $1,25(OH)_2D_3$ has a metabolic impact on cellular metabolism.

In a subsequent study, Abu El Maaty *et al*. (2018) supplemented breast cells (MCF-7 and MDA-MB-231) with $1,25(OH)_2D_3$. Using MS-based (GC-MS) metabolomics, the authors detected significant alterations in spectral regions associated with phosphoenolpyruvate, pyruvate, citrate, α-ketoglutarate, succinate, fumarate, malate, serine, glycine, L-alanine, proline, L-leucine, isoleucine, threonine, aspartic acid, valine and glutamic acid. The authors further reported that supplementary $1,25(OH)_2D_3$ induced energy metabolism reprogramming. It was shown in their study that $1,25(OH)_2D_3$ induce reprogramming of the TCA cycle and the glycolytic pathway.

Taken together, it is evident from these above-mentioned *in vitro* studies that $1,25(OH)_2D_3$ affects the metabolism of different cell types under different disease conditions, leading to metabolic reprogramming. Furthermore, these studies have shown that $1,25(OH)_2D_3$ induced metabolic changes can be profiled using both NMR and MS-based metabolomics. Hence, the aim of the current study is to use NMR and MS-based metabolomics to determine the metabolic effect of $1,25(OH)_2D_3$ supplementation in mycobacterial infection *in vitro*.

2.5. The rationale behind using the in vitro system for the present study

In vitro studies are dependent on the use of cell lines or models that resemble the *in vivo* systems of interest. Studying infectious pathogens comes with a high risk of being infected and therefore it requires a specialised and highly regulated laboratory with proper risk assessment (Patterson *et al*., 2014). Such requirements, however, come at a high cost. To overcome this, non-hazardous synthetic molecules that mimic molecules of interest are used. With the rapid growth of life sciences, the development and revolution of biotechnology in recent years, the *in vitro* approaches have become a cornerstone of basic research in many fields (Hartung and Daston, 2009). In metabolomics studies, the *in vitro* approaches provide a suitable system in the initial stages of biomarker discovery. Unlike the *in vivo* systems, the *in vitro* systems allow the investigator to strictly control the working environment. It further allows for accurate and strict control of the induction of the desired, specific variables being investigated. Furthermore, metabolomic studies concerned with pathogens performed *in vitro,* provide a clear insight into the pathogen metabolism since there is no host interfering metabolites. Such studies can be replicated easily with a high number of replicates at low costs. Despite the strengths that come with using the *in vitro* approach, the *in vitro* system has its pitfalls. Notably, the *in vitro* system does not account for the *in vivo* adaptation of the host or the microbe (Du Preez *et al*., 2019; Hartung and Daston, 2009). Also, the physiological relevance of the *in vitro* models differs from that of the *in vivo* systems. Cancer studies have

shown that *in vitro* studies only allow the investigator to capture limited aspects of the tumour microenvironment (Katt *et al*., 2016). Nonetheless, the *in vitro* models used in this study were the U937 cells as well as monocyte-macrophages.

The U937 cell line is a monocytic, histiocytic lymphoma cell line originally isolated from a 37-year-old Caucasian man. U937 cells are characterised by their oval shape with large, irregular shaped nuclei (Sundstrom and Nilsson, 1976). The popularity of the U937 cell line in research is due to its ability to resemble human macrophages, both morphologically and functionally (Mendoza-Coronel and Mastanon-Arreola, 2016). Some of these characteristics include the ability to perform antibody-induced cytotoxicity, phagocytosis of the pathogen and presentation of Fragment crystallizable (Fc) receptors that recognise subclasses of human IgG proteins (Alexander *et al*., 1979; Anderson and Abraham, 1980; Larrick *et al*., 1980). Human macrophages are terminally differentiated and non-dividing cells (Gordon and Taylor, 2005) and therefore cannot be isolated from the human body to be replicated for research *in vitro*. Hence, the U937 cell line provides a good *in vitro* model to study human macrophages. Several inducers including phorbol myristate acetate (PMA), retinoic acid (RA), interferon-Y (IFN-Y) and $1,25(OH)_2D_3$ (Pagliara *et al*., 2005; Passmore *et al*., 2001) can differentiate U937 monocytic cells to macrophages. An additional strength of the U937 cell line is its ability to retain the monocyte-macrophage features for several years, making it possible for the cell line to be used for a long period at higher passage numbers (Chanput *et al*., 2015; Strefford *et al.,* 2001).

Monocytes-macrophages form an important component of the innate and adaptive immune response, immunomodulation, inflammation and tissue repair. Monocytes originate from haematopoietic stem cells through the common myeloid progenitor lineage. They are subdivided into three subsets—Classical (with marker $CD14^{++}CD16^{-}$), intermediate ($CD14^{+(+)}$ $CD16^{+}$) and nonclassical (CD14+CD16++)—based on their function and surface marker they express (Ginhoux and Jung, 2014; Sprangers *et al*., 2016). Classical monocytes are the main subset in the immune response and phagocytosis. Monocytes are differentiated into macrophages and DCs. The functions of macrophages in the immune response have been categorised into antigen presentation, phagocytosis, and immunomodulation (Wynn *et al*., 2013). Unlike monocytes, macrophages consist of 'classical' M1 and 'alternative' M2 phenotypes that present proinflammatory and anti-inflammatory effects, respectively. Basically, M1 macrophages inhibit the pathogen whereas M2 maintains homeostasis to help repair and replace lost cells (Mills, 2012). Due to their pivotal roles in regulating the immune response and maintaining cellular homeostasis, macrophages are distributed throughout all tissues of the human body (Ballinger and Christman, 2016).

2.6. Study rationale

Previous studies have demonstrated that supplementary $1,25(OH)_2D_3$ improves the immune response against *M.tb* infection; however, the effects of $1,25(OH)_2D_3$ on the metabolism of immune cells responding to a mycobacterial infection remains elusive. Thus, the aim of the current *in vitro* study is to apply a multi-platfrom (NMR and GC-MS-based) metabolomics approach to elucidate differential metabolic changes related to the $1,25(OH)_2D_3$-supplementation in macrophages treated with mycobacterial elicitor to mimic infection. Although this is a preliminary study, it will provide necessary insights into the possible metabolic reprogramming events that define the effects of $1,25(OH)_2D_3$ on the metabolism of macrophages responding to a mycobacterial infection. Understanding these metabolic events could be of importance towards determining how $1,25(OH)_2D_3$ inhibits the activity of the mycobacteria in macrophages. Furthermore, the effectiveness of $1,25(OH)_2D_3$ in the immune response against mycobacterial infection may be estimated or predicted. The workflow of the study is given in **Figure 2.9**.

2.7. Hypothesis

Untargeted metabolomics is generally considered a hypothesis-generating approach, where a new hypothesis could be derived from the initial findings (Goodacre *et al.,* 2004). With that in mind, the accepted hypothesis for this study is as follows:

"NMR and GC-MS-based metabolic profiling can detect metabolic changes induced by Pam_3CSK_4 stimulation of macrophages supplemented with or without $1,25(OH)_2D_3$".

2.8. Research aim

The main aim of this study was to evaluate the metabolic effects of $1,25(OH)_2D_3$ on the metabolome of U937 macrophages stimulated with Pam_3CSK_4.

2.9. Research objectives

The specific objectives of the study are as follows:

1. The first objective was to differentiate the U937 monocytes to macrophages through PMA induced treatment of monocytes. Microscopic assessments of differentiated U937 cellular morphology and flow cytometry analysis of CD14 surface markers of the monocyte/macrophage cell populations were performed to determine and confirm U937 cellular differentiation.

2. The second objective was to use NMR and GC×GC-TOFMS-based metabolomics, coupled with multivariate statistical analysis, to decode metabolic reprogramming induced by Pam_3CSK_4 stimulation, $1,25(OH)_2D_3$ supplementation and a combination of both Pam_3CSK_4/$1,25(OH)_2D_3$ treatment in differentiated U937 cells. The metabolic profile of untreated (control) U937 macrophages were also determined.

3. The third objective of the study was to determine the metabolic pathways affected by each treatment condition in order to evaluate the global metabolic reprogramming associated with each treatment condition.

2.10. Research workflow

The experimental work was performed according to the workflow in **Figure 2.9.**

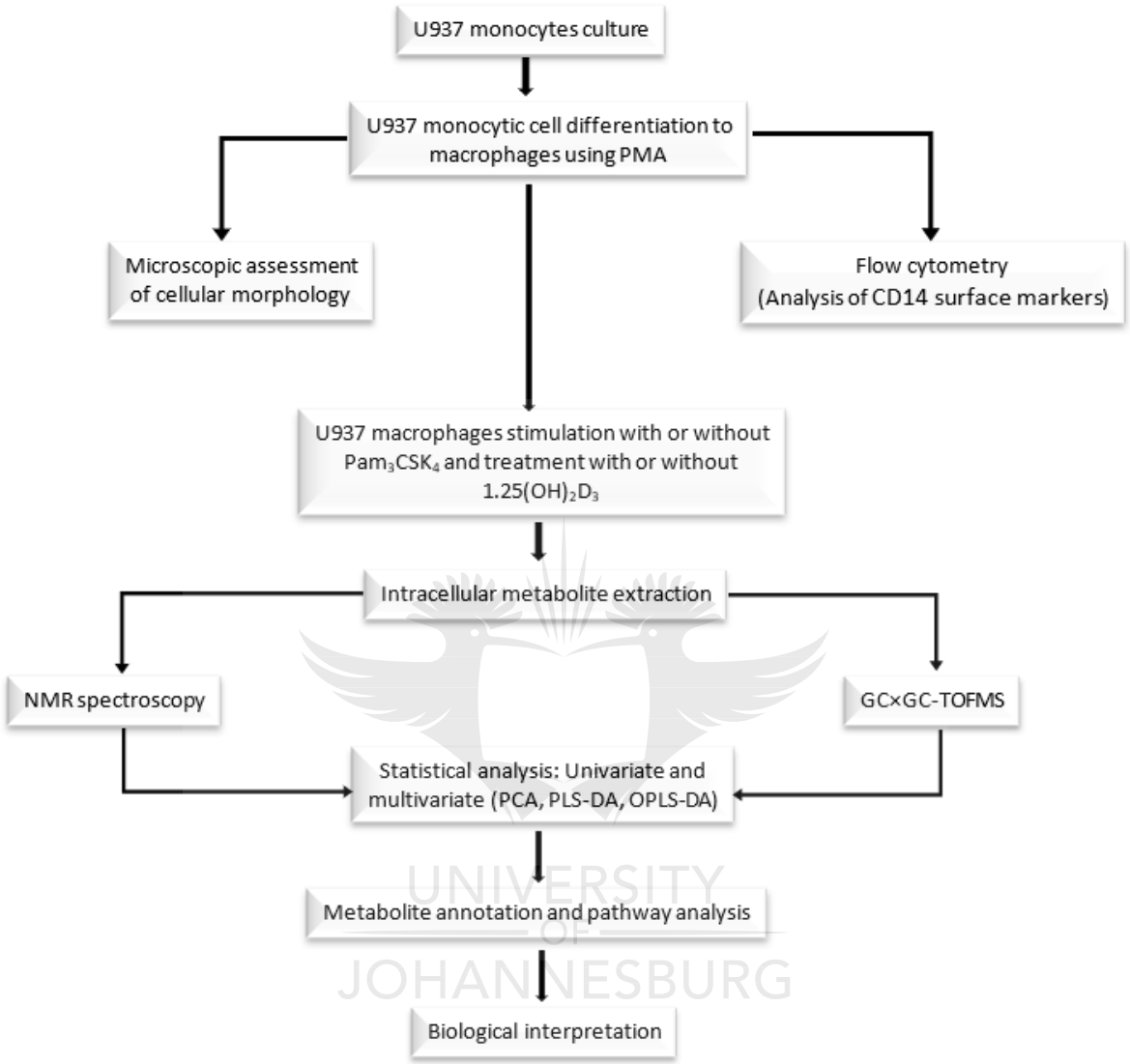

Figure 2.9: Workflow of the study. The first step of the study was to culture U937 monocytes. Viable U937 monocytes were then differentiated to macrophages using PMA. Cellular differentiation was confirmed using microscopic assessments of morphology and flow cytometry analysis of CD14 surface markers of the monocyte/macrophage cell populations. Differentiated cells were treated with Pam_3CSK_4, $1.25(OH)_2D_3$ and a combination of Pam_3CSK_4 and $1.25(OH)_2D_3$ prior to ^1H NMR spectroscopy and GC×GC-TOFMS metabolic profiling. The acquired data were subjected to univariate and multivariate statistical analysis. Statistical analysis was followed by metabolite annotation and pathway analysis. The last section of the study was the biological interpretation of the obtained metabolomics data. Abbreviations: $1.25(OH)_2D_3$: 1,25-dihydroxyvitamin D_3; CD14: Cluster of differentiation 14; GC×GC-TOFMS: Two-dimensional gas chromatography coupled with Time-of-flight mass spectrometry; NMR spectroscopy: Nuclear magnetic resonance spectroscopy; OPLS-DA: Orthogonal projections to latent structures–discriminant analysis; Pam_3CSK_4: Tripalmitoyl-S-glyceryl-L-Cys-Ser-(Lys)4; PCA: Principal component analysis; PLS-DA: Projections to latent structures-discriminant analysis; PMA: Phorbol myristate acetate.

CHAPTER 3

MATERIALS AND METHODS

The following chapter (**Chapter 3**) consists of the materials and methods used in the current study. Some of the methods used were obtained from relevant published literature sources (Sellick *et al*., 2011) with some adjustments. The first two sections (**Sections 3.1** and **3.2**) present the methodology used for the culturing of U937 monocytic cells, which were subsequently differentiated into macrophages using PMA. The succeeding section (**Section 3.3**) is divided into two sub-sections. The first sub-section (**Section 3.3.1**) presents the materials and methods used for microscopic assessment of monocyte to macrophage differentiation using a light microscope and the second sub-section (**Section 3.3.2**) consists of the methodology followed for flow cytometry-based measurement of surface maker differentiated cells. **Sections 3.4** and **3.5** provide a descriptive explanation of the stimulation of U937 macrophages in the presence and absence of Pam_3CSK_4 as well as supplementation with or without $1,25(OH)_2D_3$. This section is followed by the metabolic profiling of U937 macrophages stimulated with Pam_3CSK_4, $1,25(OH)_2D_3$ supplementation and a combination of both Pam_3CSK_4 and $1,25(OH)_2D_3$ using a multiplatform metabolomics approach, involving NMR and GC-MS analytical systems (**Sections 3.6** to **Section 3.11**). The last section of **Chapter 3** presents a detailed methodology on metabolic pathway analysis (**Section 3.12**).

3.1. U937 monocyte culturing

3.1.1. Method

The U937 monocytic cell line was obtained from the American Type Culture Collection (ATCC, Virginia, United States). The U937 cells were cultured in Roswell Park Memorial Institute medium (RPMI) 1640 (Life technologies corporation, USA) supplemented with 30% fetal bovine serum (FBS) (GE healthcare life sciences, USA), 2 mM L-glutamine (LG) (Sigma-Aldrich, USA) and 1% (w/v) Penicillin-Streptomycin (Pen-Strep); 10 000 IU/mL Penicillin with 10 mg/mL Streptomycin, made up in 0.9% sodium chloride (NaCl) solution (Invitrogen, Waltham, MA). The cells were cultured at 37°C in a humidified atmosphere with 5% CO_2. Whilst the role of FBS in cell culture is to supply nutrients to the cells, L-glutamine alternatively provides energy for cell division. Pen-Strep is crucial for preventing the growth of microbes in the medium. After 24 hrs of incubation, the cells were centrifuged at 1000 x*g* for 1 min at room temperature to remove the culture medium. The obtained cell pellet was then cultured and

maintained in 1640 RPMI medium supplemented with 10% FBS, 2 mM L-glutamine and 1% (w/v) Penicillin-Streptomycin. The concentration of FBS was changed from 30% to 10% to obtain optimal cell growth. The culture medium was refreshed every 48 hrs until the cells reached 90% confluence. Cell counting was performed using trypan blue (Sigma-Aldrich, USA) on an automated cell counter. This was achieved by adding 20 µL of trypan blue to 20 µL of culture medium containg cells. The two solutions were mixed and 20 µL of the trypan blue-culture medium was transferred to an automated cell counting slide. An automated cell counter was then used to count the cells.Upon achieving 90% cell confluence, 1 x 10^6 cells were plated in 35 mm diameter x 10 mm height cell culture dishes in 1640 RPMI containing 10% FBS, 2 mM L-glutamine and 1% (w/v) Pen-Strep.

3.2. Monocytes to macrophages differentiation

3.2.1. Principle of the method

The process of monocyte to macrophage differentiation involves both morphological and biochemical changes so that the differentiated cells can exhibit the properties and functions of the macrophages (Wallner *et al*., 2016). The reason for differentiating monocytes to macrophages is to study the response of macrophages following stimulation. Macrophages play a crucial role in the immune response. They are terminally differentiated and non-dividing cells (Gordon and Taylor, 2005). For *in vitro* studies, macrophages are derived from monocytes. Monocytes-derived macrophages can proliferate *in vitro* and are long-lived. They also develop into specialised functions (Daigneault *et al.*, 2010). Common inducers of macrophage differentiation are mentioned in **Chapter 2 Section 2.6**. In the current study, PMA was used to induce U937 monocytes differentiation to macrophages. The choice for using PMA was based on the findings from previous studies, where PMA was used successfully to differentiate U937 monocytes to macrophages (Mendoza-Coronel and Castañón-Arreola, 2016; Passmore *et al*., 2001). A total of three replicates were included.

3.2.2. Method

Monocyte differentiation was achieved by exposing the U937 monocytes (1 x 10^6 cells/mL) to PMA (Sigma-Aldrich, USA) at the final concentration of 100 ng/mL dissolved in absolute ethanol. This final concentration was based on the previous findings of Yang *et al. (2017)* who, in their study, induced differentiation of U937 monocytes to macrophages using the same concentration (Yang *et al.,* 2017). Although other compounds including tetradecanoyil-13-phorbol acetate (TPA), dimethyl sulfoxide (DMSO), zinc (Zn^{2+}), low concentration of glutamine and IFN-Y can induce monocyte to macrophage differentiation, PMA has been shown to induce monocytes differentiation with high efficiency (Pagliara *et al*., 2005; Passmore *et al*., 2001). Subsequent to PMA exposure, the cells were incubated for 24 hrs at 37°C in a

humidified atmosphere with 5% CO_2 to allow the monocytes to fully differentiate to macrophages.

3.3. Confirmation of monocytes to macrophage differentiation

3.3.1. Microscope imaging

3.3.1.1. Principle of the method

Cellular activities that occur at a molecular level are reflected in the phenotype. The relationship between the molecular system state of a cell and its phenotype can thus be evaluated using microscopic analysis (Antony *et al*., 2013). Microscopic imaging of live cells reveals the information about the cellular structures, cellular dynamics and function (Frigault *et al*., 2009). These features can be observed in real-time and over a period of time, without necessarily changing the nature of the cell (Thorn, 2016). This imaging assessment is crucial for studying and understanding cellular differentiation (Loo *et al*., 2009; Watmuff *et al*., 2012; Zaretsky *et al*., 2012). Thus, in the current study, a light microscope was used to evaluate the morphology of U937 cells supplemented with or without PMA for 24 hrs. A total of three replicates were included.

3.3.1.2. Method

Monocyte to macrophage differentiation was first confirmed by performing the microscopic analysis of the U937 cells' morphology. In this experiment, the morphology of the U937 monocytic cells treated with PMA was compared with the morphology of the U937 monocytic cells that were not exposed to PMA. This was done to assess if there were any observable differences. The assessment was performed by treating $1x10^6$ cells with PMA. The cells were then incubated for 24 hrs. At the end of the incubation period, the treated cells along with the control cells (untreated) were viewed on a Zeiss Axiovert 25 Phase Inverted light microscope using 40X magnification. Following the visual assessment of the cells under the microscope, cellular micrographs were acquired using AxioVision 3.1 for further evaluation.

3.3.2. Flow cytometry

3.3.2.1. Principle of the method

Changes in the physical properties of a cell such as size and granularity as well as molecular properties such as ribonucleic acid (RNA) and deoxyribonucleic acid (DNA) content, gene expression, extracellular and intracellular receptors can all be quantified through flow

cytometry measurements (Betters, 2015). The basic principle of flow cytometry involves the measurement of the intensity of fluorescence which depends on the properties of the cells under investigation. The properties to be quantified are preselected using relevant flow cytometry dyes or monoclonal antibodies that are specific for either extracellular molecules or intracellular molecules of interest, depending on the staining procedure followed (Adan *et al*., 2017). The components of a flow cytometer consist of fluidics, optics, electronics and a computer interface. The fluidic stream separates fluorochrome labelled cells into droplets each with a single cell (Betters, 2015; Jaye *et al.,* 2012). The optical system consists of the light sources (laser of a specific wavelength), optical filters and mirrors that selectively direct the emitted wavelengths to the relevant detector. The electronics component consists of the photomultiplier tubes (PMTs) that generate electrical signals. The generated signal is then represented graphically, simultaneously as the forward scatter (FSC) on the x-axis and the side scatter (SSC) on the y-axis. FSC represents cell size while SSC represents granularity (Betters, 2015; Knijnenburg *et al.,* 2011).

3.3.2.2. Method

Following the morphology evaluation, monocyte differentiation was quantified with a flow cytometry experiment by measuring the CD14 cell count. This experiment was carried out by first setting up an equal number of 35 mm diameter x 10 mm height cell culture dishes for positive and negative controls in triplicates. In each cell culture dish, 7 x 10^6 cells/mL were plated in 1640 RPMI medium supplemented with 200 mM LG, 10% FBS and 1% (w/v) Pen-Strep. Cells used as a positive control were treated with 100 ng/mL PMA dissolved in absolute ethanol (Sigma-Aldrich, USA). Control cells were only treated with 4 µL of absolute ethanol (Sigma-Aldrich, USA). These cells were then incubated for 24 hrs. After the incubation period, cells were scraped from each culture dish with a rubber scraper before transferring into 15 mL Falcon tubes. Cells were centrifuged at 500 *xg* for 10 min at room temperature and the supernatant was discarded. The cell pellets were resuspended in 1 mL of RPMI supplemented with 10% FBS. Cell count was performed using the trypan blue staining on an automated cell counter. For each condition, 1 x 10^6 cells/mL was added to a 96-well plate in triplicate. The RPMI medium was removed through centrifugation at 500 x*g* for 5 min at room temperature. Following the removal of the supernatant, cells were suspended and washed with 1x phosphate buffered saline (PBS), which was removed by centrifugation at 500 x*g* for 5 min at room temperature.

Subsequently, the cell pellets were resuspended in 50 µL of a blocking solution made of 10% heat-inactivated human serum diluted in PBS and incubated for 1 min. The blocking solution, as the name implies, blocks the non-specific binding of the Fc receptors of the antibodies to prevent unintended antibody binding, which could lead to background fluorescence and subsequently, incorrect results (Andersen *et al*., 2016). The cells were then incubated for 1 min at room temperature in the dark and then centrifuged at 500 x*g* for 5 min at room

temperature. The supernatant was discarded before adding a 50 µL fixation solution made of 1,5 % paraformaldehyde (Sigma-Aldrich, St Loius, MO) in PBS to the pellets. Fixation is performed to preserve the cell structure and organelles (Viryasova *et al*., 2019). The resuspended pellets were incubated at room temperature for 30 min before the next round of centrifugation at 500 x*g* for 5 min at room temperature. After the supernatant was discarded, the pellet was resuspended in a 150 µL permeabilisation solution made of 0.2% Triton X in PBS. The permeabilisation solution partially destructs both cell and nuclear membrane. The significance of permeabilisation is to allow the antibodies to penetrate the cell for staining purposes (Viryasova *et al*., 2019). The mixture of the permeabilisation solution and the pellets was incubated for 15 min at room temperature. At the end of the incubation period, the suspended pellets were centrifuged at 800 x*g* for 8 min at room temperature. The supernatant was discarded leaving the pellets in the 96-well plate. All centrifugation steps were performed at room temperature.

For CD14 labelling, the cell pellets were stained with primary and secondary antibodies. The primary antibody was anti-human CD14 immunoglobulin G2a (IgG2a) (Santa Cruz Biotechnology, Dallas, TX). The primary antibody solution was prepared by diluting 5 µL of anti-human IgG2a stock in 45 µL of 1% (w/v) bovine serum albumin (BSA)/PBS solution. The secondary antibody was a fluorescein isothiocyanate (FITC)-conjugated goat anti-mouse IgG2a (Santa Cruz Biotechnology, Dallas, TX) secondary antibody. The solution of secondary antibody was prepared by diluting 1 µL of FITC-conjugated goat anti-mouse IgG2a stock with 49 µL of 1% (w/v) BSA/PBS. The first step of CD14 labelling was performed by adding 50 µL of the primary antibody solution to the 96-well plate with the cell pellets and incubated for 30 min at room temperature in the dark. Following the incubation period, 100 µL of the wash buffer (0.1% Triton X in PBS) was added to each well. The mixture was centrifuged at 800 x*g* for 8 min at room temperature. After discarding the supernatant, another 100 µL of the wash buffer was added to each well and another round of centrifugation was performed at 800 x*g* for 8 min. The supernatant was discarded. The pellets were resuspended in 50 µL of the secondary antibody before incubation for 30 min at room temperature in the dark. The samples were washed with 100 µL of the wash buffer and centrifuged for 8 min at 800 x*g* at room temperature after which the supernatant was discarded. Another 100 µL of the wash buffer was added to each well. Again, the suspended pellets were centrifuged at 800 x*g* for 8 min at room temperature and the supernatant was discarded.

For flow cytometry analysis, the pellets were resuspended in a 150 µL BSA/PBS solution. The resuspended cell pellets were transferred to the flow cytometry tubes. Another 150 µL BSA/PBS was added to the tubes to top up the solutions to a total volume of 300 µL solution in each of the flow cytometry tubes. The fluorescence of each sample was quantified within 2 hrs on a BD FACS ARIA II flow cytometer (BD Bioscience) at an excitation wavelength of 406 nm and emission of 450 nm (BD FACSDiva™ Software 6.1.3). A total of three replicates were included for flow cytometry analysis.

3.4. In vitro U937 stimulation with Pam_3CSK_4 and $1,25(OH)_2D_3$ supplementation

3.4.1. Principle of the method

Pam_3CSK_4 is an agonist of TLR2/1 receptor that simulates bacterial stimulation and immunomodulatory effects towards bacterial lipoproteins (Aliprantis *et al.,* 1999; Akira *et al*, 2003). Pam_3CSK_4 also mimics the triacylated lipoprotein of mycobacteria (Yang *et al.,* 2015). It is, therefore, expected that Pam_3CSK_4 will have an immunomodulatory effect similar to that induced by mycobacteria. It is for this reason that U937 macrophages were stimulated with Pam_3CSK_4 in the current study. The mechanism through which Pam_3CSK_4 induces the immune response is explained in detail in **Chapter 2 Section 2.2**. Briefly, the binding and activation of TLR2/1 by Pam_3CSK_4 induce the expression of NF-kB. Subsequently, NF-kB expression favours the production of cytokines including TNF-α, IL-6 and IL-12. Furthermore, TLR2/1 activation initiates endocytosis of Pam_3CSK_4–TLR 2/1 complex via the activation of α1β1 integrin receptor. As a result, the concerned immune cell secretes IL-6 and type 1 interferon to signal neighbouring cells about the infection of the first cell.

3.4.2. Method

The following experiments were set up according to **Figure 3.1**. This includes the treatment of the U937 differentiated macrophages with or without Pam_3CSK_4 and supplementation with or without $1,25(OH)_2D_3$ for 12 hrs, 16 hrs and 24 hrs.

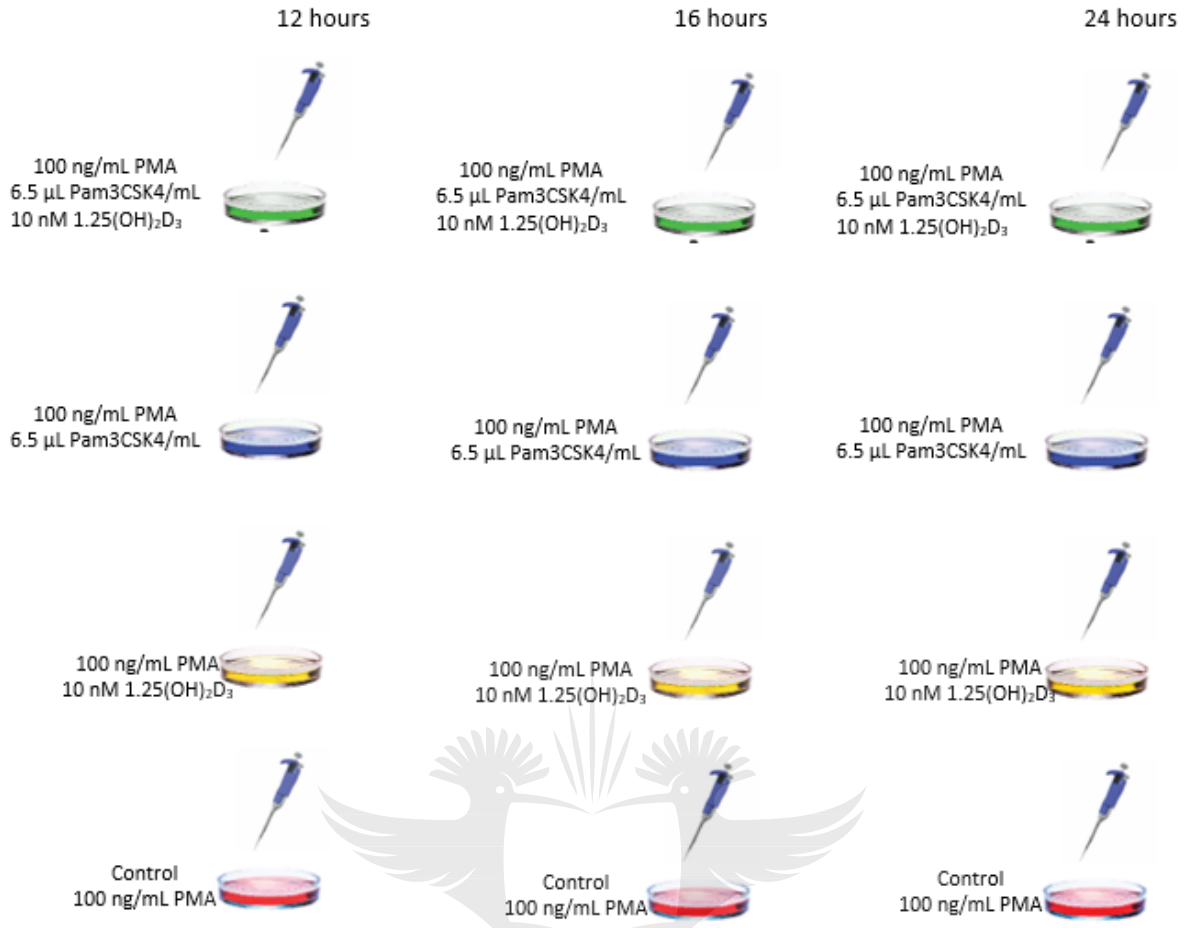

Figure 3.1: Experimental set up for differentiated U937 treatment.
The U937 monocytes were first differentiated to macrophages with 100 ng/mL PMA for 24 hrs before stimulation with or without 6.5 µL Pam_3CSK_4. The cells were then supplemented with/without $1,25(OH)_2D_3$ for 12 hrs, 16 hrs or 24 hrs.

As illustrated in **Figure 3.1**, Pam_3CSK_4 (EMC microcollections, Tuebingen, Germany) reconstituted in endotoxin-free water was used to stimulate the TLR2/1 of the macrophages. A final concentration of 6.5 µg Pam3CSK4/mL was used based on the findings of Meyer (2015), a previous PhD student from the same research group, who used this concentration to stimulate the immune response of the peripheral blood mononuclear cells (PBMCs). This was an optimal concentration after a series of Pam_3CSK_4 concentrations were evaluated. As per **Figure 3.1**, 1 x 10^6 U937 cells induced with 100 ng/mL PMA were stimulated with 6.5 µg Pam_3CSK_4/mL in triplicates for 12 hrs, 16 hrs and 24 hrs. In several studies, Pam_3CSK_4 was able to effectively induce the immune response in a 24 h incubation period. For instance, Weir and colleagues (2017) stimulated the expression of cell surface receptors in B cells with Pam_3CSK_4 at a 24 hrs incubation period. Additionally, in their study, Al-Rashed *et al*. (2017) were also able to induce matrix metalloproteinase (MMP-9) in human monocytic THP-1 cells at 24 hrs. Based on the above-mentioned studies, 24 hrs was one of the chosen time points for the current study as there is enough evidence showing that Pam_3CSK_4 can induce immune response at this time point. Regardless of these findings, it has also been found that Pam_3CSK_4

can stimulate cells earlier than 24 hrs. In a study by Hellman *et al.* (2018), PBMCs were stimulated with Pam_3CSK_4 in a 12 hrs incubation. A 12 hrs incubation period was therefore also selected. Moreover, Lee *et al*. (2014), was able to stimulate BC2 cells at a 16 hrs incubation. Based on these studies, 3 incubation periods (12, 16, and 24 hrs) were used in the present study. Performing the experiment at three different time points was crucial in determining the effect of time in each experimental condition evaluated.

3.5. U937 macrophages supplementation with $1,25(OH)_2D_3$

$1,25(OH)_2D_3$ is an important hormone with the ability to stimulate the immune response of the macrophages. To study the effect of $1,25(OH)_2D_3$ in U937 macrophages, U937 cells stimulation with/without 6.5 µg Pam_3CSK_4/mL were supplemented with/without 10 nM $1,25(OH)_2D_3$ (Sigma Aldrich, St Louis, MO). The choice of using the final concentration of 10 nM $1,25(OH)_2D_3$ was based on published literature (Edfeldt *et al.* (2010); Liu *et al.* (2006); Liu *et al*. (2009)). In these studies, it was shown that 10 nM $1,25(OH)_2D_3$ is sufficient to effectively induce the expression of VDR genes and thus increase VDR levels. Following $1,25(OH)_2D_3$ the cells were incubated for 12 hrs, 16 hrs, and 24 hrs. At the end of each incubation period, the cells were prepared to study the metabolic effect of the aforementioned treatments on the cells. The treated cells were quenched for metabolic analysis as explained in the following section.

3.6. Cell quenching

3.6.1. Principle of the method

It is crucial that the metabolic profile acquired in a metabolomic study is a true representation of the metabolism or metabolic profile of a cell at the time of metabolite extraction. Such can be achieved by quenching the cells before extracting the metabolites. Quenching is the process in which the metabolism of a cell is terminated by stopping all the cellular enzymatic activities to prevent undesired changes in composition and concentration of the metabolites to be extracted (De Koning and Van Dam, 1992; Faijes *et al*., 2007). Although several quenching methods have been published in the literature, only a few are efficient and highly reproducible. A good quenching method can be characterised by the following: (1) the ability to completely terminate and block cellular metabolism immediately when the quenching process is initiated; (2) not disruptive to the cellular membrane to prevent the leakage of intracellular metabolites; (3) ability to prevent the contamination of the sample of interest with undesired extracellular metabolites, and lastly (4) it should yield a metabolic profile that is a true representation of the cells' physiology. Thus, it should not interfere with the metabolism of the cell (Bort *et al*., 2014; Cuperlovic-Culf *et al*., 2010).

3.6.2. Method

For the NMR-based metabolomics approach, quenching was performed using liquid nitrogen. The advantage of using this quenching method lies in the fact that samples are frozen below −100°C, which allows an immediate termination of the metabolic processes. Liquid nitrogen allows quenching to be performed within a few seconds in a one-step procedure (Sellick *et al*., 2011). Quenching was performed after the specified incubation periods (12 hrs, 16 hrs and 24 hrs) were reached. Cells in culture dishes were gently scraped and transferred into 15 mL falcon tubes and the tubes were centrifuged for 1 min at 1000 x*g* at −20°C to remove the growth medium. After discarding the supernatant, the cells (pellets) were snap-frozen in liquid nitrogen (−196°C) once. The cells were then stored below -100°C. The frozen cells were allowed to thaw prior to the metabolite extraction.

3.7. Intracellular metabolite extraction

3.7.1. Principle of the NMR method

Metabolite extraction is a critical pre-analytical step in metabolomics workflow, aiming to collect (often in a solution form) metabolites of interest from a biological system or matrix. The ideal metabolite extraction process should and would lead to a wide coverage of the metabolome under investigation (Lu *et al*., 2017). A successful metabolite extraction step is necessary in for metabolomics analysis as it drastically influences the outcomes of the experiment. Despite the ability of NMR spectroscopy to measure metabolites in the whole-cell without extraction, more informative and quantitative measurements can only be achieved from the extracted metabolites (Cuperlović-Culf *et al*., 2010). Nonetheless, metabolite extraction remains challenging as there is no single extraction method that can extract all metabolites of a specimen. A single extraction method can only cover a group of metabolites with similar properties, e.g. polar *vs*. nonpolar, fatty acids or amino acids (Pinu *et al*., 2017; Cuperlović-Culf *et al*., 2010). To overcome this challenge, a combination of extraction methods is usually used to extract the largest number of metabolites from the specimen. For liquid-based extraction methods, common extraction solvents used include chloroform/methanol (De Koning and van Dam, 1992), cold methanol (De Jonge *et al.,* 2012), hot water (Bolten *et al*., 2007) and methanol/water (Sellick *et al*., 2011), among others. In the current study, cold methanol/water extraction method was used for intracellular metabolite extraction according to the extraction method developed by Sellick *et al*. (2011), with minor modification. The combination of cold methanol and water has been shown to recover the maximum number and a large range of metabolites from suspension mammalian cells (Cao *et al*., 2011; Sellick *et al*., 2011; Shin *et al*., 2010). Keeping the sample temperature lower by using cold extraction solvents minimizes variability and achieves optimal stability of most metabolites between samples (Kostidis *et al*., 2017).

3.7.2. Method

Following cell quenching, the cell pellets were resuspended in 500 µL of 100% methanol at −80°C, transferred to a microcentrifuge tube (tube 1) and snap-frozen in liquid nitrogen. The use of 100% methanol at −80°C further ensures that no enzymatic reaction or metabolic processes occur during extraction. The frozen cells were thawed and vortexed for 30 s prior to a cycle of centrifugation at 800 x*g* for 1 min at room temperature. The resulting supernatant was pooled into a fresh microcentrifuge tube (tube 2) on cold ice. The cell pellet in tube 1 was resuspended in 500 µL of 100% methanol (−80°C), snap-frozen in liquid nitrogen, thawed and vortexed for 30 s. Again, contents in tube 1 were pelleted by centrifugation at 800 x*g* for 1 min at room temperature and the supernatant was pooled into tube 2 on cold ice. The cell pellet in tube 1 was resuspended in 250 µL of Milli-Q water, snap-frozen in liquid nitrogen, thawed and vortexed for 30 s. The cells were pelleted by centrifugation at 15000 x*g* for 1 min at room temperature. The supernatant was pooled into tube 2 so that the final ratio of methanol to water in tube 2 was 1:0.25. The solution in tube 2 was centrifuged at 15000 x*g* for 1 min at room temperature and the supernatant, pooled into a fresh tube (tube 3) was dried in a centrifugal evaporator at 30°C for 2 hrs. The dried metabolite pellets were stored at −80°C until NMR spectroscopic analysis.

3.8. NMR data acquisition

3.8.1. Principle of the method

The basis of NMR spectroscopy involves measuring the magnetic properties of the atomic nuclei that have different magnetic spins (protons) such as ^{1}Hydrogen (^{1}H) and ^{13}Carbon (^{13}C). A detailed principle of NMR spectroscopy is given in **Chapter 2 Section 2.5.6**. Briefly, during the NMR spectroscopy measurements, the sample of interest is placed in a magnetic field. Subsequently, the nuclei of each molecule will either align with or against the magnetic field. As the radio frequency energy is applied, only NMR-active nuclei will resonate, each at a unique, characteristic frequency. These frequencies are given as chemical shifts on the NMR spectrum relative to a reference signal (Antcliffe and Gordon, 2016; Howard, 1998; Wilson and Walker, 2010). ^{1}H is the most abundant nucleus in almost all metabolites as compared to ^{13}C and ^{31}P nuclei, making ^{1}H easily visible by the NMR.

3.8.2. Method

In this study, all one dimensional (1D) ^{1}H NMR spectra were acquired using TOPSPIN 3.2 (Bruker, Biospin Germany) at 25°C on a Bruker Avance III 500 MHz NMR spectrometer (University of Johannesburg, Department of chemistry) operating at 500.13 MHz. The NMR

spectrometer was equipped with a double resonance broadband (BBI) probe. A 1D nuclear overhauser effect spectroscopy (NOESY)-presaturation sequence was used for water and solvent suppression. All 1D NOESY were acquired at 25°C with an acquisition time of 1.64 s, mixing time of 0.05 s, relaxation delay of 2 s and 128 scans collected with receiver gain of 203 dB and a spectral width of 10 000 Hz (20 ppm). The obtained spectra were baseline corrected and phased. The corrected spectra were referenced to the signal of TSP at δ 0.00 ppm and α-glucose at δ 5.23 ppm. All processed spectra were subjected to AMIX-viewer 3.9.15 (Bruker Biospin, Germany) for segmentation into bins with an equal width of 0.04 ppm. The water region (δ 4.4-5.5 ppm) was excluded as this region potentially interferes with low molecular weight metabolite regions on the NMR spectrum. The final binned data file was exported into a Microsoft Excel file 2013.

3.9. Chemometric and multivariate data analysis

3.9.1. Principle of the method

In untargeted metabolomics studies, sample analyses generate complex and multivariate data, which requires advanced statistical and chemometrics methodologies to meaningfully handle and mine these obtained (information-rich) datasets. Both univariate and multivariate data statistical methods are often applied, enabling the extraction of relevant, meaningful information from these highly complex data with aim of providing biological knowledge on the question under investigation (Saccenti *et al.,* 2014). When only one variable is statistically analyzed at a time, a so-called univariate statistical method is performed. The application of univariate statistical tests and analyses in a metabolomics context implies testing hundreds of metabolites, which subsequently requires imperatively correcting for multiple tests to avoid or minimize having false positives. A reflection on univariate statistical methods in metabolomics can be found in the cited literature herein (Saccenti, *et al*., 2014). It is worth noting that these univariate methods, such as *t*-test or ANOVA, allow to statistically assess one single variable (metabolite), which could contain biological information and description on the phenomenon under study (Saccenti *et al*., 2014; Vargason *et al.,* 2017).

On the other hand, MVDA, as discussed in **Chapter 2 Section 2.5.11**, is used to handle multivariate data generated in metabolomics data acquisition. MVDA methods are capable of examining multiple variables simultaneously to reveal the inherent structures and biological information contained in these multiple variables (Mengual-Macenlle *et al*., 2014). MVDA methodologies determine and quantify the relationships between variables, contained in the measured variation and expressed as covariation and/or correlation (Shiker, 2012). MVDA models are thus computed, capturing a fraction of this variation, with a certain level of prediction. The information contained in these models is then presented visually in the form of plots/graphs. In the current study, PCA, an unsupervised MDVA method, was used for

dimensionality reduction and data exploration. Such exploratory methods reveal data structures, pointing to (dis)similarities between and within sample groups, and highlighting thus sample clusters, trends and outliers (Biancolillo and Marini, 2018). To complement MVDA methods and extract more detailed information, a supervised MVDA method, OPLS-DA, was applied. For more description on PCA and OPLS-DA, refer to **Chapter 2 Section 2.5.11**. Prior to constructing the MVDA models, data pre-treatments (e.g. sample and variable normalization and missing value imputation) are applied. Furthermore, in computing these multivariate models, tuning and validation procedures are mandatorily applied to ensure statistical significance, reliability and validity of the generated models (Westad and Marini, 2015). Such validation procedures include permutation tests and CV. As mentioned in **Chapter 2 Section 2.5.12**, the basis of CV involves the decomposition of the data matrix into validation and training subsets, and through different iterations, evaluating performance estimates, model bias and predictability (Trivedi and Iles, 2012).

3.9.2. Method

The AMIX-processed data (excel file) was exported to Soft Independent Modeling of Class Analogy (SIMCA) software package, version 15 (Umetrics, Sweden) for univariate and MVDA. The data was pareto scaled before computing PCA models. The strong outliers were assessed using the Hotelling's T^2 ellipse at a 95% confidence interval on a PCA scores scatter plot. Furthermore, moderate outliers were detected using distance to the model (DModX). The generated PCA models were tuned and validated by the 7-fold CV method. This was achieved by generating the squared Pearson correlation coefficient goodness of fit (R^2) and predictive ability (Q^2) values.

In order to maximize and observe separations between the study groups, OPLS-DA modelling was performed. This is a supervised modelling which can be used to identify discriminant variables responsible for the separation between two classes, which can be useful for biomarker identification. The significance of each generated OPLS-DA model was assessed by generating the CV-ANOVA value for each model where a *p*-value of <0.05 represents a statistically good model. From the constructed OPLS-DA models, a loadings S-plot and variable importance plot (VIP) were generated to identify variables discriminating the study classes. Loadings S-plot is an S-shaped plot of modelled covariation and correlation, allowing to extract variables (metabolites) with high covariation (i.e. high magnitude) and high correlation (i.e. high reliability). These discriminating variables are thus visually found at the extreme ends of the loadings S-plot. A VIP scoring is a metric that summarizes the importance of each variable in driving the observed class separation. Variables with VIP values above 1 contribute more than average to the model, i.e. the observed group separation/classification. The fold change (equivalent to the relative concentration) for each variable was also generated. Fold change values above 1 indicates an increase in the relative concentration while fold change below 1 indicate a decrease in relative concentration.

3.10. Metabolite annotation

The identity of the metabolites associated with the variables differentiating the study groups, according to the loadings S-plot, were assigned using the chemical shift (ppm) values. These assignments were done using the Human Metabolome Database (HMDB) (http://www.hmdb.ca/) and relevant published literature (Subramani *et al.,* 2016; Govindaraju *et al*., 2000; Mickiewicz *et al.*, 2014).

3.11. Gas chromatography-mass spectrometry data acquisition

Following the analysis of the ^{1}H NMR data, it was found that the metabolic profiling of cells treated for 12 hrs yielded more potential signatory metabolites discriminating the study groups (which are, Pam_3CSK_4 stimulated cells, $1,25(OH)_2D_3$ treated cells and cells supplemented with Pam_3CSK_4/$1,25(OH)_2D_3$). For the GC-MS analysis, the 12 hrs incubation was used as the time point for the analysis. The same protocols for U937 monocyte cell culture (**Section 3.2.2**), monocyte differentiation (**Section 3.3.2**), differentiation confirmation (**Section 3.4**), and *in vitro* U937 stimulation with Pam_3CSK_4 and $1,25(OH)_2D_3$ supplementation (**Section 3.5.2** and **3.6**) were used prior to GC-MS analysis.

3.11.1. Sample preparation and quenching

The principle of quenching has already been mentioned in **Section 3.7.1**. At the end of a 12 hrs incubation period, the RPMI growth medium was removed by spinning the cells at 1000 x*g* for 1 min at room temperature. After discarding the supernatant (RPMI growth medium), the cells were washed twice with 2 mL ice-cold PBS (pH 7.4). Cells were washed by spinning the cells in PBS at 1000 x*g* for 1 min at room temperature. The resulting cell pellet was resuspended in 750 µL high performance liquid chromatography (HPLC) grade methanol (Sigma-Aldrich, St. Louis, MO). The mixture was then transferred into 2 ml Eppendorf safe-lock tubes and the samples were stored at −80°C until analysis at the Centre for Human Metabolomics at the North West University. The samples were delivered in dry ice.

3.11.2. Metabolite extraction

For the whole metabolome extraction, a single-phase extraction method proposed by Beukes *et al*. (2019) was applied to the experimental samples (1,5 million cells in 750 µL methanol), quality control (QC) sample aliquots and extraction blanks (750 µL methanol). A 50 µL internal standard (3-phenylbutyric acid), 250 µL chloroform, 250 µL H_2O and a 3mm tungsten beads were added to each sample vial. The samples were then shaken in a vibration mill at 30 Hz for

5 min and centrifuged at 14 650 *xg* for 5 min. The supernatant was then transferred into a GC vial and dried under a gentle stream of nitrogen at 40°C for 20 min. Subsequently, 50 µL methoxyamine hydrogen chloride was added and the mixture was incubated at 50°C for 90 min. This was then followed by the addition of 40 µL N,O-bis(trimethylsilyl)trifluoroacetamide (BSTFA) (Sigma Aldrich, St. Louis, MO, USA) and 1% trimethylchlorosilane (TMCS) (Sigma Aldrich, St. Louis, MO, USA) to the vial. The vial was re-incubated at 60°C for 60 min. The extracts were then transferred to a 0.25 mL insert in a GC sample vial for analysis using GCxGC-TOFMS.

3.11.3. GCxGC-TOFMS analysis

3.11.3.1. Principle of the method

Detailed principle of GC-MS is given in **Chapter 2 (Section 2.5.8)**. GC separates volatile and semi-volatile compounds in a mixture under high temperatures. The separated compounds, referred to as analytes, are then detected using MS. Before the GC-MS analysis, samples are dissolved in solvents such as acetone, methanol or heptane. The mixture is then injected to the GC, where it is vaporized under high temperature. The vaporized molecules are carried through the column by a carrier gas such as helium, hydrogen, nitrogen or argon (Sneddon *et al*., 2007; AL-Bukhaiti *et al*., 2017; Hussain and Maqbool, 2014). The vaporized analytes separate based on their differential affinity to the stationary phase coated on the column. The separated, vaporized analytes are then passed on to the mass spectrometer, where they are ionized. The formed ions are sorted in the mass analyzer and separated based on the mass to charge ratio. The separated ions are then detected by the ion detector in the MS, which produces electrical signals. The signals are represented in a histogram called mass spectrum as a function of m/z and relative abundance on the x-axis and y-axis, respectively (Murayama *et al*., 2009; Patel *et al*., 2012). In the current study, two-dimensional gas chromatography (GC×GC) coupled with time-of-flight mass spectrometry (TOFMS) was used for metabolic profiling. In GCxGC-TOFMS, sample separation is achieved using two separate GC columns (GCxGC) with different polarity of the stationary phase (Kalinova *et al*., 2006; Spanik *et al*., 2012). The separated compounds in a sample mixture are subsequently carried to the TOFMS for detection. ToF-MS can detect up to 500 spectra s^{-1} (Kalinova *et al*., 2006; Rocha *et al*., 2007). The detected compounds are represented in a mass spectrum.

3.11.3.2. Method

The GCxGC-TOFMS analysis was performed on a Pegasus 4D GCxGC-TOFMS (Leco Corporation, St. Joseph, MI, USA), using an Agilent 7890A GC (Agilent, Atlanta, GA) coupled to a time of flight mass spectrometer (Leco Corporation, St. Joseph, MI, USA) equipped with

a Gerstel Multi-Purpose Sampler (MPS) (Gerstel GmbH & co. KG, Eberhard-Gerstel- Platz 1, D-45473 Mülheim an der Ruhr), equipped with a cryogenic cooler. The primary column was fused with Rxi-5Sil-MS phase. The length of the column was 30 m with an internal diameter of 0,25 mm with the film thickness of 0,25 µm. The secondary column was fused with the Rxi-17 phase. The column was 1,400 m long with the internal diameter of 0,25 mm and the film thickness of 0,25 µm. Both columns were supplied by Restek (Bellafonte, PA, USA). The inlet was operated in a split ratio of 1:10 at 270°C with an injection volume of 1µl (derivatized sample). Helium (He) was used as a carrier gas at a constant flow of 1 mL/min. The temperature of the primary GC oven was initially programmed at 70°C for 2 min after which it was gradually increased at 4°C/min to a final temperature of 300°C, where it was maintained for 2 min. The temperature of the secondary GC oven was initially programmed at 85°C for 2 min. The temperature was then increased at 4.5°C/min to a final temperature of 300°C with a 4.5 min hold. The modulator was programmed to have an initial temperature of 100°C for 2 min. The temperature was then increased by 4°C/min to a final temperature of 310°C with a 12 min hold. The effluent emerging from the primary column onto the secondary column was controlled using cryomodulation and a hot pulse of nitrogen gas of 0.5 s every 3 s. For TOFMS, sample ionization was performed using electron ionization with 70 eV. The ion source temperature was kept constant at 200°C while the transfer line temperature was held at 270°C. The m/z was between 50–800 at an acquisition rate of 200 spectra/second after a 350 s solvent delay. The detector voltage was programmed at 150 V offset.

3.11.4. Peak identification and data matrix creation

Peak identification and mass spectral deconvolution were performed using Leco Corporation ChromaTOF software (version 4.50) at an S/N ratio of 100, with a minimum of 3 apexing peaks. Peak identification was achieved using a level 3 identification according to Schymanski *et al*. (2014). The mass fragmentation patterns together with their respective GC retention times as generated by the MS were used to determine the identities of the peaks by comparing it to in-house and commercially available National Institute of Standards and Technology (NIST) spectral libraries (mainlib, replib).

3.11.5. MVDA analysis

Following peak alignment from the ChromaTOF software, peaks identified in the blank samples (system blanks and extraction blanks) were deleted from the dataset as these were considered to be contaminants. Compound areas were then normalised according to the total useful signal detected for each sample. The resulting dataset was subjected to MetaboAnalyst 4.0 (https://www.metaboanalyst.ca/) for statistical analyses. The data was pareto scaled before analysis. Univariate statistics (student's t-test and volcano plot) were used to identify features

that vary significantly between cells stimulated with Pam_3CSK_4, Pam_3CSK_4/1,25$(OH)_2D_3$ supplemented cells and control cells (untreated). Furthermore, multivariate methods, PCA, PLS-DA and OPLS-DS were performed to extract more biologically meaningful information from the data. PCA was applied to reduce the dimensionality of the data and for data exploration. In addition, OPLS-DA was applied for binary classification analyses.

3.12. Pathway analysis

The annotated signatory metabolites from ^{1}H NMR spectroscopy and GCxGC-TOFMS analysis were subjected to MetaboAnalyst version 4.0 (https://www.metaboanalyst.ca/) for metabolic pathway analysis. MetaboAnalyst allows the identification of metabolic pathways associated with the given metabolites. These are the metabolic pathways that are altered under the given conditions. Metabolic pathways were selected based on the level of significance with $p<0.05$ considered to be significant. These metabolic pathways contain most of the identified metabolites.

CHAPTER 4

RESULTS

The results generated in the study are presented in the current chapter. The first section (**Section 4.1**.) presents the results of U937 cellular differentiation. This section is divided into two sub-sections which consist of the results of the microscopic assessment of differentiated cells (**Section 4.1.1**) and flow cytometry-based measurement of surface maker differentiated cells (**Section 4.1.2**). The succeeding section (**section 4.2**) presents the results of the metabolic profiling of U937 macrophages stimulated with Pam_3CSK_4, $1,25(OH)_2D_3$ supplementation and a combination of both Pam_3CSK_4 and $1,25(OH)_2D_3$. This section is also divided into two sub-sections: Nuclear magnetic resonance (NMR) spectroscopy-based metabolic profiling (**Section 4.2.1**) and gas chromatography–mass spectrometry (GC-MS) based metabolic profiling (**Section 4.2.2**). The metabolic pathways associated with signatory metabolites identified in metabolic profiling are presented in **Section 4.3.,** which is the last section of **Chapter 4**.

4.1. Phorbol myristate acetate-induced cellular differentiation assessment

4.1.1. Microscopic assessments of differentiated U937 cellular morphology

The confirmation of PMA-induced monocytes to macrophage cellular differentiation was first performed by assessing the morphology of the U937 cells supplemented with or without 100 ng/mL PMA for 24 hrs. The aim of this experiment was to evaluate if there are morphological differences between U937 cells cultured in the presence and absence of PMA. At the end of the incubation period (24 hrs), the morphological changes of the cells were examined using an inverted light microscope under 40X magnification. Cells cultured in the absence of PMA (**Figure 4.1A**) were shiny and round in shape with smooth edges, a typical morphology of U937 monocytic cells (Shu *et al.,* 2013; Zamani *et al.,* 2013). On the contrary, PMA-treated cells (**Figure 4.1B**) showed a differential irregular cellular shape, with an elongation, rough edges and pseudopods. This PMA-induced cellular shape resembles an adhesion morphology of macrophages (Marcuello *et al*., 2018; McWhortera *et al*., 2013; Zamani *et al.,* 2013).

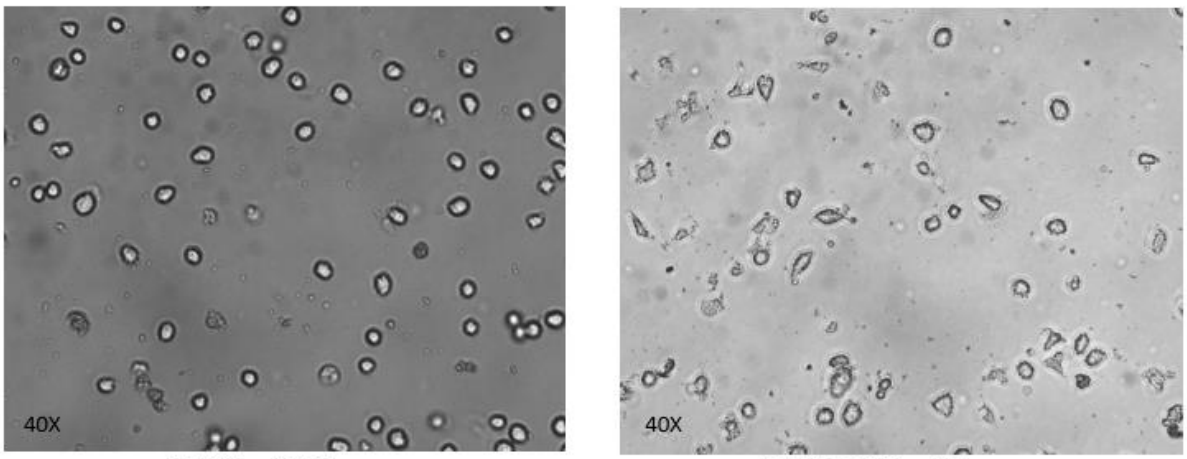

A. Without PMA. B. With PMA for 24 hrs.

Figure 4.1: Cellular morphology assessment under the microscope: Micrographs of U937 cells supplemented without (A) or with PMA (B) for 24-hrs treatment. The micrographs show the differences in the morphology of cells between the two conditions. In the absence of PMA, cells are round in shape and have smooth edges. On the contrary, PMA supplemented cells have uneven, irregular shape with rough edges. Cells were viewed under 40X magnification on a Zeiss Axiovert 25 Phase Inverted light microscope before the micrographs were acquired using AxioVision 3.1.

4.1.2. Flow cytometry analysis of CD14 surface markers of the monocyte/macrophage cell populations

Cellular differentiation of monocytes to macrophages was also evaluated by measuring the level of the expressed surface marker CD14 on the U937 cells, following a 24 hrs incubation in the presence or the absence of 100 ng/mL PMA. Cells were stained with anti-human IgG2a primary antibody and a FITC-conjugated goat anti-mouse IgG2a secondary antibody. The flow cytometry analysis enabled the observation of whether treatment of U937 cells with PMA induced the expression of CD14 surface marker — a maker of monocyte to macrophage differentiation. **Figure 4.2A** illustrates the forward scatter (FSC-A) and the side scatter (SSC-A) properties of the cell population. The FSC-A and SSC-A measure the size and granularity or density of the cell. The gate P1 on **Figure 4.2B** represents the U937 cells that abundantly expressed CD14 surface markers. The gate P1 confirms that the majority of the U937 cells in the measured population expressed CD14 cells. The quantification of CD14 count between PMA-treated and the control (untreated) cells showed that PMA-supplemented cells expressed a high-levels of CD14 as compared to the control cells (**Figure 4.3**). PMA supplementation significantly increased the intensity of CD14 ($p< 0.001$).

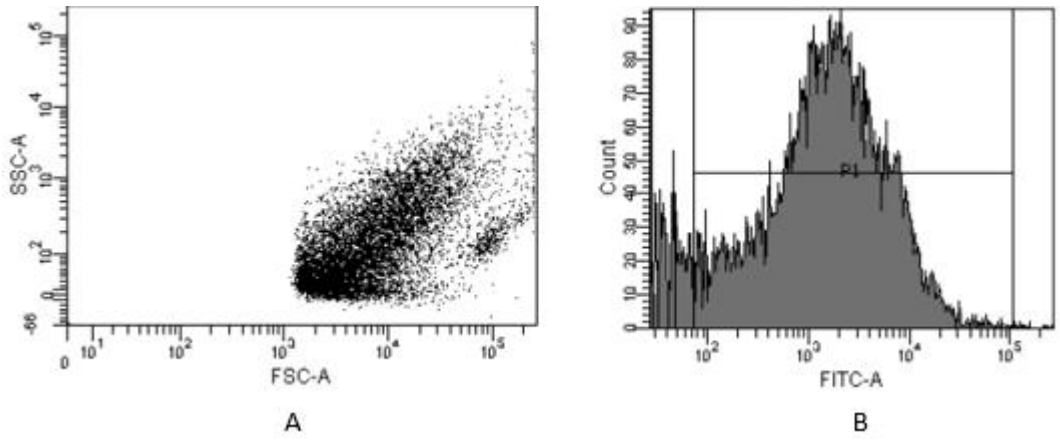

Figure 4.2: Flow cytometry analysis of monocyte-macrophage CD14 count. (A) A **dot plot** provides the forward scatter (FSC-A) which is the measure of the size of cells and the side scatter (SSC-A), the granularity or density of the cell. (B) A **histogram** of CD14 labelled monocyte-macrophage cell populations. Gate P1 is the CD14 expressing cells labelled with antibody fluorochrome, FITC-A.

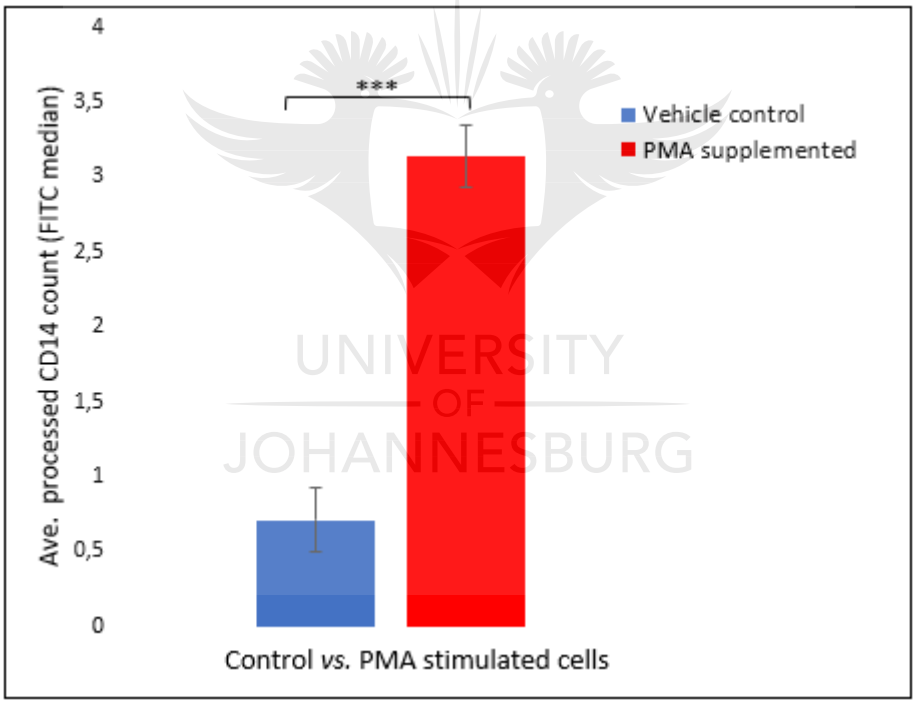

Figure 4.3: Flow cytometry CD14 count. CD14 count of U937 cells supplemented with 100 ng/mL PMA *vs*. control cells incubated for 24 hrs. Each error bar represents the standard deviation. The two groups show statistically significant differences in CD414 counts, with $p<0.001$ ***.

4.2. Multiplatform metabolic profiling of U937 macrophages treated with Pam_3CSK_4, $1,25(OH)_2D_3$ and a combination of both Pam_3CSK_4 and $1,25(OH)_2D_3$

To decode metabolic reprogramming induced by Pam_3CSK_4 stimulation, $1,25(OH)_2D_3$ supplementation and a combination of both Pam_3CSK_4/$1,25(OH)_2D_3$ treatment in differentiated U937 cells, NMR spectroscopy and GC-MS platforms were used in an

untargeted approach. For NMR spectroscopy analysis, proton (^{1}H) NMR spectroscopy was used to detect the extracted metabolites. In addition to ^{1}H NMR spectroscopy, GCxGC–TOFMS was used as a complimentary technique to expand the metabolome coverage. The results of these metabolic analyses are presented in the following sub-sections: **Section 4.2.1** for NMR spectroscopy analysis and **Section 4.2.2** for GC-MS-based metabolic profiling.

4.2.1. NMR-based metabolic profiling of U937 cells treated with Pam_3CSK_4, $1,25(OH)_2D_3$ and a combination of both Pam_3CSK_4 and $1,25(OH)_2D_3$

The extracted metabolites of cells treated with Pam_3CSK_4, $1,25(OH)_2D_3$, a combination of both Pam_3CSK_4 and $1,25(OH)_2D_3$, as well as that of untreated cells, were analysed using ^{1}H NMR spectroscopy. To monitor the changes over time, the treated cells were incubated for 12 (**Figure 4.4**), 16 (**Figure A1**) and 24 hrs (**Figure A2**). Visually, treatment-related differences in the overlaid spectra were observed (**Figure 4.4**) and these included the presence or absence of peaks and changes in peak intensities. Furthermore, to adequately extract information from these spectral data, chemometrics methods were applied. Unsupervised modelling, particularly PCA, was applied for dimensionality reduction and data exploration. Furthermore, the supervised OPLS-DA was carried out for binary classification analyses.

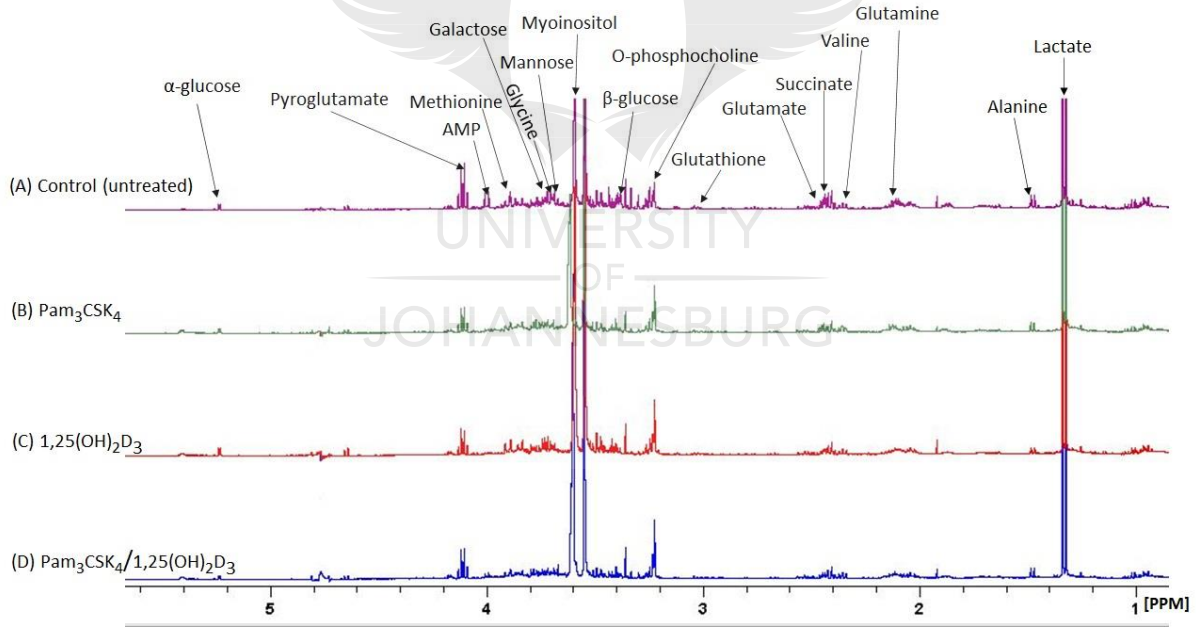

Figure 4.4: Representative overlaid ^{1}H NMR spectra acquired using a 500 MHz Bruker NMR spectrometer (12-hrs treatment). The spectra represent the metabolic profiling of (A) **control cells (untreated)**, (B) **Pam_3CSK_4 stimulated cells**, (C) **$1,25(OH)_2D_3$** treated cells and (D) **$Pam_3CSK_4/1,25(OH)_2D_3$ supplemented cells**. The labelled peaks are signatory metabolites identified from the Human Metabolome Database (HMDB) (http://www.hmdb.ca/) and relevant published literature (Govindaraju *et al*., 2000; Mickiewicz *et al*., 2014; Subramani *et al*., 2016). All spectra were referenced to TSP at δ 0.0 ppm and α-glucose at δ 5.53 ppm. $1,25(OH)_2D_3$: 1,25-dihydroxyvitamin D_3; AMP: Adenosine monophosphate.

4.2.1.1. PCA-based data exploration: Hidden internal data structures and sample groupings

PCA revealed the between-group and within-group variation, the trend and outliers as depicted in **Figures 4.5, Figure A3** and **A4**. Using the first two principal components, treatment-related sample grouping of control (untreated) cells, Pam_3CSK_4 and $1,25(OH)_2D_3$ treated cells can be evidently seen in scores space, even though there is some sample overlap (**Figures 4.5A, A3A** and **4A**). Furthermore, Hotelling's T^2 at 95% confidence level was used to detect strong outliers; and there were no strong outliers, i.e. there is no observation that is found outside the ellipse of scores scatter plots (**Figures 4.5A, A3A** and **4A**). Distance to the model (DModX) was also computed to visually assess moderate outliers. The latter are observations with a value greater than the critical value denoted DCrit (0.05) (red dotted line) on the DModX infographics (**Figure 4.5B** and **Figure A3B** and **A4B** for 12, 16, and 24 hrs treatment, respectively); however, these outliers had no variable(s) with critical deviation from the rest of the dataset, hence they were retained. To further investigate the sample grouping revealed by PCA modelling, a supervised binary classification, OPLS-DA, was applied, as presented in the following section.

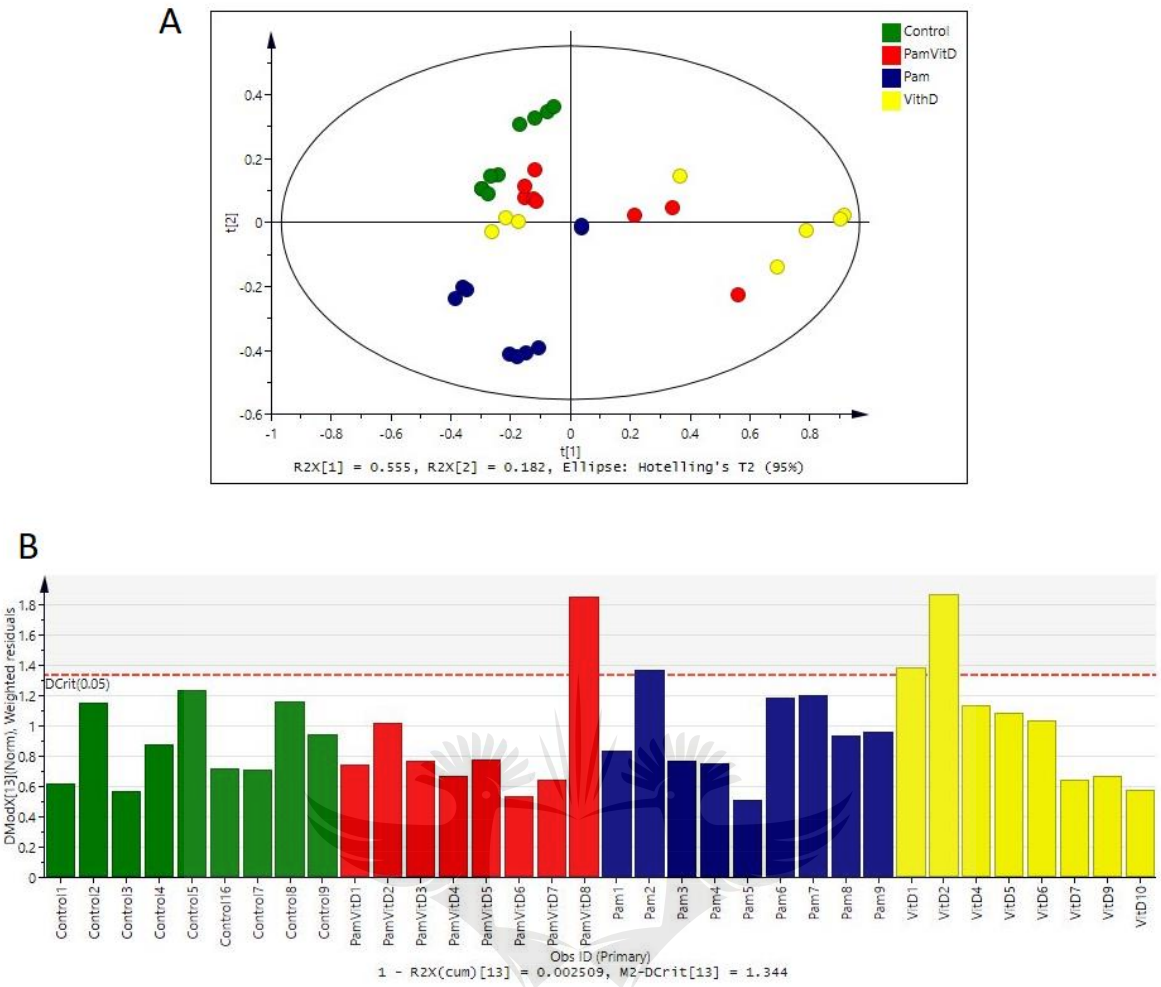

Figure 4.5: PCA modelling. (A) **PCA scores scatter plot** showing sample grouping of control cells (untreated), Pam (Pam_3CSK_4), VitD ($1.25(OH)_2D_3$), and Pam_3CSK_4/Vit D (Pam_3CSK_4/$1.25(OH)_2D_3$) treated cells without any strong outliers as per Hotelling's T^2 (95% confidence level). Component t[1] shows the between-groups variation and t[2] shows the within-group variation. The description of the computed PCA model are R^2= 0.997, Q^2= 0.969, components = 13. (B) **DModX** shows four moderate outliers with DModX values greater than critical value, DCrit (0.05) (red dotted line).

4.2.1.2. Sample classification and variable selection — OPLS-DA modelling

Supervised multivariate modelling, OPLS-DA, was performed to maximize the separation between the sample classes. This OPLS-DA binary classification and sample discrimination modelling allow for the extraction of more detailed and descriptive information from the dataset. Different OPLS-DA models were thus computed investigating the following classes: the control cells *vs*. Pam_3CSK_4 (**Figure 4.6A**), control cells *vs*. $1,25(OH)_2D_3$ (**Figure 4.6C**), and control cells *vs*. Pam_3CSK_4/$1,25(OH)_2D_3$ (**Figure 4.6E**) for 12 hrs treatment. The OPLS-DA modelling infographs for the 16 and 24 hrs treatment is given in **Figure A5 and A6, respectively.** A clear separation was observed between the aforementioned classes, indicating that there were differences in the metabolome of the experimental groups

compared. A seven-fold CV procedure was applied as a tuning method in building the models; and the quality of each OPLS-DA model was assessed by inspecting R^2X (the explained variation of the X variable by the model) and R^2Y (the explained variation of the Y variable by the model), as well as the predictive ability of the model, Q^2. Generally, the metrics Q^2 with a minimum value of 0.05 (50%) and R^2 close to 1 are desirable as indicative of valid models (Triba *et al*., 2015). However, in practice, it is not possible to set a general limit for good predictability (Q^2) since this strongly depends on the properties of the dataset, such as the number of observations included. Q^2 of 0.04 (40%) or below can be accepted and have been published (Cai *et al*., 2012; Dong *et al*., 2013). Such models with poor predictability are further validated by other methods such as a permutation test. In this study, in addition to *k*-fold CV metrics (R^2 and Q^2), permutation tests were applied and the statistical reliability of the models was assessed using cross validated-analysis of variance (CV-ANOVA) by generating the probability (*p*) value with a cut-off value of $p<0.05$, which indicates a statistically significant model. All models met these validation requirements.

For the selection of discriminant variables responsible for class separation, the OPLS-DA loadings S-plot for each model were generated and evaluated (**Figure 4.6B, 4.6D and 4.6F**, respectively). The discriminant variables are those located at the extreme ends of the S-plot (bottom left and top right). These are the variables that are significantly different between the classes. Such variables have a high correlation and covariation in a multivariate space and have a $p<0.05$. The selected variables were annotated by using the Human Metabolome Database (HMDB) (http://www.hmdb.ca/) and relevant published literature (Govindaraju *et al*., 2000; Mickiewicz *et al*., 2014; Subramani *et al*., 2016). The confidence in metabolite annotation was level 2, as classified by the current metrics of the Metabolomics Standard Initiative (MSI) (Sumner *et al.,* 2007). The selected and annotated potential signatory metabolites are thus tabulated in **Table 4.1.**

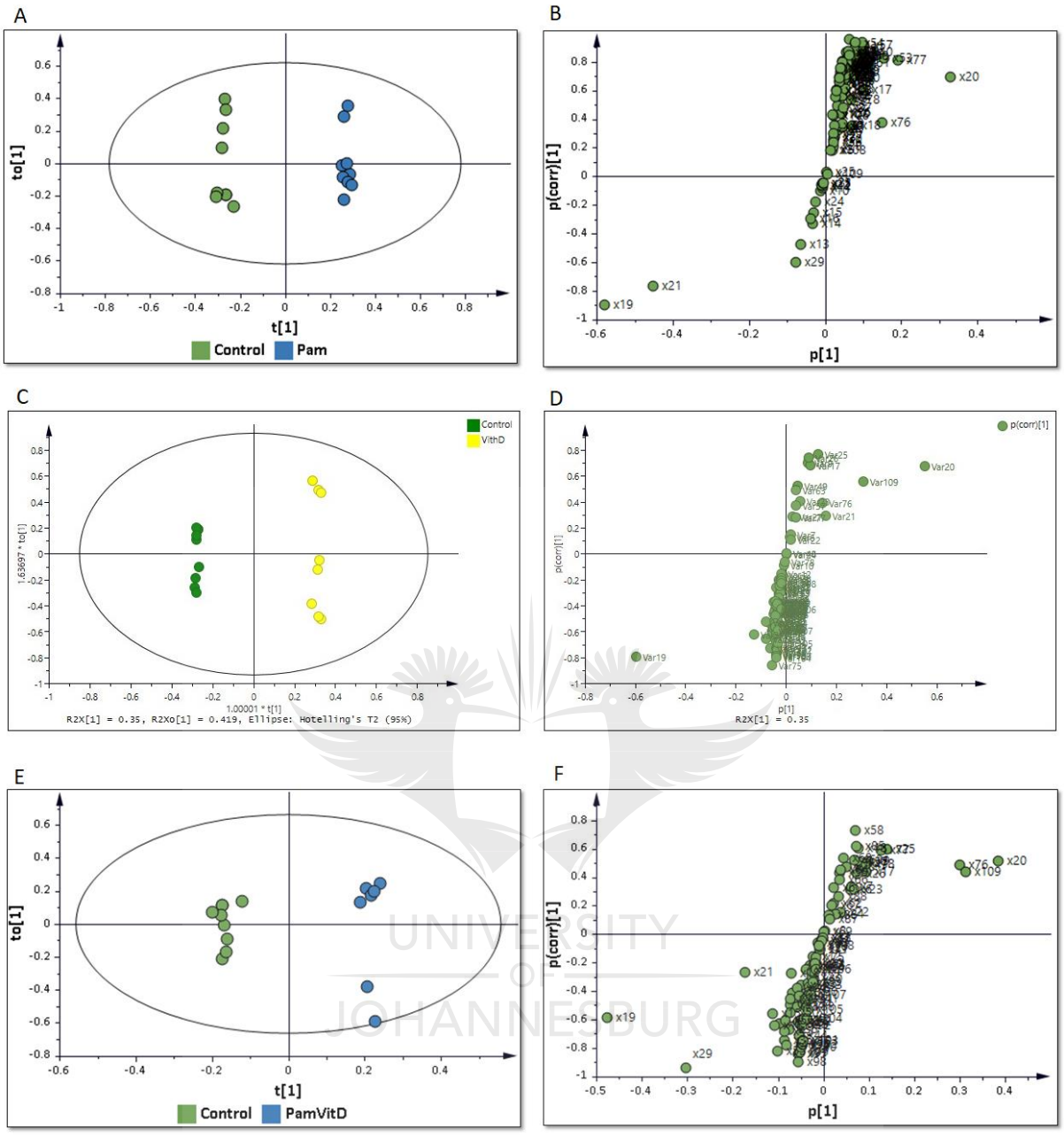

Figure 4.6: OPLS-DA modelling and variable selection. An OPLS-DA model separating control cells *vs*. Pam_3CSK_4 (1+4+0 components, $R^2X = 0.989$, $R^2Y = 0.995$, $Q^2 = 0.99$, CV-ANOVA *p*-value = 4.87×10^{-8}) (**A**) the **scores scatter plot** of t1 *vs*. t1o, a window in the X space displaying the separation of the two classes in horizontal (t1) direction; and orthogonal variation or within-class variability (i.e., unrelated to the discrimination between the two classes) is expressed in the vertical (to[1]) direction. (**B**) the **loading S-plot**, a predictive component loading, which displays discriminant variables – the variables that are situated in the extreme ends of the loadings S-plot are statistically relevant and represent prime candidates as discriminating variables. **(C)** An **OPLS-DA scores scatter plot** separating the control cells *vs*. VitD ($1,25(OH)_2D_3$) supplemented cells (Components: 1+5+0, $R^2X = 0.993$, $R^2Y = 0.998$, $Q^2 = 0.99$, CV-ANOVA *p*-value = 4.1535×10^{-06}); and **(D)** the **loading S-plot** displaying discriminant variables. **(E)** An **OPLS-DA scores scatter plot** and **(F)** the **loading S-plot** of Control *vs*. $Pam_3CSK_4/1,25(OH)_2D_3$. A clear separation can be seen between the two classes (1+3+0 components, $R^2X = 0.848$, $R^2Y = 0.991$, $Q^2 = 0.975$, CV-ANOVA *p*-value = 8.41×10^{-6}).

Table 4.1: OPLS-DA-derived signatory metabolites discriminating between controls (untreated) and cells treated with Pam_3CSK_4, $1,25(OH)_2D_3$ and a combination of both Pam_3CSK_4 and $1,25(OH)_2D_3$ detected using ^1H NMR spectroscopy.

		12 hrs						16 hrs						24 hrs					
PPM	**Metabolite**	**Pam_3CSK_4**		**$1,25(OH)_2D_3$**		**Pam_3CSK_4/ $1,25(OH)_2D_3$**		**Pam_3CSK_4**		**$1,25(OH)_2D_3$**		**Pam_3CSK_4/ $1,25(OH)_2D_3$**		**Pam_3CSK_4**		**$1,25(OH)_2D_3$**		**Pam_3CSK_4/ $1,25(OH)_2D_3$**	
		Fold change	***p*-value**	**Fold change**	***p*-value**	**Fold change**	***p*-value**	**Fold change**	**p-value**	**Fold change**	**p-value**	**Fold change**	**p-value**	**Fold change**	**p-value**	**Fold change**	**p-value**	**Fold change**	**p-value**
3.85	Methionine	0.899	0.049	—	—	0.891	0.006	—	—	—	—	0.813	0.003	—	—	0.871	0.166	—	—
3.69	Galactose	1.190	0.008	—	—	1.109	0.100	—	—	0.916	0.379	0.840	0.018	0.728	0.024	0.788	0.013	0.786	0.030
3.61	Myoinositol	0.612	4.15×10^{-7}	0.459	0.0001	0.802	0.017	0.677	0.235	1.021	0.923	0.902	0.738	1.331	0.262	1.311	0.295	1.214	0.410
3.57	Threonine/ glycine	2	0.001	4.351	0.003	1.879	0.047	1.480	0.265	1.171	0.499	1.377	0.473	0.687	0.251	0.863	0.653	0.623	0.235
3.53	Beta-glucose	0.807	0.0002	1.070	0.248	0.962	0.340	0.993	0.803	0.987	0.881	1.159	0.089	0.959	0.433	1.078	0.237	0.915	0.195
3.21	o-Phosphocholine	0.920	0.009	0.744	0.008	0.604	7.13×10^{-8}	0.914	0.342	0.762	0.016	0.828	0.049	1.084	0.666	0.886	0.479	—	—
2.25	Valine	2.463	2.04×10^{-5}	—	—	—	—	—	—	—	—	—	—	1.394	0.289	—	—	—	—
1.33	Lactate	1.143	0.117	1.144	0.118	—	—	1.045	0.444	0.957	0.397	0.912	0.209	1.061	0.461	1.004	0.963	1.339	0.006
3.65	Mannose	—	—	1.419	0.0003	1.290	0.011	1.162	0.011	—	—	0.741	0.033	1.203	0.158	—	—	—	—
3.41	Taurine	—	—	—	—	—	—	—	—	0.883	0.243	—	—	0.772	0.002	0.800	0.002	0.841	0.007
4.01	Adenosine monophosphate (AMP)	—	—	—	—	1.310	0.042	1.210	0.070	1.142	0.006	—	—	1.375	0.006	—	—	1.262	0.056
3.77	Ornithine/ glycerol	—	—	—	—	0.863	0.021	—	—	—	—	0.788	0.0008	—	—	—	—	—	—
2.41	Succinate	—	—	—	—	1.123	0.051	—	—	0.889	0.161	—	—	—	—	0.838	0.003	—	—
3.97	Tyrosine/ Phenylalanine	—	—	—	—	—	—	—	—	—	—	—	—	1.374	0.024	—	—	—	—
2.45	Glutamate	—	—	—	—	1.111	0.013	—	—	—	—	—	—	—	—	0.834	0.002	—	—
0.97	Leucine	—	—	—	—	—	—	—	—	—	—	—	—	—	—	0.875	0.006	—	—
4.17	Pyroglutamate	—	—	—	—	0.748	0.008	—	—	—	—	—	—	—	—	—	—	—	—
2.97	Glutathione	—	—	—	—	0.747	0.001	—	—	—	—	—	—	—	—	—	—	—	—
2.53	Beta-Alanine	—	—	—	—	0.850	0.0004	—	—	—	—	—	—	—	—	—	—	—	—
2.17	Glutamine	—	—	—	—	0.817	9.82×10^{-5}	—	—	—	—	—	—	—	—	—	—	—	—

As it can be seen in **Table 4.1** and depicted in **Figure 4.7,** the discriminatory metabolites, which are biologically potential markers for the specific treatment in consideration, were up- or down-regulated. Furthermore, these metabolites were either unique to a treatment or overlapped. Their relative concentrations differ between the 12, 16 and 24 hrs treatment, indicating the changes in metabolic activities of the treated cells overtime. The identified discriminatory metabolites are members of different chemical classes including amino acids, carbohydrates, organic compounds and antioxidants.

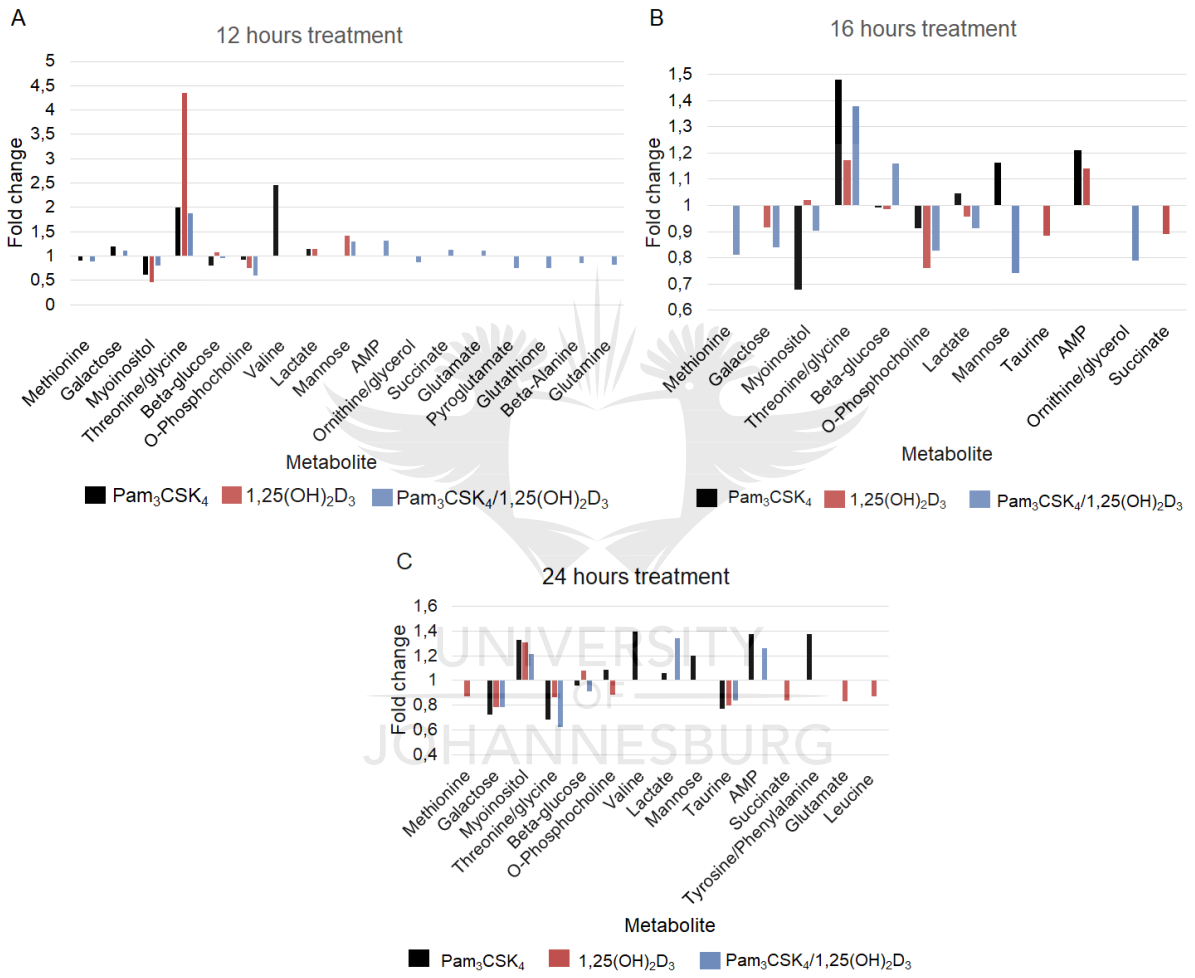

Figure 4.7: Graphical representation of potential signatory metabolites differentiating Pam_3CSK_4 stimulation, $1,25(OH)_2D_3$ treatment and $Pam_3CSK_4/1,25(OH)_2D_3$ supplementation at three time points. Figure 4.7 A, B and C show the signatory metabolites resulting from the metabolic profiling of the treated U937 cells treated for 12-, 16- and 24 hrs. Fold change value above 1 represents an increase in the relative concentration of metabolite whereas fold change value below 1 represents a decrease in the relative concentration of metabolite.

4.2.2. GS-MS–mass spectrometry based metabolic profiling of U937 cells treated with Pam_3CSK_4, $1,25(OH)_2D_3$ and a combination of both Pam_3CSK_4 and $1,25(OH)_2D_3$

For GCxGC-TOFMS metabolic profiling, U937 differentiated cells treated with Pam_3CSK_4 or a combination of both Pam_3CSK_4 and $1,25(OH)_2D_3$ were incubated for 12 hrs only. The choice of incubating the treated cells for 12 hrs was motivated by the ^1H NMR spectroscopy analysis results. Meaning, in the ^1H NMR spectroscopy analysis, more potential signatory metabolites were identified from the metabolic profiling of cells incubated for 12 hrs in comparison to 16 and 24 hrs (**Figure 4.7**). Data generated from GCxGC-TOFMS metabolic profiling was subjected to both univariate and multivariate data analysis. For univariate statistical analysis, student's t-test was performed to determine the features (metabolites) that are significantly different between control cells *vs*. Pam_3CSK_4; and control cells *vs.* $Pam_3CSK_4/1,25(OH)_2D_3$ (**Figure 4.8**). Furthermore, volcano plots of control *vs*. Pam_3CSK_4; and that of control cells *vs.* $Pam_3CSK_4/1,25(OH)_2D_3$ (**Figure A7A** and **A7B**, respectively) were generated to identify significant features (metabolites) discriminating the aforementioned groups. Significant features that are highly altered between the groups are those located far from the origin of the volcano plot at the far right or left. These metabolites, together with their fold changes and *p*-value are tabulated in **Table 4.2**.

Thereafter multivariate methods, PCA, PLS-DA and OPLS-DA modelling were performed. PCA was performed to explore the internal structure of the GCxGC-TOFMS spectral data. The between-group and within-group variation was also revealed (**Figure A8**). To further extract descriptive information from the dataset, PLS-DA (**Figure A9**) was performed for sample classification and discrimination between the aforementioned groups. The generated PLS-DA scores models of both control cells *vs*. Pam_3CSK_4 (**Figure A9A**); and control cells *vs.* $Pam_3CSK_4/1,25(OH)_2D_3$ (**Figure A9B**) were not at all predictive, as indicated by a low or negative predictivity (Q^2) value. Hence, OPLS-DA modelling was performed to maximize separation between classes. The generated OPLS-DA scores models (**Figure A11A and A11B**) were also not predictive. The OPLS-DA models were further validated using a permutation test. However, the predictivity of each model remained as a negative value, showing that the models are not predictive. Therefore, the only features (metabolites) that were considered to be significant from PLS-DA VIP scores (**Figure A10**) and OPLS-DA loadings S-plot (**Figure A11C and 11D**) are those that were identified by univariate statistics (**Figure 4.8** (Generated from box plot) and **Table 4.2** (generated from volcano plot)).

4.2.2.1. Boxplot representing the relative abundance of metabolites between control cells vs. Pam_3CSK_4 stimulated cells and control cells vs. $Pam_3CSK_4/1,25(OH)_2D_3$ supplemented cells

GCxGC-TOFMS detected metabolites that are significantly altered between control cells *vs*. Pam_3CSK_4 stimulated cells, and control cells *vs.* $Pam_3CSK_4/1,25(OH)_2D_3$ supplemented cells as determined by the student's t-test are shown in **Figure 4.8**. The box plots show the distribution of the potential marker metabolite between the aforementioned groups. These metabolites belong to chemical classes including fatty acids, amino acids, organic and inorganic compounds.

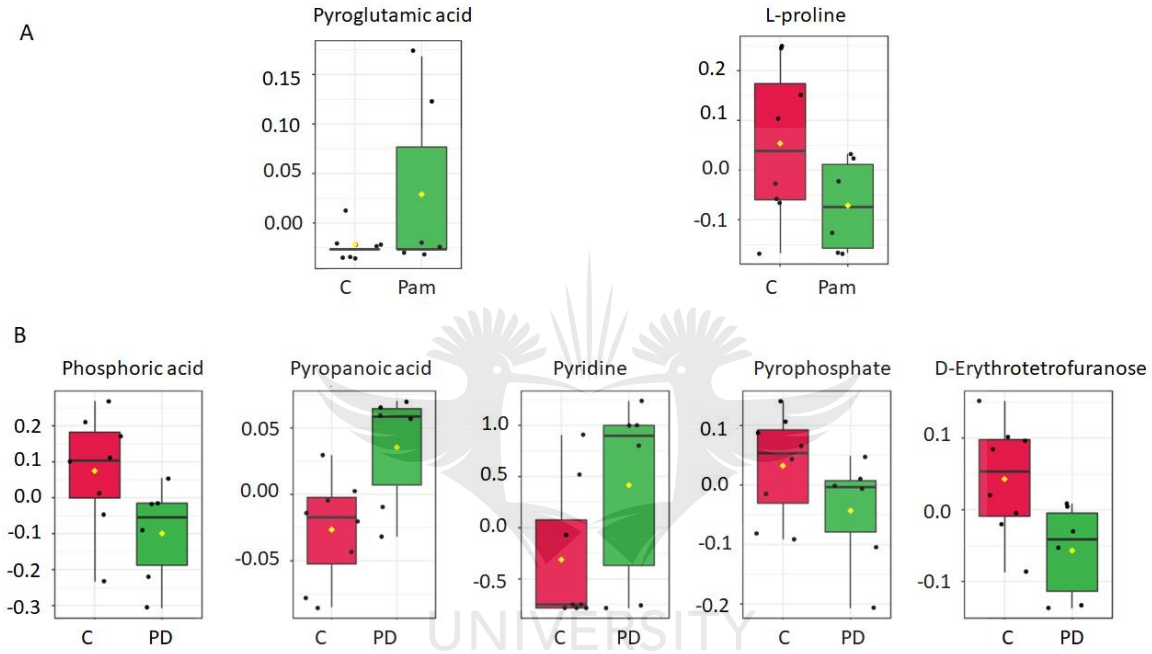

Figure 4.8: Box plots of significant metabolites identified by t-test. These are metabolites that significantly contribute to the variance between (A) **control cells *vs*. Pam_3CSK_4** stimulated cells, and (B) **control cells *vs*. $Pam_3CSK_4/1,25(OH)_2D_3$** supplemented cells. The relative concentrations of these metabolites differ significantly between the experimental groups. Abbreviations: C: Control; PAM: Pam_3CSK_4; PD: $Pam_3CSK_4/1,25(OH)_2D_3$.

Table 4.2: Signatory metabolites discriminating U937 macrophages cells stimulated with Pam_3CSK_4 and those supplemented with a combination of both Pam_3CSK_4 and $1,25(OH)_2D_3$ detected using GCxGC-TOFMS. These are important metabolites selected by the volcano plot.

Metabolite	Control vs. Pam_3CSK_4		Control vs. $Pam_3CSK_4/1,25(OH)_2D_3$	
	Fold change	***P*-value**	**Fold change**	***P*-value**
Meso-2,5-Dimethyl-3,4-hexanediol	0.054542	2.9986×10^{-5}	0.12252	0.0006246
Taurine	-	-	20.396	0.086935
Niacinamide	11.084	0.027165	-	-
Unknown	-	-	4.7544	0.083741
Unknown	0.34438	0.038087	-	-

4.3. Analysis of metabolic pathways associated with the treatment of differentiated U937 cells with Pam_3CSK_4, $1,25(OH)_2D_3$ and a combination of both Pam_3CSK_4 and $1,25(OH)_2D_3$

Metabolic pathways associated with signatory metabolites identified from ^1H NMR spectroscopy analysis (12 hrs treatment) and GCxGC-TOFMS analysis are given in **Figure 4.9.** The labelled metabolic pathways are the most significant pathways with the highest hits (the actual number of metabolites matched from the uploaded data) (**Table A1**).

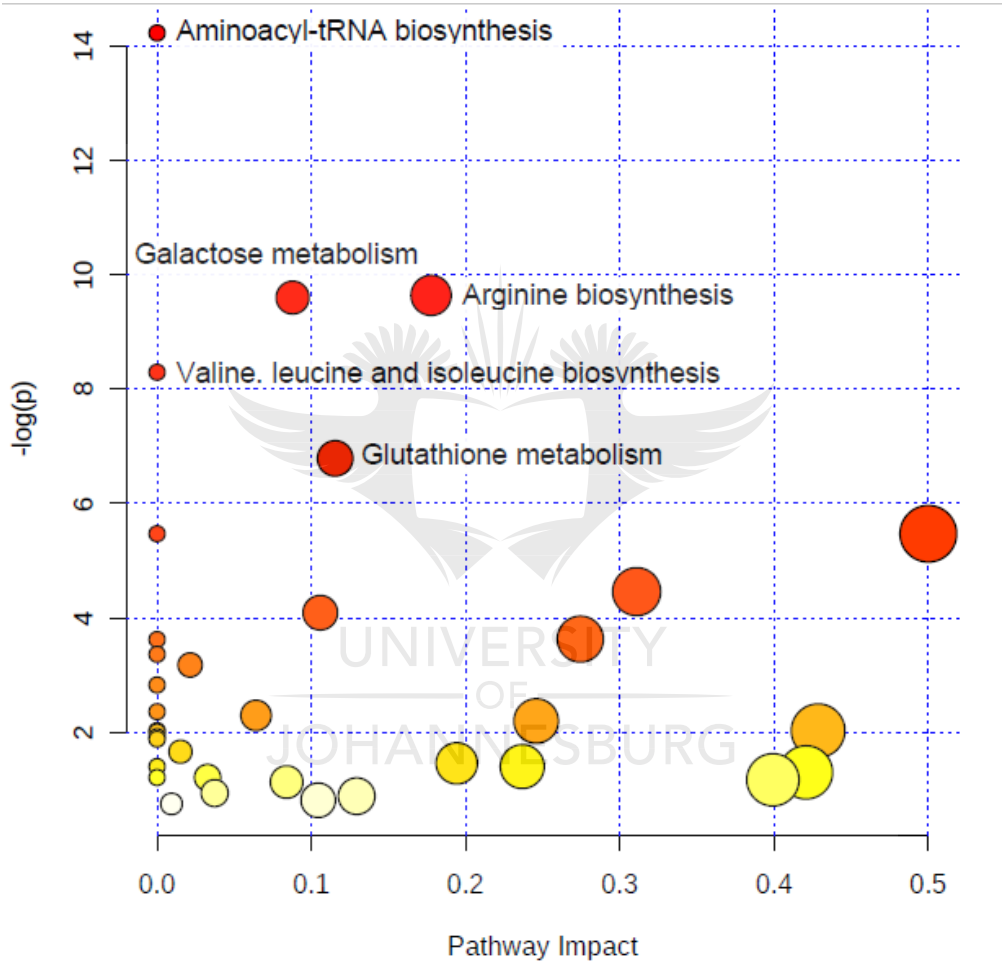

Figure 4.9: Topology analysis of metabolic pathways affected in control cells *vs*. Pam_3CSK_4 stimulated cells; control cells *vs*. and $1,25(OH)_2D_3$, and control cells *vs*. Pam_3CSK_4/$1,25(OH)_2D_3$ supplemented U937 macrophages. The pathway analysis is based on Kyoto Encyclopedia of Genes and Genome (KEGG) and was generated from MetaboAnalsyt 4.0. using metabolites that were significantly altered in the aforementioned study groups. Each circle represents a metabolic pathway. The size and the colour of the cycle reflect the pathway impact and *p*-value, respectively. Pathways with greater pathway impact are represented with bigger cycles. Dark red cycles represent metabolic pathways with a $p < 0.05$ or lower. The significance decrease from dark red to white

Metabolic pathway analysis was performed to identify the metabolic reprogramming induced by U937 macrophage treatment with Pam_3CSK_4, $1,25(OH)_2D_3$ or a combination of both Pam_3CSK_4 and $1,25(OH)_2D_3$. The metabolic pathway analysis gives a snapshot of the metabolism of the U937 macrophages associated with the aforementioned treatment.

In summary, the results clearly illustrate that PMA induced U937 monocytes to macrophage differentiation as determined using macroscopic analysis of U937 cells treated with or without PMA (**Section 4.1.1**). Flow cytometry analysis of CD14 surface markers of the monocyte/macrophage cell populations further confirms that U937 monocytes treated with PMA were differentiated to macrophages (**Section 4.1.2**)**.** Metabolic profiling differentiated cells treated with Pam_3CSK_4, $1,25(OH)_2D_3$ and a combination of both Pam_3CSK_4 and $1,25(OH)_2D_3$ (**Section 4.2**) illustrated that each treatment induced metabolic reprogramming. Metabolic reprogramming was depicted via NMR and GC-MS (**Section 4.2.1** and **4.2.2**, respectively) differential metabolic profiles. The differential metabolic profiles were explained by PCA/OPLS-DA models. Metabolic pathways associated with metabolic reprogramming were also identified (**Section 4.3, Figure 4.9**).

CHAPTER 5

DISCUSSION

Macrophages play a pivotal role in many biological processes including metabolic regulation, maintenance of tissue homeostasis and most importantly, in the immune response. These phagocytic cells are normally the primary regulators in the immune response during infections, including various bacterial infections (De Sousa *et al.,* 2019). For *in vitro* studies on human macrophages, U937 monocytes-derived macrophages are a good model as they resemble the human macrophages in morphology, function, and metabolism (Mendoza-Coronel and Mastanon-Arreola, 2016). As described in **Chapter 2**, the aim of the present study was to evaluate the effects of $1,25(OH)_2D_3$ on the metabolome of U937 macrophage stimulated with Pam_3CSK_4. Experimentally, this metabolic profiling was carried out by applying a multi-platform approach that included NMR and GC-MS-based untargeted analyses (**Chapter 3**). This allowed a wide coverage of the intracellular metabolome.

As presented in **Chapter 4**, applying various statistical analyses and modelling to mine the generated spectral data (from both NMR and GC-MS platforms) allowed the extraction of information that indicated a significant difference in the metabolome of the compared experimental groups (**Figure 4.6A, 4.6C and 4.6E**). From the variable selection (**Figure 4.6B, 4.6D and 4.6F**), the identified discriminating metabolites (explaining group separation) were mapped onto metabolic pathways in an integrative manner, inferring thus significant pathways related to treatment effects. The results (**Chapter 4**) showed that treatment-related reprogramming of (macrophage) cellular metabolism spanned several amino acid pathways including galactose metabolism, arginine biosynthesis, glutathione metabolism, valine, leucine and isoleucine synthesis. This chapter interprets and discusses the obtained results (**Chapter 4**), in reference to the current literature, formulating and drawing relevant knowledge and conclusions regarding the metabolic effect of $1,25(OH)_2D_3$ on U937 macrophage stimulated with Pam_3CSK_4. The chapter is subdivided into three main sections: The results of U937 differentiation are discussed in **Section 5.1**, and the profiling of the U937 macrophage cellular metabolome is discussed in **Sections 5.2–5.3**.

5.1. U937 monocytes to macrophage differentiation

As described in **Chapter 3**, the study was designed to firstly differentiate the U937 monocytes to macrophages. The latter mimics the *in vivo* immune cells responsible for the containment of *M.tb* during infection, providing a good (*in vitro*) model to study metabolomic reprogramming related to cellular immune responses to infection and/or other treatments,

such as $1,25(OH)_2D_3$ in this case. Monocytes-derived macrophages can proliferate in culture and develop specialised functions. Furthermore, responses such as the inhibition of *M.tb* growth by macrophages *in vivo* can be observed in U937 macrophages *in vitro* (Daigneault *et al*., 2010).

PMA is known as an effective inducer of macrophages from monocytes through mechanisms that include the activation of protein kinase C (PKC) (Song *et al*., 2015). In this study, the observed morphological changes in PMA-treated U937 cells (**Figure 4.1B**) evidently suggest that PMA successfully differentiated the U937 monocytes to macrophages. From our observations, PMA-treated cells were elongated, irregular in shape with rough edges and protrusions, which is a typical morphology of macrophages (Marcuello *et al*., 2018; McWhortera *et al*., 2013; Zamani *et al.,* 2013). The morphology of macrophages correlates with their functions including proliferation, apoptosis, nuclear organisation and their phagocytic role in immunity (Rosales and Uribe-Querol, 2017; Versaevel *et al*., 2012). Macrophage elongation results from the uniaxial stretch of the cell (Pugin *et al*., 1998) whereas the cyclic biaxial stretch triggers an increase in the spread cell area (Matheson *et al*., 2006). Both cell elongation and increase in spread cell area were observed in PMA-treated cells (**Figure 4.1B**). Functionally, the significance of such morphology is to form a link/bridge between the bacterial surface and the receptor of the macrophage that recognises the pathogen. Once the link has been established, the macrophage protrusions form a surrounding structure around the bacterial antigen. Subsequently, the antigen is absorbed into a phagosome created by the macrophage (Hirayama *et al*., 2018; Ueno and Wilson, 2012).

As presented in the results chapter (**Section 4.1.1.**), to complement morphological assessments (under a microscope), the differentiation of monocyte to macrophage was further confirmed by measuring CD14 count in both PMA supplemented cells and untreated cells using flow cytometry. The CD14 markers were measured as they are the main differentiation surface markers of myeloid lineage cells (Zamani *et al.,* 2013). CD14 genes are among the macrophage-specific genes. During monocytes/macrophage differentiation, CD14 proteins are abundantly expressed by macrophages (Contreras *et al*., 2015; Lehtonen *et al.,* 2007). The results (**Chapter 4**, **Figure 4.3**) showed that the expression of CD14 was higher in PMA-stimulated cells than in the U937 monocytes cultured in the absence of PMA. These findings are similar to those of Zhang *et al.* (2014), who differentiated THP-1 monocytes to macrophages using PMA, and found a significant increase in the expression of CD14 following cell treatment with PMA. Thus, an increase in CD14 expression is associated with the differentiation of monocytes to macrophages. Macrophages abundantly express CD14 as to detect pathogens during infection. Macrophages sense bacterial lipopolysaccharides through TLR2 and TLR4 to initiate phagocytosis (Anas *et al*., 2010). Both microscopic analyses and flow cytometry CD14 count measurements provided sufficient evidence to confidently confirm that PMA effectively differentiated U937 monocytes to macrophages.

To evaluate the effects of $1,25(OH)_2D_3$ on the metabolome of U937 macrophage stimulated with Pam_3CSK_4, the multi-platform metabolomic analyses of U937 macrophages treated with Pam_3CSK_4, $1,25(OH)_2D_3$, and a combination of Pam_3CSK_4 and $1,25(OH)_2D_3$ was performed. These analyses showed differential changes in various metabolic pathways between the treatment conditions. The changes include an increase or decrease in levels of metabolites in pathways such as galactose metabolism, arginine biosynthesis, glutathione metabolism, valine, leucine and isoleucine biosynthesis as well as aminoacyl-tRNA biosynthesis. Biologically, these pathways are involved in different cellular functions and activities such as energy metabolism, regulation of redox reaction and protein synthesis. Thus, the following sections discuss these metabolic results in relation to biological functions: **Section 5.2** looks at the regulation of energy metabolism and **Section 5.3** discusses the reprogramming of metabolic pathways associated with amino acids.

5.2. Regulation of energy metabolism

The change in galactose metabolism observed in our study is associated with the metabolic reprogramming of energy metabolism. In our study, galactose metabolism was identified as the energy metabolism pathway reprogrammed in Pam_3CSK_4 stimulated cells, and in cells co-treated with Pam_3CSK_4 and $1,25(OH)_2D_3$ (**Chapter 4**, **Table 4.1** and **Figure 4.7**). Galactose metabolism is associated with glycolysis and the Warburg effect, as discussed below. In mycobacterial infection, the reprogramming of the energy metabolism by the host determines survival, the virulence and persistence of *M.tb* in the host. The host usually utilises additional or alternative energy sources to improve energy production for the control of *M.tb* (Cumming *et al*., 2018; Shi *et al.,* 2005).

5.2.1. Galactose metabolism – "The Warburg effect"

The presence of galactose during mycobacterial infection has been extensively described (Gough, 1932; Haworth *et al*., 1948). Galactose is a naturally occurring monosaccharide sugar with a similar chemical formula as glucose. Galactose only differs from glucose in the positioning of the carbon 4 (C4) hydroxyl (OH) group. The C4 OH positioning introduces some chemical and biochemical differences between galactose and glucose (Blackstock *et al.,* 1989). In a mammalian biological system, galactose serves as a source of energy and a substrate for the biosynthesis of several macromolecules (Liu *et al*., 2000). Galactose can be metabolised to glucose-6-phosphate (G6P) which can enter the glycolysis pathway. The conversation of galactose to G6P occurs via the Leloir pathway which was first described by Leloir in 1951. In the first step of the Leloir pathway, galactose is phosphorylated into galactose-1-phosphate (Gal1P) by galactokinase. Following that, Gal1P uridyltransferase catalyses the conversion of UDP-glucose and Gal1P to glucose-1-phosphate (G1P) and UDP-galactose. The resulting G1P is converted to G6P by phosphoglucomutase.

Phosphoglucomutase catalyses the transfer of the phosphate group from C1 to C4 of glucose. G6P serves as a substrate for glycolysis. Cells, however, efficiently take up more glucose than galactose. Furthermore, galactose prevents the net production of ATP via glycolysis (Garedew *et al.,* 2010). Hence, glucose-dependent energy production is preferred over the galactose-dependent pathway.

The UDP-galactose formed in the Leloir pathway can be converted to UDP-glucose by UDP-galactose 4-epimerase. UDP-glucose plays a functional role in the synthesis of glycoconjugates via glycosylation reactions (Guo and Ye, 2010; Moradi *et al*., 2016). Glycosylation is an essential process for secondary protein processing and determines protein functioning (Arey, 2012). In our study, there was no significant difference in the relative concentration of galactose in cells treated with Pam_3CSK_4 only, $1,25(OH)_2D_3$ only or co-treated with Pam_3CSK_4 and $1,25(OH)_2D_3$. The relative concentration of galactose, however, decreased as the incubation period was increased from 12 hrs to 24 hrs. A gradual decrease in the relative concentration of galactose was also observed in the 16 and 24 hrs treatment conditions (**Chapter 4**, **Table 4.1** and **Figure 4.7**). The gradual decline of galactose in the 16 and 24 hrs treatment conditions suggest that galactose was metabolised over time. This gradual decrease is most likely associated with the up-regulation of glycolysis. The possibility of glycolysis up-regulation is supported by the findings obtained in Pam_3CSK_4 stimulated cells and in cells co-treated with Pam_3CSK_4 and $1,25(OH)_2D_3$. Under these treatment conditions, a decrease in the relative concentration of glucose and an increase in the relative concentration of lactate was observed. These observations evidently suggest that glycolysis was up-regulated. Our results correspond to those findings of Gleeson *et al*. (2016) and Shi *et al*. (2015), who also reported that glycolysis is up-regulated during *M.tb* infection in macrophages. This up-regulation has been linked with the containment of intracellular *M.tb* by the hosts' immune response. This observation is similar to the Warburg effect in cancer cells.

The Warburg effect is the metabolic phenomenon that is used to describe the up-regulation of glycolysis with the formation of lactate as the final product in cancer cells (Warburg, 1956). In recent years, the Warburg effect has been observed in non-cancerous cell types (Abdel-Haleem *et al.,* 2017). Our data further corresponds to the findings of Salamon *et al.* (2014), who reported that vitamin D enhanced the Warburg effect in *M.tb* infection. A shift in energy metabolism to glycolysis during *M.tb* infection is crucial for controlling the activity of *M.tb* as glycolysis promote inflammatory response against the bacteria through the generation of proinflammatory cytokines and ROS (O'Neill and Hardie, 2013).

5.3. Reprogramming of metabolic pathways associated with amino acids

The presence or absence of certain amino acids produced by the host during the mycobacterial infection can determine the inhibition, growth/survival and virulence of the mycobacterium in the host (Burke *et al.,* 2018; Gouzy *et al.,* 2014; Lyon *et al*., 1970). Amino acids detected in our study play an important role in the regulation of oxidation-reduction (redox) reaction, regulation of energy metabolism, synthesis of antimycobacterial compounds, nucleic acids synthesis and protein synthesis, including structure folding and function (Garrett *et al*., 2018; Kocic *et al*., 2012; Morris *et al*., 2017). Taken together, these amino acids shape the host's immune response against mycobacterial infection.

5.3.1. Arginine biosynthesis down-regulation by 1,25(OH)$_2$D$_3$ in Pam$_3$CSK$_4$ stimulated U937 macrophages

The role of arginine in mycobacterial infection has been sufficiently investigated (Peteroy-Kelly *et al.,* 2003). Previous studies have shown that metabolic reprogramming during infection is associated with the changes in the metabolism of arginine (Luiking *et al*., 2003). Arginine is a semi-essential amino acid synthesised mainly from glutamate (Mizrahi and Warner, 2018). L-arginine serves as a precursor for the synthesis of reactive nitrogen species (RNS), polyamines, creatine, ornithine and urea cycle (Morris *et al*., 2017).

Although in the current study arginine was not detected in all treatment conditions, significant changes in the concentration of metabolites associated with arginine biosynthesis—glutamate, ornithine and proline—were detected. A relatively high concentration of glutamate was observed in cells co-treated with Pam$_3$CSK$_4$ and 1,25(OH)$_2$D$_3$ as compared to the untreated cells. A decrease in the relative concentration of glutamate was observed in cells treated with 1,25(OH)$_2$D$_3$ only. These changes were not observed in U937 macrophages treated with Pam$_3$CSK$_4$ only. An increase in glutamate concentrations in cells co-treated with Pam$_3$CSK$_4$ and 1,25(OH)$_2$D$_3$ suggest that this treatment condition downregulates arginine biosynthesis—the conversion of glutamate to arginine. This could explain the relatively high concentration of glutamate observed in Pam$_3$CSK$_4$ and 1,25(OH)$_2$D$_3$ co-treated U937 macrophages (**Chapter 4**, **Table 4.1** and **Figure 4.7A**). The down-regulation of the arginine biosynthesis could be one of the metabolic effects of 1,25(OH)$_2$D$_3$ in Pam$_3$CSK$_4$ treated U937 macrophages. 1,25(OH)$_2$D$_3$ probably initiates this arginine biosynthesis down-regulation as the immune response against Pam$_3$CSK$_4$ action. In *M.tb* infection, arginine is used as a source of both carbon and nitrogen (Gupta *et al*., 2018; Hampel *et al*., 2015). Arginine starvation leads to the death of *M.tb* infected cells and ultimately, the killing of *M.tb* (Mizrahi and Warner, 2018; Tiwari *et al.*, 2018). Our suggestion of arginine biosynthesis down-regulation by 1,25(OH)$_2$D$_3$ in Pam$_3$CSK$_4$ treated U937 macrophages, however, contradicts the findings of Andrukhova *et al.* (2014), who reported that 1,25(OH)$_2$D$_3$ increases the availability of arginine, which subsequently leads to an increase in the synthesis of arginine-derived nitric oxide (NO). Furthermore, Rockett *et al.* (1998) reported that 1,25(OH)$_2$D$_3$ induces the

expression of the *nitric oxide synthase 2 (NOS2*) gene in *M.tb* infected human HL-60 macrophage-like cell line. NOS2 encodes for NO synthase, an enzyme that catalyses the conversion of arginine to NO. NO has an antimycobacterial activity (Jamaati *et al*., 2017). We propose that the down-regulation of arginine biosynthesis seen in U937 macrophages co-treated with Pam_3CSK_4 and $1,25(OH)_2D_3$ could be the biochemical mechanism induced by $1,25(OH)_2D_3$ in U937 macrophages to inhibit NO synthesis. This suggests that $1,25(OH)_2D_3$ induces U937 macrophages to inhibit the mycobacterial-like effect of Pam_3CSK_4 through arginine starvation other than the use of NO. Although RNS such as NO has antimicrobial properties, overproduction of NO can cause mitochondrial dysfunction, DNA damage, changes in structure and function of protein mediators, as well as cell injury and cell death (Abdelmegeed *et al*., 2014; Groves *et al*., 1995; Song *et al.,* 2014). Hence, NO downregulation is crucial in protecting the cells from these NO side effects. Hence, we propose arginine starvation rather than NO production by $1,25(OH)_2D_3$ as the immune response against Pam_3CSK_4 stimulation.

In addition to these observations, a relatively low concentration of ornithine was observed in cells co-treated with Pam_3CSK_4 and $1,25(OH)_2D_3$. No significant changes in ornithine relative concentration were observed in the other treatments. Ornithine is a non-proteinogenic amino acid synthesised from the reaction of arginine with water, catalysed by arginase (Dimski, 1994). Our observation further supports the notion that arginine biosynthesis was down-regulated in Pam_3CSK_4 and $1,25(OH)_2D_3$ co-treated cells. Arginine is a precursor of ornithine, and therefore, decreases in the synthesis of arginine will result in a decrease in ornithine synthesis. It has been shown that in *M.tb* infection, arginine is converted into ornithine, resulting in an increase in this metabolite (Hampel *et al*., 2015). Low concentration of arginine inhibits this reaction. A similar phenomenon was observed in our study, which further shows that arginine synthesis was inhibited by $1,25(OH)_2D_3$ in Pam_3CSK_4 treated cells. In addition to arginine biosynthesis down-regulation, a relative decrease in ornithine could have been enhanced by ornithine decarboxylase. $1,25(OH)_2D_3$ increases the activity of ornithine decarboxylase, an enzyme that catalyses the decarboxylation of ornithine. The increased activity of ornithine decarboxylase leads to a low concentration of ornithine (Sömjen *et al.,* 1983). Further enzyme-based investigations are needed to confirm this speculation.

Taken together, the observed relative decrease in the concentration of arginine and ornithine suggest that $1,25(OH)_2D_3$ decreases arginine biosynthesis in Pam_3CSK_4 treated U937 macrophages. The decrease in arginine biosynthesis could be the metabolic mechanism induced by $1,25(OH)_2D_3$ to activate the U937 macrophages immune response against Pam_3CSK_4 stimulation. Down-regulation of arginine biosynthesis is of importance in controlling the mycobacterial-like effect of Pam_3CSK_4. This speculation is based on the findings of Tiwari *et al.* (2018), who reported that arginine deprivation leads to *M.tb* killing through ROS accumulation, DNA damage, and rapid sterilisation of *M.tb.* Arginine is a crucial source of both carbon and nitrogen needed for *M.tb* survival (Hampel *et al*., 2015).

5.3.2. Glutathione metabolism down-regulation in U937 macrophages co-treated with Pam_3CSK_4 and $1,25(OH)_2D_3$

Changes in the cellular glutathione (GSH) concentration in the presence of mycobacteria have been previously investigated (Dayaram *et al.,* 2006; Guerra *et al*., 2011). GSH is an essential tripeptide antioxidant synthesised from glutamate, cysteine and glycine in two sequential ATP-dependent steps (Lu, 2009). The first step is the synthesis of γ-glutamylcysteine from glutamate and cysteine in a reaction catalysed by glutamate-cysteine ligase (GCL). The second step is the addition of glycine to γ-glutamylcysteine to form GSH in a reaction catalyzed by GSH synthetase (Mari *et al*., 2010). GSH maintains the cellular redox state through the active thiol group present in the cysteine residue of GSH. The thiol group of cysteine regulates the redox state by directly detoxifying ROS and RNS (Cooper *et al*., 2011). A decrease in intracellular GSH leads to an increase in ROS, which ultimately leads to oxidative stress (OS). The latter is a process by which cells and tissues produce excessive ROS compared to antioxidants. The imbalance between ROS and antioxidants can lead to chronic inflammation (Hussain *et al*., 2016). OS is a common phenomenon in mycobacterial infections such as TB. In active TB, OS is induced to counteract the disease and kill *M.tb* (Goyal *et al.,* 2017; Shastri *et al*., 2018).

Previous studies have shown that GSH can protect the host against microbial infection by activating T lymphocytes and natural killer cells (Guerra *et al*., 2011; Guerra *et al.,* 2012). Additionally, GSH reacts with NO to form S-nitrosoglutathione (GSNO). The latter increases the activity of NO in inhibiting microbial growth. NO from the GSNO complex is released at the site of infection to induce microbial death (Venketaraman *et al*., 2003). In cases where GSH levels are decreased, an increase in OS is usually observed (Mohod *et al.,* 2008). For instance, patients with active TB have decreased levels of GSH during the initial stages of infection (Venketaraman *et al*., 2008). Decreased levels of GSH lead to OS, which contributes towards the control of M.tb infection (Wu et al., 2018). In the present study, decreased GSH was detected in U937 macrophages treated with a combination of Pam_3CSK_4 and $1,25(OH)_2D_3$ in the 12 hrs treatment. GSH was not detected in the 16 and 12 hrs treatment conditions. In U937 macrophages treated with a combination of Pam_3CSK_4 and $1,25(OH)_2D_3$ in the 12 hrs treatment, GSH concentration was relatively low. These findings suggest that Pam_3CSK_4 and $1,25(OH)_2D_3$ co-treatment down-regulates glutathione synthesis. A decrease in GSH would favour U937 macrophages oxidative response to the mycobacterial-like effect of Pam_3CSK_4. The effect of supplementary $1,25(OH)_2D_3$ on GSH metabolism in mycobacterial infection is still enigmatic and remains to be investigated. To our knowledge, this is the first study to show the relationship between mycobacterial infection, supplementary $1,25(OH)_2D_3$ and GSH metabolism in macrophages using metabolomics. A recent study by Vrieling *et al*. (2020) only investigated the relationship between mycobacterial infection and GSH metabolism. In their study, Vrieling *et al*. (2020) reported an increase in GSH concentration following *M.tb* infection. In our study, however, we observed a decrease in GSH when Pam_3CSK_4 treated

U937 macrophages are supplemented with $1,25(OH)_2D_3$. This observation suggests that $1,25(OH)_2D_3$ down-regulates GSH synthesis in Pam_3CSK_4 treated U937 macrophages. This could be the immune response mechanism to induce OS for the inhibition of Pam_3CSK_4 mycobacterial-like activity. Our observation of the decrease in GSH in the presence of $1,25(OH)_2D_3$ contradicts the findings of Jain and Micinski (2013). These authors reported that $1,25(OH)_2D_3$ up-regulates GSH synthesis by up-regulating glutamate-cysteine ligase (GCL) in U937 monocytes. The differences observed in our study and that of Jain and Micinski (2013) suggest that the metabolic effect of $1,25(OH)_2D_3$ on GSH metabolism differs between monocytes and macrophages. Further studies should be done to confirm the absence of increased GSH concentrations using standard biochemical assays.

Subsequently, glycine and glutamate (GSH precursors) were also observed in our study. Glycine and glutamate are nonessential amino acids that are key excitatory neurotransmitters involved in metabolic, bioenergetic, biosynthetic and oncogenic signalling pathways (Alves *et al.,* 2019; Willard and Koochekpour, 2013). Mycobacteria utilise these metabolites as a nitrogen source needed for mycobacterial growth and replication (Cowley *et al.,* 2004; Lyon *et al*., 1970; Ratledge, 1976). In the current study, glutamate concentration was not significantly affected in Pam_3CSK_4 stimulated macrophages, however, the concentration of glutamate was relatively increased in cells co-treated with Pam_3CSK_4 and $1,25(OH)_2D_3$. This observation suggests that $1,25(OH)_2D_3$ inhibits the consumption of glutamate in Pam_3CSK_4 treated U937 macrophages, meaning that the use of glutamate in GSH synthesis was inhibited. Accordingly, the GSH concentration was relatively decreased in cells co-treated with Pam_3CSK_4 and $1,25(OH)_2D_3$. These observations further show that Pam_3CSK_4 and $1,25(OH)_2D_3$ co-treatment down-regulated GSH synthesis. The increase of glutamate and the decrease in GSH levels observed in cells co-treated with Pam_3CSK_4 and $1,25(OH)_2D_3$ could be the mechanism used by the cells relating to allow OS. In this instance, OS would be necessary to produce ROS, which would inhibit the mycobacterial-like activity of Pam_3CSK_4. Our suggestion agrees with the study by Kelly *et al*. (2015), who reported an increase in ROS production in Pam_3CSK_4 treated macrophages. Furthermore, Matta and Kumar (2016) also reported an increase in ROS in *M.tb* infected macrophages as as an immune response against this bacterium. ROS, such as hydrogen peroxide, diffuses through the cell membrane of the pathogen into the cytoplasm and damages the DNA, thus leading to the death of the pathogen (Slauch, 2011).

In addition to glutamate, the concentration of glycine was relatively increased in all treatment conditions at 12 hrs. A gradual decrease in the relative concentration of glycine was also observed in the 16 and 24 hrs treatment conditions (**Chapter 4**, **Table 4.1** and **Figure 4.7**). This gradual decrease could be associated with glycine degradation over time. The relative concentration of glycine was slightly higher in Pam_3CSK_4 treated U937 macrophages as compared to Pam_3CSK_4 and $1,25(OH)_2D_3$ co-treated U937 macrophages over time. This suggests that $1,25(OH)_2D_3$ induces glycine degradation in Pam_3CSK_4 treated U937 macrophages. We propose that the relative low glycine concentration in U937 macrophages

is associated with biochemical processes such as energy metabolism and protein synthesis other than GSH synthesis. This suggestion is based on the evidence that GSH concentration was relatively low in U937 macrophages co-treated with Pam_3CSK_4 and $1,25(OH)_2D_3$ (**Chapter 4**, **Table 4.1** and **Figure 4.7A**). Taken together, our findings suggest that one of the metabolic effects of $1,25(OH)_2D_3$ in Pam_3CSK_4 treated U937 macrophages is the down-regulation of GSH synthesis. Hence, GSH was relatively decreased in U937 macrophages co-treated with Pam_3CSK_4 and $1,25(OH)_2D_3$. GSH synthesis is probably inhibited by $1,25(OH)_2D_3$ in order to allow the oxidative response against Pam_3CSK_4 in U937 macrophages.

5.3.3. Reprogramming of valine, leucine and isoleucine biosynthesis in U937 macrophages treated with Pam_3CSK_4 only and $1,25(OH)_2D_3$ only

The role of branched-chain amino acids (BCAAs)— valine, leucine and isoleucine—in microbial infection has been extensively described (Lobel *et al.,* 2015; Kaiser and Heinrichsa, 2018; Kim *et al.,* 2017). BCAAs are essential amino acids that consist of hydrophobic side chains. They are the main contributors to the hydrophobic side chains required for the structure and function of proteins (Shimomura and Harris, 2006). BCAA catabolism starts with the conversion of BCAAs in a transamination reaction catalysed by branched-chain aminotransferase (BCAT) into their respective α-keto acids (branched-chain keto acids; BCKAs). These include α-keto-β-methylvaleric acid, α-ketoisovaleric acid and α-ketoisocaproic acid. The second step is the oxidative decarboxylation of BCKAs by the branched-chain ketoacid dehydrogenase complex. This reaction yields isovaleryl-CoA, α-methylbutyryl-CoA and isobutyryl-CoA. These are precursors of acetoacetate, acetyl-CoA and succinyl-CoA (Burrage *et al.,* 2014). Acetoacetate, acetyl-CoA and succinyl-CoA are utilised in energy metabolism (TCA cycle) and for biosynthetic purposes (e.g. lipid biosynthesis) (Wanders *et al*., 2012). BCAAs are essential in protein synthesis, energy metabolism and the immune response (Holeček, 2018; Nie *et al*., 2018; Platell *et al*., 2000).

Valine and leucine were detected in the current study. Stimulation of U937 macrophages with only Pam_3CSK_4 induced a relative increase in the concentration of valine in the 12 and 24 hrs treatment conditions (**Chapter 4**, **Table 4.1** and **Figure 4.7A**). These changes were, however, not detected in the 16 hrs treatment conditions. The relative increase in valine concentration in Pam_3CSK_4 is most likely associated with an up-regulation of BCAA (particularly valine) biosynthesis. The biosynthesis of BCAAs by the U937 macrophages probably support the activity of Pam_3CSK_4. Our suggestion is supported by the study of Awasthy *et al.* (2009) who reported that BCAAs biosynthesis is crucial for intracellular survival of *M.tb*. BCAAs (particularly valine) is used as a nitrogen donor by intracellular *M.tb* in macrophages (Borah *et al*., 2019).

In cells treated with $1,25(OH)_2D_3$ only (24 hrs treatment), a relatively low concentration of leucine was observed (**Chapter 4**, **Table 4.1** and **Figure 4.7C**). Leucine was, however, not

detected in the 12 and 16 hrs treatment conditions. A decrease in leucine in cells treated with $1,25(OH)_2D_3$ only in 24 hrs treatment suggests that $1,25(OH)_2D_3$ supplementation to U937 macrophages downregulates BCAA biosynthesis. We, therefore, propose that a decrease of leucine could be the results of BCAA oxidation (particularly leucine) by the U937 macrophages supplemented with $1,25(OH)_2D_3$. The relationship between $1,25(OH)_2D_3$ and BCAA biosynthesis in macrophages is yet to be investigated in the literature. Previous studies, however, have reported that immune cells including macrophages, oxidise BCAAs to produce precursors for energy metabolism and the synthesis of new immune cells (Calder, 2006; Negro *et al*., 2008; Platell *et al*., 2000; Zhang *et al*., 2017). The metabolic profiling of U937 macrophages co-treated with Pam_3CSK_4 and $1,25(OH)_2D_3$ did not show any changes in BCAAs (**Chapter 4**, **Table 4.1** and **Figure 4.7**). The metabolic effect of $1,25(OH)_2D_3$ on BCAA synthesis in Pam_3CSK_4 treated cells remains unclear. Further investigations are needed to elucidate the effect of $1,25(OH)_2D_3$ on BCAA biosynthesis in Pam_3CSK_4 stimulated cells.

5.3.4. Easing of Pam_3CSK_4 effects by aminoacyl-tRNA biosynthesis reprogramming

Aminoacyl-tRNA or transfer RNA (tRNA) biosynthesis is another pathway altered in *M.tb* infection. This pathway is concerned with the attachment of amino acids to relevant tRNA in the process catalysed by a multi-enzyme aminoacyl-tRNA synthetase. This process is a requirement for protein synthesis (Gadakh and Van Aerschot, 2012; Yanagisawa *et al*., 2010). Inhibiting aminoacyl-tRNA synthetase prevents the synthesis of proteins required by the pathogen for growth and virulence (Van de Vijver *et al*., 2009). Our detection of significant alterations in the aminoacyl-tRNA biosynthesis pathway could be due to an immune response mechanism following U937 macrophages stimulation with Pam_3CSK_4. Supplementing the cells with $1,25(OH)_2D_3$ most likely counteracts the activity of Pam_3CSK_4 by targeting aminoacyl-tRNA synthetases. Aminoacyl-tRNA synthetases are validated targets for many therapeutic strategies against infectious diseases. Most therapeutics control infections by inhibiting the messenger RNA (mRNA) translation machinery (Dewan *et al*., 2014). Previous studies have shown that anti-TB compounds can inhibit *M.tb* by targeting specific *M.tb* aminoacyl-tRNA synthetases (Hu *et al.,* 2013; Kovalenko *et al*., 2019; Soto *et al.,* 2018; Zhu *et al*., 2015). Unfortunately, it cannot be determined from the results generated in our study whether aminoacyl-tRNA biosynthesis was down- or up-regulated in each treatment condition. This is due to the fact that aminoacyl-tRNA biosynthesis involves all the standard amino acids. In this instance, one cannot pinpoint a specific amino acid that is responsible for the changes observed. Nonetheless, the results show that aminoacyl-tRNA biosynthesis was significantly altered in Pam_3CSK_4 treated cells supplemented with or without $1,25(OH)_2D_3$. The exact metabolic effects of $1,25(OH)_2D_3$ on aminoacyl-tRNA biosynthesis in Pam_3CSK_4 treated U937 macrophages remain unclear in the present study. Little is known about the effect of $1,25(OH)_2D_3$ on aminoacyl-tRNA biosynthesis in literature. Future studies using enzyme assays are needed to measure the activity of specific aminoacyl-tRNA synthetases involved in protein

synthesis in U937 macrophages treated with Pam_3CSK_4, $1,25(OH)_2D_3$ and a combination of Pam_3CSK_4 and $1,25(OH)_2D_3$. This will help to determine the regulation of aminoacyl-tRNA synthetases of interest under the aforementioned treatment conditions.

CHAPTER 6

CONCLUSION AND FUTURE PERSPECTIVES

^{1}H NMR spectroscopy and GCxGC-TOFMS based metabolomics successfully detected and identified metabolites discriminating metabolic profiles of U937 macrophages treated with Pam_3CSK_4, $1,25(OH)_2D_3$ and a combination of Pam_3CSK_4 and $1,25(OH)_2D_3$. Discriminatory metabolites that distinguish the study groups have been linked to energy metabolism (galactose metabolism, glycolysis—the Warburg effect), regulation of redox reaction (arginine biosynthesis and glutathione metabolism), amino acid and protein synthesis (aminoacyl-tRNA biosynthesis). Together, these metabolic pathways have also been implicated in the immune responses during mycobacterial infection.

Novel aspect

Previous metabolomics-based mycobacterial studies focused solely on evaluating the metabolic changes induced by mycobacterial infection from biological sample matrices such as serum, plasma, lung tissue and spleen tissue. In addition, a limited number of studies have investigated the metabolic effects of $1,25(OH)_2D_3$ in the presence of mycobacterial infection. The aim of the present study was to evaluate the metabolic effects of supplementary $1,25(OH)_2D_3$ in mycobacterial stimulated macrophages using ^{1}H NMR spectroscopy and GCxGC-TOFMS metabolomics. Although this is an *in vitro* study, the metabolic changes in mycobacterial stimulated cells co-treated with Pam_3CSK_4 and $1,25(OH)_2D_3$ have been identified. The generated data revealed that supplementary $1,25(OH)_2D_3$ induces metabolic reprogramming in mycobacteria stimulated cells. The results suggest that $1,25(OH)_2D_3$ promotes the elimination of bacterial infection by the macrophages and is therefore beneficial in the immune response against mycobacterial infection. To further substantiate our findings, additional confirmatory investigations using actual *M.tb* are needed. Such studies may contribute to the understanding of whether or not $1,25(OH)_2D_3$ is significantly beneficial in eliminating *M.tb* infection.

Revisiting hypothesis

It was hypothesized that: *Metabolomics can detect the metabolic changes induced by Pam_3CSK_4 stimulation of macrophages supplemented with or without $1,25(OH)_2D_3$.*

The results (**Chapter 4**, **Section 4.2 and appendix data**) showed differences in the metabolic profiles of U937 macrophages stimulated with Pam_3CSK_4 and supplemented with or without $1,25(OH)_2D_3$. Based on these findings, the proposed hypothesis was accepted.

The null hypothesis was therefore rejected as it states that: *Metabolomics cannot detect the metabolic changes induced by Pam_3CSK_4 stimulation of macrophages supplemented with or without $1,25(OH)_2D_3$.*

Limitations of the study

- The present study used *in vitro* models (U937 macrophages and Pam_3CSK_4) due to the limitation in specialised equipment and *M.tb* infected serum samples. The *in vitro* models do not give the exact metabolic events that occur *in vivo* during *M.tb.* Thus, the physiological relevance of the *in vitro* models differs from that of the *in vivo* systems. Nonetheless, the present study gives the possible metabolic events that occur in *M.tb* infection with or without *$1,25(OH)_2D_3$.*

- The study only focused on the intracellular metabolome. The results obtained do not account for the extracellular metabolome. Hence, the obtained results do not give the complete picture of all the metabolic events associated with each treatment condition. Nevertheless, the metabolites detected in this study allowed us to speculate on the possible metabolic events occurring under each treatment condition.

Future perspectives

- Quantitative analysis of metabolites implicated in U937 macrophages treated with Pam_3CSK_4, supplemented with $1,25(OH)_2D_3$ and co-treated with Pam_3CSK_4 and $1,25(OH)_2D_3$. Quantitative analysis will provide the actual concentration of each significantly altered metabolite in the study groups. This information will help understand the extent to which $1,25(OH)_2D_3$ effects a specific metabolites in U937 macrophages stimulated with or without Pam_3CSK_4. Such knowledge can be used to further confirm whether $1,25(OH)_2D_3$ is significant in eliminating the mycobacterial infection.

- Future studies will also require the use of additional analytical techniques such as LC-MS to detect as many metabolites as possible. The use of LC-MS will allow the detection of thermally unstable, involatile and ionic compounds that could not be detected using NMR and GCxGC-TOFMS. This additional analytical technique will expand the number of metabolites detected and possibly the number of metabolic pathways reprogrammed in each treatment group.

CHAPTER 7

REFERENCES

Abdel-Haleem AM, Lewis NE, Jamshidi N, Mineta K, Gao X, Gojobori T. The emerging facets of non-cancerous Warburg effect. *Front Endocrinol (Lausanne)* 2017;8:279.

Abdelmegeed MA, Song BJ. Functional roles of protein nitration in acute and chronic liver diseases. *Oxid Med Cell Longev* 2014;2014:149627.

Abu El Maaty MA, Alborzinia H, Khan SJ, Büttner M, Wölfl S. 1,25$(OH)_2D_3$ disrupts glucose metabolism in prostate cancer cells leading to a truncation of the TCA cycle and inhibition of TXNIP expression. *Biochim Biophys Acta Mol Cell Res* 2017;1864(10):1618-30.

Abu El Maaty MA, Dabiri Y, Almouhanna F, Blagojevic B, Theobald J, Büttner M, Wölfl S. Activation of pro-survival metabolic networks by 1,25$(OH)_2D_3$ does not hamper the sensitivity of breast cancer cells to chemotherapeutics. *Cancer Metab* 2018;6:11. doi: 10.1186/s40170-018-0183-6.

Adan A, Alizada G, Kiraz Y, Baran Y, Nalbant A. Flow cytometry: basic principles and applications. *Crit Rev Biotechnol* 2017;37(2):163-176. doi: 10.3109/07388551.2015.1128876.

Akira S, Uematsu S, Takeuchi O. Pathogen recognition and innate immunity. *Cell* 2006; 124:783–801.

AL-Bukhaiti WQ, Noman A, Qasim AS, AL-Farga A. Gas chromatography: principles, advantages and applications in food analysis. *IJAIR* 2017;6(1):123-8.

Alexander MD, Andrews JA, Leslie RGQ, Wood NJ. The binding of human and guinea-pig IgG subclasses to homologous macrophage and monocyte Fc receptors. *Immunology* 1978;35:115-23.

Aliprantis AO, Yang R-B, Mark MR, Shelly S, Devaux B, Radolf JD, Klimpel GR, Godowski P, Zychlinsky A. Cell activation and apoptosis by bacterial lipoproteins through toll-like receptor-2. *Science* 1999;285:736-9. DOI: 10.1126/science.285.5428.73.

Alonso A, Marsal S, Julià A. Analytical methods in untargeted metabolomics: state of the art in 2015. *Front Bioeng Biotechnol* 2015;3:23. doi: 10.3389/fbioe.2015.00023.

Al-Rashed F, Kochumon S, Usmani S, Sindhu S, Ahmad R. Pam3CSK4 induces MMP-9 expression in human monocytic THP-1 cells. *Cell Physiol Biochem* 2017;41(5):1993-2003. doi: 10.1159/000475298.

Al-Rubaye AF, Hameed IH, Kadhim MJ. A Review: Uses of Gas Chromatography-Mass Spectrometry (GC-MS) technique for analysis of bioactive natural compounds of some plants. *IJTPR* 2017;9(1);81-5.

Alves A, Bassot A, Bulteau A-L, Pirola L, Morio B. Glycine metabolism and its alterations in obesity and metabolic diseases. *Nutrients* 2019;11(6):1356. doi: 10.3390/nu11061356.

Anas A, van der Poll T, de Vos AF. Role of CD14 in lung inflammation and infection. *Critical Care* 2010; 14:209. http://ccforum.com/content/14/2/209.

Andersen MN, Al-Karradi SNH, Kragstrup TW, Hokland M. Elimination of erroneous results in flow cytometry caused by antibody binding to fc receptors on human monocytes and macrophages. *Cytometry A* 2016;89A:1001-9.

Anderson CL, Abraham GN. Characterization of the Fc receptor for IgG on a human macrophage cell line, U937. *J Immunol* 1980;125:2735-41.

Andrukhova O, Slavic S, Zeitz U, Riesen SC, Heppelmann MS, Ambrisko TD, Markovic M, Kuebler WM, Erben RG. Vitamin D is a regulator of endothelial nitric oxide synthase and arterial stiffness in mice. *Mol Endocrinol* 2014;28(1):53–64. doi: 10.1210/me.2013-1252.

Antcliffe D, Gordon AC. Metabonomics and intensive care. *Crit Care* 2016;20(1):68. doi: 10.1186/s13054-016-1222-8.

Antony PM, Trefois C, Stojanovic A, Baumuratov AS, Kozak K. Light microscopy applications in systems biology: opportunities and challenges. *Cell Commun Signal* 2013;11(1):24. doi: 10.1186/1478-811X-11-24.

Aretz I, Meierhofer D. Advantages and pitfalls of mass spectrometry based metabolome profiling in systems biology. *Int J Mol Sci* 2016;17:632; doi:10.3390/ijms17050632.

Arey BJ. The role of glycosylation in receptor signalling, in Petrescu S. (ed.). *Glycosylation*. United Kingdom: InTechOpen; 2012. pp. 273-86.

Arnedo-Pena A, Juan-Cerdán JV, Romeu-García A, García-Ferrer D, Holguín-Gómez R, Iborra-Millet J, Gil-Fortuño M, Gomila-Sard B, Roach-Poblete F. Vitamin D status and incidence of tuberculosis among contacts of pulmonary tuberculosis patients. *Int J Tuberc Lung Dis 2015*;19(1):65-9. doi: 10.5588/ijtld.14.0348.

Atan NAD, Koushki M, Ahmadi NA, Rezaei-Tavirani M. Metabolomics-based studies in the field of Leishmania/leishmaniasis. *Alexandria J Med* 2018;54:383–90.

Awasthy D, Gaonkar S, Shandil RK, Yadav R, Bharath S, Marcel N, Subbulakshmi V, Sharma U. Inactivation of the *ilvB1* gene in *Mycobacterium tuberculosis* leads to branched-chain amino acid auxotrophy and attenuation of virulence in mice. *Microbiology* 2009;155(Pt 9):2978-87. doi: 10.1099/mic.0.029884-0.

Baeke F, Takiishi T, Korf H, Gysemans C, Mathieu C. Vitamin D: modulator of the immune system. *Curr Opin Pharmacol* 2010;10(4):482-96.

Ballinger MN, Christman JW. Pulmonary macrophages: Overlooked and underappreciated. *Am J Respir Cell Mol Biol* 2016;54(1):1-2. doi: 10.1165/rcmb.2015-0270ED.

Banerjee S, Mazumdar S. Electrospray ionization mass spectrometry: A technique to access the information beyond the molecular weight of the analyte. *Int J Anal Chem* 2012; doi:10.1155/2012/28257.

Bardoel BW, Kenny EF, Sollberger G, Zychlinsky A. The balancing act of neutrophils. *Cell Host Microbe* 2014;15:526–36.

Bartel J, Krumsiek J, Theis FJ. Statistical methods for the analysis of high throughput metabolomics data. *Comput Struct Biotechnol J* 2013;4:e201301009.

Barter DM, Agboola SO, Murray MB, Bärnighausen T. Tuberculosis and poverty: the contribution of patient costs in sub-Saharan Africa – a systematic review. *BMC Public Health* 2012;12:980. doi: 10.1186/1471-2458-12-980.

Beckonert O, Keun HC, Ebbels TMD, Bundy J, Holmes E, Lindon JC, Nicholson JK. Metabolic profiling, metabolomic and metabonomic procedures for NMR spectroscopy of urine, plasma, serum and tissue extracts. *Nat Protoc* 2007;2(11):2692-703. doi: 10.1038/nprot.2007.376.

Behrends V, Williams KJ, Jenkins VA, Robertson BD, Bundy JG. Free glucosylglycerate is a novel marker of nitrogen stress in Mycobacterium smegmatis. *J Proteome Res* 2012;11:3888–96.

Betters, D. M. Use of flow cytometry in clinical practice. *J Adv Pract Oncol* 2015;6(5):435–40. doi: 10.6004/jadpro.2015.6.5.4.

Beukes D, du Preez I, Loots DT. Total metabolome extraction from mycobacterial cells for GC-MS metabolomics analysis. *Methods Mol Biol* 2019;1859:121-31.

Biancolillo A, Marini F. Chemometric methods for spectroscopy-based pharmaceutical analysis. Analysis. *Front Chem* 2018;6:576. doi: 10.3389/fchem.2018.00576.

Bingol K, Brüschweiler R. Two elephants in the room: New hybrid nuclear magnetic resonance and mass spectrometry approaches for metabolomics. *Curr Opin Clin Nutr Metab Care* 2015;18(5):471-7. doi: 10.1097/MCO.0000000000000206.

Blackstock JC. *Guide to biochemistry.* United Kingdom: Elsevier Ltd; 1989. pp. 20-31.

Bolten CJ, Kiefer P, Letisse F, Portais JC, Wittmann C. Sampling for metabolome analysis of microorganisms. *Anal Chem* 2007;79(10):3843-9.

Booth SC, Weljie AM, Turner RJ. Computational tools for the secondary analysis of metabolomics experiments. *Comput Struct Biotechnol J* 2013;4:e201301003. doi: 10.5936/csbj.201301003.

Borah K, Beyß M, Theorell A, Wu H, Basu P, Mendum TA, Nöh K, Beste DJV, McFadden J. Intracellular *Mycobacterium tuberculosis* exploits multiple host nitrogen sources during growth in human macrophages. *Cell Rep* 2019;29(11):3580-91.e4. doi: 10.1016/j.celrep.2019.11.037.

Bort JAH, Shanmukam V, Pabst M, Windwarder M, Neumann L, Alchalabi A, Krebiehl G, Koellensperger G, Hann S, Sonntag D, Altmann F, Heel C, Borth N. Reduced quenching and extraction time for mammalian cells using filtration and syringe extraction. *J Biotechnol* 2014 Jul 20;182-183(100):97-103. doi: 10.1016/j.jbiotec.2014.04.014.

Bowler RP, Wendt CH, Fessler MB, Foster MW, Kelly RS, Lasky-Su J, Rogers AJ, Stringer KA, Winston BW. New Strategies and Challenges in Lung Proteomics and Metabolomics: An Official American Thoracic Society Workshop Report. *Ann Am Thorac Soc* 2017;14(12):1721-43. doi: 10.1513/AnnalsATS.201710-770WS.

Boyer RF. Biochemistry Laboratory: modern theory and techniques. 2nd ed. United States of America: Pearson Education, Inc; 2012. pp.225-37.

Burke C, Abrahams KA, Richardson EJ, Loman NJ, Alemparte C, Lelievre J, Besra GS. Development of a whole-cell high-throughput phenotypic screen to identify inhibitors of mycobacterial amino acid biosynthesis. *FASEB BioAdvances* 2019;1:246–54.

Burrage LC, Nagamani SCS, Campeau PM, Lee BH. Branched-chain amino acid metabolism: from rare Mendelian diseases to more common disorders. *Hum Mol Genet* 2014;23(R1): R1–R8.doi: 10.1093/hmg/ddu123.

Cai HL, Li HD, Yan XZ, Sun B, Zhang Q, Yan M, Zhang WY, Jiang P, Zhu RH, Liu YP, Fang PF, Xu P, Yuan HY, Zhang XH, Hu L, Yang W, Ye HS. Metabolomic analysis of biochemical changes in the plasma and urine of first-episode neuroleptic-naïve schizophrenia patients after treatment with risperidone. *J Proteome Res* 2012;11:4338-50. doi: 10.1021/pr300459d.

Calder PC. Branched-chain amino acids and immunity. *J Nutr* 2006;136(1 Suppl):288S-93S. doi: 10.1093/jn/136.1.288S.

Cantorna MT, Zhu Y, Froicu M, Wittke A. Vitamin D status, 1,25-dihydroxyvitamin D3, and the immune system. *Am J Clin Nutr* 2004;80(6):1717S–20S. doi: 10.1093/ajcn/80.6.1717S.

Cao B, Aa J, Wang G, Wu X, Liu L, Li M, Shi J, Wang X, Zhao C, Zheng T, Guo S, Duan J. GC-TOFMS analysis of metabolites in adherent MDCK cells and a novel strategy for identifying intracellular metabolic markers for use as cell amount indicators in data normalization. *Anal Bioanal Chem* 2011;400(9):2983-93. doi: 10.1007/s00216-011-4981-8.

Carlos C, Maretto DA, Poppi RJ,.Sato MIZ, Ottoboni LMM. Fourier transform infrared microspectroscopy as a bacterial source tracking tool to discriminate fecal *E. coli* strains. *Microchem J* 2011;99(1):15-19.

Chagoyen M, Pazos F. Tools for the functional interpretation of metabolomic experiments. *Brief. Bioinform* 2012;14(6):737-44. doi:10.1093/bib/bbs055.

Chandra P, Rajmani RS, Verma G, Bhavesh NS, Kumar D. targeting drug-sensitive and -resistant strains of mycobacterium tuberculosis by inhibition of *Src* family kinases lowers disease burden and Pathology. *mSphere* 2016;1(2). pii: e00043-15. doi: 10.1128/mSphere.00043-15.

Chanput W, Peters V, Wichers H. THP-1 and U937 cells, in Verhoeckx K, Cotter P, López-Expósito I, Kleiveland C, Lea T, Mackie A, Requena T, Swiatecka D, Wichers H. (ed). *The impact of food bioactives on health: in vitro and ex vivo models.* Cham (CH): Springer; 2015. pp. 147-59.

Chatham JC, Blackban SJ. Nuclear magnetic resonance spectroscopy and imaging in animal research. *ILAR J* 2001;42:189-208.

Chen J, MacEachren AM, Peuquet DJ. Constructing overview + detail dendrogram-matrix views. *IEEE Trans Vis Comput Graph* 2009;15(6):889–96. doi: 10.1109/TVCG.2009.130.

Christakos S, Dhawan P, Verstuyf A, Verlinden L, Carmeliet G. Vitamin D: metabolism, molecular mechanism of action, and pleiotropic effects. *Physiol Rev* 2016;96(1):365-408.

Christakos S. In search of regulatory circuits that control the biological activity of vitamin D. *J Biol Chem* 2017;292:17559–60.

Chun RF, Liu PT, Modlin RL, Adams JS, Hewison M. Impact of vitamin D on immune function: lessons learned from genome-wide analysis. *Front Physiol* 2014;5:151. doi:10.3389/fphys.2014.00151.

Clarke CJ, Haselden JN. Metabolic profiling as a tool for understanding mechanisms of toxicity. *Toxicol Pathol* 2008;36(1):140-7. doi: 10.1177/0192623307310947.

Clayton TA, Lindon JC, Cloarec O, Antti H, Charuel C, Hanton G, Provost J-P, Le Net J-L, Baker D, Walley RJ, Everett JR, Nicholson JK. Pharmaco-metabonomic phenotyping and personalized drug treatment. *Nature* 2006;440:1073-7. doi: 10.1038/nature04648.

Clish CB. Metabolomics: an emerging but powerful tool for precision medicine. *Cold Spring Harb Mol Case Stud* 2015;1:a000588. doi: 10.1101/mcs.a000588.

Contreras GA, Kabara E, Brester J, Neuder L, Kiupel M. Macrophage infiltration in the omental and subcutaneous adipose tissues of dairy cows with displaced abomasum. *J Dairy Sci* 2015;98:6176–87.

Cooper AJL, Pinto JT, Callery PS. Reversible and irreversible protein glutathionylation: biological and clinical aspects, *Expet Opin Drug Metabol Toxicol* 2011;7(7):891e910.

Cowley S, Ko M, Pick N, Chow R, Downing KJ, Gordhan BG, Betts JC, Mizrahi V, Smith DA, Stokes RW, Av-Gay Y. The *Mycobacterium tuberculosis* protein serine/threonine kinase PknG is linked to cellular glutamate/glutamine levels and is important for growth *in vivo*. *Mol Microbiol* 2004;52:1691–702. doi: 10.1111/j.1365-2958.2004.04085.x.

Cumming BM, Addicott KW, Adamson JH, Steyn AJ. *Mycobacterium tuberculosis* induces decelerated bioenergetic metabolism in human macrophages. *Elife* 2018;7:e39169. doi: 10.7554/eLife.39169.

Cuperlovic-Culf M, Cormier K, Touaibia M, Reyjal J, Robichaud S, Belbraouet M, Turcotte S. 1H NMR metabolomics analysis of renal cell carcinoma cells: Effect of VHL inactivation on metabolism. *Int J Cancer* 2016;138(10):2439-49. doi: 10.1002/ijc.29947.

Daigneault M, Preston JA, Marriott HM, Whyte MK, Dockrell DH. The identification of markers of macrophage differentiation in PMA-stimulated THP-1 cells and monocyte-derived macrophages. *PLoS One* 2010;5(1):e8668. doi: 10.1371/journal.pone.0008668.

Dang NA, Janssen HG, Kolk AH. Rapid diagnosis of TB using GC-MS and chemometrics. *Bioanalysis* 2013;5:3079–97.

Davis R, Mauer LJ. Fourier transform infrared (FT-IR) spectroscopy: a rapid tool for detection and analysis of foodborne pathogenic bacteria. *Curr Res Technol Educ Top Appl Microbiol Microb Biotechnol* 2010;2:1582–94.

Dayaram YK, Talaue MT, Connell ND, Venketaraman V. Characterization of a glutathione metabolic mutant of *Mycobacterium tuberculosis* and Its resistance to glutathione and nitrosoglutathione. *J Bacteriol* 2006;88(4):1364–72.

De Buck J, Shaykhutdinov R, Barkema HW, Vogel HJ. Metabolomic profiling in cattle experimentally infected with *Mycobacterium avium* subsp. paratuberculosis. *PLoS One* 2014;9:e111872.

De Jonge LP, Douma RD, Heijnen JJ, van Gulik WM. Optimization of cold methanol quenching for quantitative metabolomics of *Penicillium chrysogenum*. *Metabolomics* 2012;8(4):727-35.
De Koning W, van Dam K. A method for the determination of changes of glycolytic metabolites in yeast on a subsecond time scale using extraction at neutral pH. *Anal Biochem* 1992;204(1):118-23.

De Sousa JR, Da Costa Vasconcelos PF, Quaresma JAS. Functional aspects, phenotypic heterogeneity, and tissue immune response of macrophages in infectious diseases. *Infect Drug Resist* 2019;12:2589-611. doi: 10.2147/IDR.S208576.

De Villiers L, Loots DT. Using metabolomics for elucidating the mechanisms related to tuberculosis treatment failure. *Curr Metabolomics* 2013;1:306-17.

Dekeirsschieter J, Stefanuto P-H, Brasseur C, Haubruge E, Focant J-F. Enhanced characterization of the smell of death by comprehensive two-dimensional gas chromatography-time-of-flight mass spectrometry (GCxGC-TOFMS). *PLoS ONE* 2012;7(6): e39005. doi:10.1371/journal.pone.0039005.

Demarest H. Fundamental properties and the laws of nature. *Philos. Compass* 2015;10(5):334–44.

Dewan V, Reader J, Forsyth KM. Role of aminoacyl-tRNA synthetases in infectious diseases and targets for therapeutic development. *Top Curr Chem* 2014;344:293-329.

Diamandis EP, Sidransky D, Laird PW, Cairns P, Bapat B. Epigenomics-based diagnostics. *Clin Chem* 2010;56(8):1216-9. doi: 10.1373/clinchem.2010.148007.

Dimski DS. Ammonia metabolism and the urea cycle: function and clinical implications. *J Vet Intern Med* 1994;8:73-78.

Dini C, Bianchi A. The potential role of vitamin d for prevention and treatment of tuberculosis and infectious diseases. *Ann Ist Super Sanita* 2012;48(3):319-27.

Dong B, Jia J, Hu W, Chen Q, Jiang C, Pan J, Huang Y, Xue W, Gao H. Application of ^{1}H NMR metabonomics in predicting renal function recoverability after the relief of obstructive uropathy in adult patients. *Clin Biochem* 2013;46:346-53.

Draghici S, Khatri P, Eklund AC, Szallasi Z. Reliability and reproducibility issues in DNA microarray measurements. *Trends Genet* 2006;22:101–9.

Du Preez I, Loots DT. New sputum metabolite markers implicating adaptations of the host to *Mycobacterium tuberculosis*, and vice versa. *Tuberculosis (Edinb)* 2013; 93:330–7.

Du Preez I, Luies L, Loots DT. Metabolomics biomarkers for tuberculosis diagnostics: current status and future objectives. *BIomark Med* 2017; DOI: 10.2217/bmm-2016-0287.

Du Preez I, Luies L, Loots DT. The application of metabolomics toward pulmonary tuberculosis research. *Tuberculosis* 2019;115:126–39.

Du X, Fleiss B, Li H, D'angelo B, Sun Y, Zhu C, Hagberg H, Levy O, Mallard C, Wang X. Systemic stimulation of TLR2 impairs neonatal mouse brain development. *PLoS ONE* 2011;6(5): DOI: 10.1371/journal.pone.0019583.

Duft RG, Castro A, Chacon-Mikahil MPT, Cavaglieri CR. Metabolomics and Exercise: possibilities and perspectives. *Motriz Rio Claro* 2017;23(2):e101634.

Dunn WB, Ellis DI. Metabolomics: Current analytical platforms and methodologies. *TrAC* 2005;24:285-94.

Edfeldt K, Liu PT, Chun R, Fabri M, Schenk M, Wheelwright M, Keegan C, Krutzik SR, Adams JS, Hewison M, Modlin RL. T-cell cytokines differentially control human monocyte antimicrobial responses by regulating vitamin D metabolism. *Proc Natl Acad Sci U S A* 2010;107(52):22593-8. doi: 10.1073/pnas.1011624108.

Faghihzadeh F, Anaya NM, Schifman LA, Oyanedel-Craver V. Fourier transform infrared spectroscopy to assess molecular-level changes in microorganisms exposed to nanoparticles. *Nanotechnol Environ Eng* 2016;1:1. DOI 10.1007/s41204-016-0001-8.

Faijes M, Mars AE, Smid EJ. Comparison of quenching and extraction methodologies for metabolome analysis of *Lactobacillus plantarum. Microb Cell Fact* 2007;6:27. doi: 10.1186/1475-2859-6-27.

Feng S, Du YQ, Zhang L, Zhang L, Feng RR, Liu SY. Analysis of serum metabolic profile by ultra-performance liquid chromatography-mass spectrometry for biomarkers discovery: application in a pilot study to discriminate patients with tuberculosis. *Chin Med J (Engl)* 2015;128:159–68.

Fliser D, Novak J, Thongboonkerd V, Argiles A, Jankowski V, Girolami MA, Jankowski Jo, Mischak H. Advances in urinary proteome analysis and biomarker discovery. *J Am Soc Nephrol* 2007;18:1057–71.

Frediani JK, Jones DP, Tukvadze N, Uppal K, Sanikidze E, Kipiani M, Tran VT, Hebbar G, Walker DI, Kempker RR, Kurani SS, Colas RA, Dalli J, Tangpricha V, Serhan CN, Blumberg HM, Ziegler TR. Plasma metabolomics in human pulmonary tuberculosis disease: a pilot study. *PLoS One* 2014;9:e108854.

Frigault MM, Lacoste J, Swift JL, Brown CM. Live-cell microscopy - tips and tools. *J Cell Sci* 2009;22(Pt 6):753-67. doi: 10.1242/jcs.033837.

Gadakh B, Van Aerschot A. Aminoacyl-tRNA synthetase inhibitors as antimicrobial agents: A patent review from 2006 till present. *Expert Opin Ther Pat* 2012;22(12):1453-65.

Ganz T. Hepcidin and iron regulation, 10 years later. *Blood* 2011;17:4425–33.

Gao W-W, Wang Y, Zhang X-R, Yin C-Y, Hu C-M, Tian M, Wang H-W, Zhang X. Levels of $1,25(OH)_2D_3$ for patients with pulmonary tuberculosis and correlations of $1,25(OH)_2D_3$ with the clinical features of TB. *J Thorac Dis* 2014;6:760–64.

Garedew A, Henderson SO, Moncada S. Activated macrophages utilize glycolytic ATP to maintain mitochondrial membrane potential and prevent apoptotic cell death. *Cell Death Differ* 2010;17:1540-50.

Garg D, Sharma VK, Karnawat BS. Association of serum vitamin D with acute lower respiratory infection in Indian children under 5 years: a case control study. *Int J Contemp Pediatr* 2016;3:1164-69.

Garrett T, Abrahem R, Cao R, Gyurjian K, Islamoglu H, Lucero M, Martinez A, Paredes E, Salaiz O, Robinson B, Venketaraman V. Glutathione as a marker for human disease. *Adv Clin Chem.* 2018;87:141-59. doi: 10.1016/bs.acc.2018.07.004.

German JB, Hammock BD, Watkins SM. Metabolomics: building on a century of biochemistry to guide human health. *Metabolomics* 2005;1:3–9.

Gibney KB, MacGregor L, Leder K, Torresi J, Marshall C, Ebeling PR, Biggs BA. Vitamin D deficiency is associated with tuberculosis and latent tuberculosis infection in immigrants from Sub-Saharan Africa. *Clin Infect Dis* 2008;46:443-6. doi: 10.1086/525268.

Ginhoux F, Jung S. Monocytes and macrophages: developmental pathways and tissue homeostasis. *Nat Rev Immunol* 2014;14:392-404. doi: 10.1038/nri3671.

Giraldi GA, Rodrigues PS, Kitani EC, Sato JR, Thomaz CE. Statistical learning approaches for discriminant features selection. *J Braz Comp Soc* 2008;14:7-22.

Gleeson LE, Sheedy FJ, Palsson-McDermott EM, Triglia D, O'Leary SM, O'Sullivan MP, O'Neill LA, Keane J. Cutting edge: Mycobacterium tuberculosis induces aerobic glycolysis in human alveolar macrophages that is required for control of intracellular bacillary replication. *J Immunol* 2016;196:2444–9.

Gomez-Casati DF, Zanor MI, Busi MV. Metabolomics in plants and humans: Applications in the prevention and diagnosis of diseases. *Biomed Res Int* 2013;2013:792527. doi: 10.1155/2013/792527.

Goodacre R, Broadhurst D, Smilde AK, Kristal BS, Baker JD, Beger R, Bessant C, Connor S, Capuani G, Craig A, Ebbels T, Kell DB, Manetti C, Newton J, Paternostro G, Somorjai R, Sjostrom M, Trygg J, Wulfert F. Proposed minimum reporting standards for data analysis in metabolomics. *Metabolomics* 2007;3:231–41.

Goodacre R, Vaidyanathan S, Dunn WB, Harrigan GG, Kell DB. Metabolomics by numbers: acquiring and understanding global metabolite data. *Trends Biotechnol* 2004;22:245–52.

Gordon S, Taylor PR. Monocyte and macrophage heterogeneity. *Nat Rev Immunol* 2005 Dec;5(12):953-64. doi: 10.1038/nri1733.

Gough GA. The specific carbohydrate of the tubercle bacillus. *Biochem J* 1932;26:248–54.

Gouzy A, Poquet Y, Neyrolles O. Amino acid capture and utilization within the *Mycobacterium tuberculosis* phagosome. *Future Microbiol*. 2014;9(5):631-7.

Gouzy A, Poquet Y, Neyrolles O. Nitrogen metabolism in *Mycobacterium tuberculosis* physiology and virulence. *Nat Rev Microbiol* 2014; 12(11):729-37. doi: 10.1038/nrmicro3349.

Govindaraju V, Young K, Maudsley AA. Proton NMR chemical shifts and coupling constants for brain metabolites. *NMR Biomed* 2000;13:129–53.

Goyal N, Kashyap B, Singh N, Kaur IR. Neopterin and oxidative stress markers in the diagnosis of extrapulmonary tuberculosis. *Biomarkers* 2017;22(7):648–53.

Green RJ, Samy G, Miqdady MS, El-Hodhod M, Akinyinka OO, Saleh G, Haddad J, Alsaedi SA, Mersal AY, Edris A, Salah M. Vitamin D deficiency and insufficiency in Africa and the middle east, despite year-round sunny days. *S Afr Med J* 2015;105:603-5.

Gromski PS, Howbeer M, Ellis DI, Xu Y, Correa E, Turner ML, Goodacre R. A tutorial review: Metabolomics and partial least squares-discriminant analysis – a marriage of convenience or a shotgun wedding. *Anal Chim Acta* 2015;879:10-23.

Groves JT, Marla SS. Peroxynitrite-induced DNA strand scission mediated by a manganese porphyrin. *J Am Chem Soc* 1995;117:9578–9.

Guerra C, Johal K, Morris D, Moreno S, Alvarado O, Gray D, Tanzil M, Pearce D, Venketaraman V. Control of *Mycobacterium tuberculosis* growth by activated natural killer cells. *Clin Exp Immunol* 2012;168(1):142–52.

Guerra C, Morris D, Sipin A, Kung S, Franklin M, Gray D, Tanzil M, Guilford F, Khasawneh FT, Venketaraman V. Glutathione and adaptive immune responses against *Mycobacterium tuberculosis* infection in healthy and HIV infected individuals. *PLoS One* 2011;6(12):e28378. doi: 10.1371/journal.pone.0028378.

Guo J, Ye X-S. Protecting groups in carbohydrate chemistry: Influence on stereoselectivity of glycosylations. *Molecules* 2010;15:7235–65. doi: 10.3390/molecules15107235.

Gupta RS, Lo B, Son J. Phylogenomics and comparative genomic studies robustly support division of the genus *Mycobacterium* Into an emended genus *Mycobacterium* and four novel genera. *Front Microbiol* 2018;9:67. doi: 10.3389/fmicb.2018.00067.

Halouska S, Fenton RJ, Zinniel DK, Marshall DD, Barletta RG, Powers R. Metabolomics analysis identifies D-alanine-D-alanine ligase as the primary lethal target of D-cycloserine in mycobacteria. *J Proteome Res* 2014;13:1065–76.

Hampel A, Huber C, Geffers R, Spona-Friedl M, Eisenreich W, Bange F-C. *Mycobacterium tuberculosis* Is a Natural Ornithine Aminotransferase (rocD) mutant and depends on rv2323c for growth on arginine. *PLoS One* 2015;10(9):e0136914. doi: 10.1371/journal.pone.0136914

Handono K, Daramatasia W, Pratiwi, Sunarti S, Wahono S, Kalim H. Low level of vitamin D increased dendritic cell maturation and expression of interferon-γ and interleukin-4 in systemic lupus erythematosus. *J Pharm Biol Sci* 2012;2(4):37-43.

Hartung T, Daston G. Are *in vitro* tests suitable for regulatory use? *Toxicol Sci* 2009;111:233–37.

Hassanein EG, Mohamed EE, Baess AI, EL-Sayed ET, Yossef AM. The role of supplementary vitamin D in treatment course of pulmonary tuberculosis. *Egypt J Chest Dis Tuberc* 2016;65:629–35.

Hatzakis E. Nuclear magnetic resonance (NMR) spectroscopy in food science: A comprehensive review. *Compr Rev Food Sci Food Saf* 2019;18:189-220.

Haworth N, Kent PW, Stacey M. The constitution of a lipoid-bound polysaccharide from *M. tuberculosis*, human strain. *J Chem Soc* 1948;10:1220–4.

Heine G, Niesner U, Chang HD, Steinmeyer A, Zügel U, Zuberbier T, Radbruch A, Worm M. 1,25-dihydroxyvitamin D(3) promotes IL-10 production in human B cells. *Eur J Immunol* 2008; 38:2210-8.

Hellman Stina, Hjertner B, Morein B, Fossum C. The adjuvant G3 promotes a Th1 polarizing innate immune response in equine PBMC. *Vet Res* 2018;49:108. https://doi.org/10.1186/s13567-018-0602-2.

Hewison M. Vitamin D and immune function: an overview. *Proc Nutr Soc* 2012;71:50-61.

Hirayama D, Iida T, Nakase H. The phagocytic function of macrophage-enforcing innate immunity and tissue homeostasis. *Int J Mol Sci* 2018;19:92. doi:10.3390/ijms19010092.

Holeček M. Branched-chain amino acids in health and disease: Metabolism, alterations in blood plasma, and as supplements. *Nutr Metab (Lond)* 2018;15:33. doi: 10.1186/s12986-018-0271-1.

Holick MF. Medical progress: vitamin D deficiency. *N Engl J Med* 2007;357:266–81.

Howard MJ. Protein NMR spectroscopy. *Curr Biol* 1998;8(10):PR331-PR3. DOI:https://doi.org/10.1016/S0960-9822(98)70214-3.

Hu Q-H, Huang Q, Wang E-D. Crucial role of the C-terminal domain of *Mycobacterium tuberculosis* leucyl-tRNA synthetase in aminoacylation and editing. *Nucleic Acids Res* 2013;41(3):1859–72. doi: 10.1093/nar/gks1307.

Hussain SZ, Maqbool K. GC-MS: principle, technique and its application in food science. *Int J Curr Sci 2014*;13:E116-26.

Hussain T, Tan B, Yin Y, Blachier F, Tossou MCB, Rahu N. Oxidative stress and inflammation: What polyphenols can do for us? *Oxid Med Cell Longev* 2016;2016:7432797. doi: 10.1155/2016/7432797.

Jain SK, Micinski D. Vitamin D upregulates glutamate cysteine ligase and glutathione reductase, and GSH formation, and decreases ROS and MCP-1 and IL-8 secretion in high-glucose exposed U937 monocytes. *Biochem Biophys Res Commun* 2013;437(1):7–11.

Jamaati H, Mortaz E, Pajouhi Z, Folkerts G, Movassaghi M, Moloudizargari M, Adcock IM, Garssen J. Nitric oxide in the pathogenesis and treatment of tuberculosis. *Front Microbiol* 2017;8:2008. doi: 10.3389/fmicb.2017.02008.

Jax E, Wink M, Kraus RHS. Avian transcriptomics: opportunities and challenges. *J. Ornithol* 2018;159:599–629.

Jaye DL, Bray RA, Gebel HM, Harris WAC, Waller EK. Translational applications of flow cytometry in clinical practice. *J Immunol* 2012;188(10):4715-9. doi: 10.4049/jimmunol.1290017.

Johnson CH, Gonzalez FJ. Challenges and opportunities of metabolomics. *J Cell Physiol* 2012; 227:2975–81.

Johnson CH, Ivanisevic J, Siuzdak G. Metabolomics: beyond biomarkers and towards mechanisms. *Nat Rev Mol Cell Biol* 2016;17:451–59.

Jones G, Prosser DE, Kaufman M. 25-Hydroxyvitamin D-24-hydroxylase (CYP24A1): Its important role in the degradation of vitamin D. *Arch Biochem Biophys* 2012;523:9-18.

Kaiser JC, Heinrichs DE. Branching Out: Alterations in bacterial physiology and virulence due to branched-chain amino acid deprivation. *mBio* 2018;9:e01188-18. doi.org/10.1128/mBio.01188-18.

Kalantari S, Jafari A,2 Moradpoor R, Ghasemi E, Khalkhal E. Human urine proteomics: analytical techniques and clinical applications in renal diseases. *Int J Proteomics* 2015; http://dx.doi.org/10.1155/2015/782798.

Kalantri PP, Somani RR, Makhija DT. Raman spectroscopy: A potential technique in analysis of pharmaceuticals. *Der Chemica Sinica* 2010;1:1-12.

Kalinova B, Jiros P, Zd'arek J, Wen X, Hoskovec M. GC×GC/TOF MS technique—A new tool in identification of insect pheromones: Analysis of the persimmon bark borer sex pheromone gland. *Talanta* 2006;69:542–47.

Kanehisa M, Goto S. KEGG: Kyoto Encyclopedia of Genes and Genomes. *Nucleic Acids Res* 2000;1:28:27–30.

Kang JY, Nan X, Jin MS, Youn S-J, Ryu YH, Mah S, Han SH, Lee H, Paik S-G, Lee J-O. Recognition of lipopeptide patterns by toll-like receptor 2-toll-like receptor 6 heterodimer. *Immunity* 2009;31(6):873-84. doi: 10.1016/j.immuni.2009.09.018.

Katt ME, Placone AL, Wong AD, Xu ZS, Searson PC. *In vitro* tumor models: advantages, disadvantages, variables, and selecting the right platform. *Bioeng Biotechnol* 2016; 4:12. doi: 10.3389/fbioe.2016.00012.

Kearns MD. The role of vitamin D in tuberculosis. *J Clin Transl Endocrinol* 2014;1(4):167–69.

Kell DB, Oliver SG. The metabolome 18 years on: a concept comes of age. *Metabolomics* 2016;12:148. DOI 10.1007/s11306-016-1108-4.

Kelly B, Tannahill GM, Murphy MP, O'Neill LAJ. Metformin inhibits the production of reactive oxygen species from NADH:Ubiquinone oxidoreductase to limit induction of interleukin-1β (IL-1β) and boosts interleukin-10 (IL-10) in lipopolysaccharide (LPS)-activated macrophages. *J Biol Chem* 2015;290(33):20348-59. doi: 10.1074/jbc.M115.662114.

Kennel KA, Drake MT, Hurley DL. Vitamin D Deficiency in Adults: When to Test and How to Treat. *Mayo Clin Proc* 2010;85:752–58. doi: 10.4065/mcp.2010.0138.

Khammissa RAG, Fourie J, Motswaledi MH, Ballyram R, Lemmer J, Feller L. The biological activities of vitamin d and its receptor in relation to calcium and bone homeostasis, cancer, immune and cardiovascular systems, skin biology, and oral health. *Biomed Res Int* 2018; 2018:9276380. doi: 10.1155/2018/9276380.

Kim GL, Lee S, Luong TT, Nguyen CT, Park SS, Pyo S, Rhee DK. Effect of decreased BCAA synthesis through disruption of *ilvC* gene on the virulence of Streptococcus pneumoniae. *Arch Pharm Res* 2017;40:921-32.

Kim K, Yeom S. Investigation on the growth of green bean sprouts with linear discriminant analysis. *International Journal of Fuzzy Logic and Intelligent Systems* 2017;17(4):315-22.

Kinoshita Y, Uo T, Jayadev S, Garden GA, Conrads TP, Veenstra TD, Morrison RS. Potential applications and limitations of proteomics in the study of neurological disease. *Arch Neurol. 2006*;63:1692-96.

Kirkwood JS, Maier C, Stevens JF. Simultaneous, untargeted metabolic profiling of polar and non-polar metabolites by LC-Q-TOF mass spectrometry. *Curr Protoc Toxicol* 2013;4: 4.39. doi:10.1002/0471140856.tx0439s56.

Klee MS, Blumberg LM. Theoretical and practical aspects of fast gas chromatography and method translation. *J Chromatogr Sci* 2002;40:234-47.

Knijnenburg TA, Roda O, Wan Y, Nolan GP, Aitchison JD, Shmulevich, I. A regression model approach to enable cell morphology correction in high-throughput flow cytometry. *Mol Syst Biol* 2011;7:531. doi: 10.1038/msb.2011.64.

Kochupillai N. The physiology of vitamin D: current concepts. *Indian J Med Res* 2008;127:256-62.

Kocic G, Nikolic J, Jevtovic-Stoimenov T, Sokolovic D, Kocic H, Cvetkovic T, Pavlovic D, Cencic A, Stojanovic D. L-arginine intake effect on adenine nucleotide metabolism in rat parenchymal and reproductive tissues. *Sci World J* 2012;2012:208239. doi: 10.1100/2012/208239.

Korn T, Oukka M, Kuchroo V, Bettelli E. Th17 cells: Effector T cells with inflammatory properties. *Semin Immunol* 2007;19(6):362–71.

Kostidis S, Addie RD, Morreau H, Mayboroda OA, Giera M. Quantitative NMR analysis of intra- and extracellular metabolism of mammalian cells: A tutorial. *Anal Chim Acta* 2017;980:1-24. doi: 10.1016/j.aca.2017.05.011.

Kovalenko OP, Volynets GP, Rybak MY, Starosyla SA, Gudzera OI, Lukashov SS, Bdzhola VG, Yarmoluk SM, Boshoff HI Tukalo MA. Dual-target inhibitors of mycobacterial aminoacyl-tRNA synthetases among N-benzylidene-N'-thiazol-2-yl-hydrazines. *Med Chem Commun* 2019;10:2161–9.

Kuehnbaum NL, Britz-McKibbin P. New advances in separation science for metabolomics: Resolving chemical diversity in a post-genomic era. *Chem Rev* 2013;113:2437–68.

Kuhn M, von Mering C, Campillos M, Jensen LJ, Bork P. STITCH: Interaction networks of chemicals and proteins. *Nucleic Acids Res* 2008;36:D684–D8. doi:10.1093/nar/gkm795.

Kulie T, Groff A, Redmer J, Hounshell J, Schrager S. Vitamin D: an evidence-based review. *J Am Board Fam Med* 2009;22:698-706.

Kupiec T. Quality control Analytical Methods: Gas Chromatography. *Int J Pharm Comp* 2004;8:305-9.

Larrick JW, Fischer DG, Anderson SJ, Koren HS. Characterization of a human macrophage-like cell line stimulated in vitro: A model of macrophage functions. *J Immunol* 1980;125:6-12.

Lauri I, Savorani F, Iaccarino N, Zizza P, Pavone LM, Novellino E, Engelsen SB, Randazzo A. Development of an optimized protocol for NMR metabolomics studies of human colon cancer cell lines and first insight from testing of the protocol using DNA G-Quadruplex ligands as novel anti-cancer drugs. *Metabolites* 2016;4. doi:10.3390/metabo6010004.

Lazar AG, Romanciuc F, Socaciu MA, Socaciu C. Bioinformatics tools for metabolomic data processing and analysis using untargeted liquid chromatography coupled with mass spectrometry. *Bull Univ Agric Sci Vet Med* 2015;72:103-115.

Lee SK, Chwee JY, Ma CAP, Le Bert N, Huang CW, Gasser S. Synergistic anticancer effects of Pam_3CSK_4 and Ara-C on B-cell Lymphoma Cells. *Clin Cancer Res* 2014;20:3485-95.

Lehtonen A, Ahlfors H, Veckman V, Miettinen M, Lahesmaa R, Julkunen I. Gene expression profiling during differentiation of human monocytes to macrophages or dendritic cells. *J Leukoc Biol* 2007;82:710-20.

Leloir LF. The enzymatic transformation of uridine diphosphate glucose into a galactose derivative. *Arch Biochem Biophys* 1951;33(2):186-90. doi: 10.1016/0003-9861(51)90096-3.

Likić VA, McConville MJ, Lithgow T, Bacic A. Systems biology: the next frontier for bioinformatics. *Adv Bioinformatics* 2010;2010:268925. doi: 10.1155/2010/268925.

Liu G, Hale GE, Hughes CL. Galactose metabolism and ovarian toxicity. *Reprod Toxicol* 2000;14:377–84.

Liu J, Li Z, Liu H, Wang X, Lv C, Wang R, Zhang D, Li Y, Du X, Li Y, Wang B, Huang Y. Metabolomics-based clinical efficacy and effect on the endogenous metabolites of tangzhiqing tablet, a chinese patent medicine for type 2 diabetes mellitus with hypertriglyceridemia. *Evid Based Complement Alternat Med* 2018;2018:5490491. doi: 10.1155/2018/5490491.

Liu PT, Schenk M, Walker VP, Dempsey PW, Kanchanapoomi M, Wheelwright M, Vazirnia A, Zhang X, Steinmeyer A, Zügel U, Hollis BW, Cheng G, Modlin RL. Convergence of IL-1beta and VDR activation pathways in human TLR2/1-induced antimicrobial responses. *PLoS One* 2009; 4: e5810. doi: 10.1371/journal.pone.0005810.

Liu PT, Stenger S, Li H, Wenzel L, Tan BH, Krutzik SR, Ochoa MT, Schauber J, Wu K, Meinken C, Kamen DL, Wagner M, Bals R, Steinmeyer A, Zügel U, Gallo RL, Eisenberg D, Hewison M, Hollis BW, Adams JS, Bloom BR, Modlin RL. Toll-like receptor triggering of a vitamin D-mediated human antimicrobial response. *Science* 2006;311:1770-3.

Lobel L, Sigal N, Borovok I, Belitsky BR, Sonenshein AL, Herskovits AA. The metabolic regulator CodY links *Listeria monocytogenes* metabolism to virulence by directly activating the virulence regulatory gene *prfA*. *Mol Microbiol* 2015;95(4):624–44. doi:10.1111/mmi.12890.

Loo LH, Lin HJ, Singh DK, Lyons KM, Altschuler SJ, Wu LF. Heterogeneity in the physiological states and pharmacological responses of differentiating 3T3-L1 preadipocytes. *J Cell Biol* 2009;187(3):375-84. doi: 10.1083/jcb.200904140.

Looker AC, Johnson CL, Lacher DA, Pfeiffer CM, Schleicher RL, Sempos CT. Vitamin D status: United States, 2001-2006. *NCHS data brief* 2011;(59):1-8.

Loots T. An altered Mycobacterium tuberculosis metabolome induced by *katG* mutations resulting in isoniazid resistance. *Antimicrob Agents Chemother* 2014;58:2144–9.

Lorincz AT. The promise and the problems of epigenetics biomarkers in cancer. *Expert Opin Med Diagn* 2011;5:375-9.

Lu J. NMR in biomedical research. *Mater methods* 2013;3:170.

Lu SC. Regulation of glutathione synthesis. *Mol Aspects Med* 2009;30(1-2):42–59. doi: 10.1016/j.mam.2008.05.005

Lu W, Su X, Klein MS, Lewis IA, Fiehn O, Rabinowitz JD. Metabolite measurement: pitfalls to avoid and practices to follow. *Annu Rev Biochem* 2017;86:277-304. doi: 10.1146/annurev-biochem-061516-044952.

Luiking YC, Steens L, Poeze M, Ramsay G, Deutz NEP. Low plasma arginine concentration in septic patients is related to diminished *de novo* arginine production from citrulline. *Clin Nutr* 2003;22(1). DOI: 10.1016/S0261-5614(03)80098-5.

Lyon RH, Hall WH, Costas-Martinez C. Utilization of amino acids during growth of *Mycobacterium tuberculosis* in rotary cultures. *Infect Immun* 1970;1(6):513-20.

Mahapatra S, Hess AM, Johnson JL, Eisenach KD, DeGroote MA, Gitta P, Joloba ML, Kaplan G, Walzl G, Boom WH, Belisle JT. A metabolic biosignature of early response to anti-tuberculosis treatment*. BMC Infect Dis* 2014;14:53.

Marcuello M, Mayol X, Felipe-Fumero E, Costa J, López-Hierro L, Salvans S, Alonso S, Pascual M, Grande L, Pera M. Modulation of the colon cancer cell phenotype by pro-inflammatory macrophages: A preclinical model of surgery-associated inflammation and tumor recurrence. *PLoS One* 2018;13(2):e0192958. doi: 10.1371/journal.pone.0192958.

Mari M, 1 Colell A, Morales A, von Montfort C, Garcia-Ruiz C, Fernandez-Checa JC. Redox control of liver function in health and disease. *Antioxid Redox Signal* 2010;12(11):1295-331. doi: 10.1089/ars.2009.2634.

Marion D. An introduction to biological NMR spectroscopy. *Mol Cell Proteomics* 2013;12(11):3006–25. doi: 10.1074/mcp.O113.030239.

Markley JL, Brüschweiler R, Edison AS, Eghbalnia HR, Powers R, Raftery D, Wishart DS. The future of NMR-based metabolomics. *Curr Opin Biotechnol* 2017;43:34–40.

Marques CD, Dantas AT, Fragoso TS, Duarte AL. The importance of vitamin D levels in autoimmune diseases. *Bras J Rheumatl* 2010;50:67-80.

Marre ML, Petnicki-Ocwieja T, DeFrancesco AS, Darcy, CT, Hu LT. Human integrin α3β1 regulates TLR2 recognition of lipopeptides from endosomal compartments. *PLoS ONE* 2010; 5(9):e12871.

Matheson LA, Fairbank NJ, Maksym GN, Paul Santerre, J. Labow, RS. Characterization of the Flexcell Uniflex cyclic strain culture system with U937 macrophage-like cells. *Biomaterials* 2006;27:226–33.

Matta SK, Kumar D. Hypoxia and classical activation limits *Mycobacterium tuberculosis* survival by Akt-dependent glycolytic shift in macrophages. *Cell Death Discov* 2016;2:16022. doi: 10.1038/cddiscovery.2016.22.

McWhortera FY, Wanga T, Nguyena P, Chunga T, Liua WF. Modulation of macrophage phenotype by cell shape. *PNAS* 2013;10:17253–8.

Mendoza-Coronel E, Castanon-Arreola M. Comparative evaluation of in vitro human macrophage models for mycobacterial infection study. *Pathogens and Disease* 2016;74(6): doi: 10.1093/femspd/ftw052.

Mengual-Macenlle N, Marcos PJ, Golpe R, González-Rivas D. Multivariate analysis in thoracic research. *J Thorac Dis* 2015;7(3):E2–E6. doi: 10.3978/j.issn.2072-1439.2015.01.43.

Mesri M. Advances in proteomic technologies and its contribution to the field of cancer. *Adv Med* 2014; http://dx.doi.org/10.1155/2014/238045.

Meyer, V. (2015) *Vitamin D, genetic variation of the vitamin D pathway and methylation of the vitamin D receptor gene: functional impact on the innate immune response to the mycobacterial lipopeptide Pam_3CSK_4*. PhD. (Biochemistry). [Unpublished]: University of Johannesburg. Retrieved from: https://ujcontent.uj.ac.za/vital/access/manager/Index?site_name=Research%20Output (Accessed: May 2019)

Mickiewicz B, Duggan GE, Winston BW, Doig C, Kubes P, Vogel HJ. Metabolic profiling of serum samples by 1H nuclear magnetic resonance spectroscopy as a potential diagnostic approach for septic shock. *Crit Care Med* 2014;42(Online supplementary):E1-E13.

Mills CD. M1 and M2 macrophages: Oracles of health and disease. *Crit Rev Immunol* 2012; 32(6):463-88.

Mirsaeidi M, Banoei MM, Winston BW, Schraufnagel DE. Metabolomics: applications and promise in mycobacterial disease. *Ann Am Thorac Soc* 2015;12(9):1278–87.

Mizrahi V, Warner DF. Death of *Mycobacterium tuberculosis* by L-Arginine starvation. *Proc Natl Acad Sci U S A* 2018;115:9658-60.

Mogilevsky G, Borland L, Brickhouse M, Fountain III AW. Raman spectroscopy for homeland security applications. *Int J Spectrosc* 2012; doi:10.1155/2012/808079.

Mohler RE, Dombek KM, Hoggard JC, Young ET, Synovec RE. Comprehensive two-dimensional gas chromatography time-of-flight mass spectrometry analysis of metabolites in fermenting and respiring yeast cells. *Anal Chem* 2006;78:2700–9.

Mohod K, Gangane N, Kumar S. Oxidants and antioxidants in lymph node tuberculosis. *J MGIMS* 2008;13:35–41.

Moradi SV, Hussein WM, Varamini P, Simerska P, Toth I. Glycosylation, an effective synthetic strategy to improve the bioavailability of therapeutic peptides. *Chem Sci* 2016;7:2492–500.

Morris CR, Hamilton-Reeves J, Martindale RG, Sarav M, Gautier JBO. Acquired amino acid deficiencies: A focus on arginine and glutamine. *Nutr Clin Pract*. 2017;32(1_suppl):30S-47S. doi: 10.1177/0884533617691250.

Murayama C, Kimura Y, Setou M. Imaging mass spectrometry: principle and application. *Biophys Rev* 2009;1:131. doi: 10.1007/s12551-009-0015-6.

Nägele T. Linking metabolomics data to underlying metabolic regulation. *Front Mol Biosci 2014*;1:22. doi: 10.3389/fmolb.2014.00022.

Negro M, Giardina S, Marzani B, Marzatico F. Branched-chain amino acid supplementation does not enhance athletic performance but affects muscle recovery and the immune system. *J Sports Med Phys Fitness* 2008;48:347–51.

Nicholson JK, Lindon JC, Holmes E. 'Metabonomics': understanding the metabolic responses of living systems to pathophysiological stimuli via multivariate statistical analysis of biological NMR spectroscopic data. *Xenobiotica* 1999;29:1181–9.

Nie C, He T, Zhang W, Zhang G, Ma X. Branched chain amino acids: Beyond nutrition metabolism. *Int J Mol Sci* 2018;19(4):954. doi: 10.3390/ijms19040954.

Nighat H, Abdul Ghaffare N, Khalid Mehmood A.Khan. Frequency nutritional rickets in children admitted with severe pneumonia. *J Pak Med Assoc* 2010;60:729-32.

Nyirenda MH, Crooks J, Gran B. The role of toll-like receptors in multiple sclerosis and experimental autoimmune encephalomyelitis, in Yamamura T, Gran B. (eds.), *Multiple Sclerosis Immunology*. Springer Science+Business Media: New York; 2008. pp. 149-76.

O'Neill LA, Hardie DG. Metabolism of inflammation limited by AMPK and pseudo-starvation. *Nature* 2013;493:346–55.

Okhovat-Isfahani B, Bitaraf S, Mansournia MA, Doosti-Irani A. Inequality in the global incidence and prevalence of tuberculosis (TB) and TB/HIV according to the human development index. *Med J Islam Repub Iran* 2019;33:45. doi: 10.34171/mjiri.33.45.

Oliver SG, Winson MK, Kell DB, Baganz F. Systematic functional analysis of the yeast genome. *Trends in biotechnology* 1998;16:373–8.

Oña-Ruales JO, Wilson WB, Nalin F, Sander LC, Schubert-Ullrich P, Wise SA. The influence of the aromatic character in the gas chromatography elution order: the case of polycyclic aromatic hydrocarbons. *Mol Phys* 2016;114:3533-45.

Osman SA, Saeed WSE, Musa AM, Younis BM, Bashir AEA, Idris FEM, Ahmed AEH, Khalil EAG. Prevalence of latent tuberculosis Infection (LTBI) among household contacts of Sudanese patients with pulmonary tuberculosis in Eastern Sudan: Revisiting the tuberculin skin test. *J Tuberc Res* 2017;5:69-76.

Owens DJ, Allison R, Close GL. Vitamin D and the athlete: current perspectives and new challenges. *Sports Med* 2018;848(Suppl 1):3-16. doi: 10.1007/s40279-017-0841-9.

Pagliara P, Lanubile R, Dwikat M, Abbro L, Dini L. Differentiation of monocytic U937 cells under static magnetic field exposure. *Eur J Histochem* 2005;49:75-86.

Palomino JC. Nonconventional and new methods in the diagnosis of tuberculosis: feasibility and applicability in the field. *Eur Respir J* 2005;26:339-50.

Passmore JS, Lukey PT, Ress SR. The human macrophage cell line U937 as an in vitro model for selective evaluation of mycobacterial antigen-specific cytotoxic T-cell function. *Immunology* 2001;102:146-56.

Patel RS, Roy M, Dutta GK. Mass spectrometry- A review. *Vet World* 2012;5:185-92.

Patterson A, Fennington K, Bayha R, Wax D, Hirschberg R, Boyd N, Kurilla M. Biocontainment laboratory risk assessment: perspectives and considerations. *Pathog Dis* 2014;71(2):102-8.

Patterson DG, Welch SM, Turner WE, Sjodin A, Focant JF. Cryogenic zone compression for the measurement of dioxins in human serum by isotope dilution at the attogram level using modulated gas chromatography coupled to high resolution magnetic sector mass spectrometry? *J Chromatogr A 2011*;1218:3274–81.

Perwad F, Portale AA. Vitamin D metabolism in the kidney: regulation by phosphorus and fibroblast growth factor 23. *Mol Cell Endocrinol* 2011;347:17–24.

Peteroy-Kelly MA, Venketaraman V, Talaue M, Seth A, Connell ND. Modulation of J774.1 macrophage L-arginine metabolism by Intracellular *Mycobacterium bovis* BCG. *Infect Immun* 2003;71(2):1011–5.

Pinu FR, Villas-Boas SG, Aggio R. Analysis of intracellular metabolites from microorganisms: quenching and extraction protocols. *Metabolites* 2017;7(4):53.doi: 10.3390/metabo7040053.

Platell C, Kong S-E, McCauley R, Hall JC. Branched-chain amino acids. *J Gastroenterol Hepatol* 2000;15:706–17.

Prietl B, Treiber G, Pieber TR, Amrein K. Vitamin D and immune function. *Nutrients* 2013;5: 2502–21.

Pugin J, Dunn I, Jolliet P, Tassaux D, Magnenat JL, Nicod LP, Chevrolet JC. Activation of human macrophages by mechanical ventilation in vitro. *Am J Physiol* 1998;275:L1040–L50.

Purnamasari D, Soewondo P, Djauzi S. The adaptive immune response in graves' disease: does vitamin D have a role? *JAFES* 2014;29:8-16.

Raamsdonk LM, Teusink B, Broadhurst D, Zhang N, Hayes A, Walsh MC, Berden JA, Brindle KM, Kell DB, Rowland JJ, Westerhoff HV, van Dam K, Oliver SG. A functional genomics strategy that uses metabolome data to reveal the phenotype of silent mutations. *Nat Biotechnol* 2001;19:45-50.

Ramsden JJ. Metabolomics and Metabonomics, in *Bioinformatics. Computational Biology.* London: Springer; 2009. pp. 257-9.

Raoult D, Leone M, Roussel Y, Rolain JM. Attributable deaths caused by infections with antibiotic-resistant bacteria in France. *Lancet Infect Dis* 2019;19:128-9.

Ratledge C. The physiology of the mycobacteria. *Adv Microb Physiol* 1976;13:115–244.

Regmi S, Regmi AP, Adhikari S, Shakya D. Prevalence of vitamin D deficiency/insufficiency among children and adolescents. *JCMC* 2017;7:11-15.

Ren S, Hinzman AA, Kang EL, Szczesniak V, Lu LJ. Computational and statistical analysis of metabolomics data. *Metabolomics* 2015;11:1492–1513.

Riekeberg E, Powers R. New frontiers in metabolomics: From measurement to insight. *F1000Research* 2017;6(F1000 Faculty Rev):1148.

Roberts J, Middleton A. Genetics in the 21st Century: Implications for patients, consumers and citizens. *F1000Res* 2017 [revised 2018];6:2020. doi: 10.12688/f1000research.12850.2. eCollection 2017.

Rocha SM, Coelho E, Zrostlıkova J, Delgadillo I, Coimbra MA. Comprehensive two-dimensional gas chromatography with time-of-flight mass spectrometry of monoterpenoids as a powerful tool for grape origin traceability. *J Chromatogr A* 2007;1161:292–9.

Rockett K, Brookes R, Udalova I, Vidal V, Hill AV, Kwiatkowski D. 1,25-Dihydroxyvitamin D3 induces nitric oxide synthase and suppresses growth of *Mycobacterium tuberculosis* in a human macrophage-like cell line. *Infect Immun* 1998;66:5314–21.

Rosales C, Uribe-Querol E. Phagocytosis: A fundamental process in immunity. *Biomed Res Int.* 2017; 2017:9042851. doi: 10.1155/2017/9042851.

Rosen CJ, Adams JS, Bikle DD, Black DM, Demay MB, Manson JE, Murad MH, Kovacs CS. The nonskeletal effects of vitamin D: an Endocrine Society scientific statement. *Endocr Rev* 2012; 33:456-92.

Saccenti E, Hoefsloot HC, Smilde AK, Westerhuis JA, Hendriks MM. Reflections on univariate and multivariate analysis of metabolomics data. *Metabolomics* 2014;10:361–74.

Salahuddin N, Ali F, Hasan Z, Rao N, Aqeel M, Mahmood F. Vitamin D accelerates clinical recovery from tuberculosis: results of the SUCCINCT Study [Supplementary Cholecalciferol in recovery from tuberculosis]. A randomized, placebo-controlled, clinical trial of vitamin D supplementation in patients with pulmonary tuberculosis'. *BMC Infect Dis* 2013;13:22. doi: 10.1186/1471-2334-13-22.

Salamon H, Bruiners N, Lakehal K, Shi L, Ravi J, Yamaguchi KD, Pine R, Gennaro ML. Cutting edge: vitamin D regulates lipid metabolism in mycobacterium tuberculosis infection. *J Immunol*. 2014;193(1):30-34. doi: 10.4049/jimmunol.1400736.

Santos ADC, Dutra LM, Menezes LRA, Santos MFC, Barison A. Forensic NMR spectroscopy: Just a beginning of a promising partnership. *TrAC* 2018;107;31-42.

Santos GC, Zeidler JD, Pérez-Valencia JA, Sant'Anna-Silva AC, Da Poian AT, El-Bacha T, Almeida FCL. Metabolomic Analysis Reveals Vitamin D-induced Decrease in Polyol Pathway and Subtle Modulation of Glycolysis in HEK293T Cells. *Sci Rep* 2017;7:9510. doi: 10.1038/s41598-017-10006-9.

Scalbert A, Brennan L, Fiehn O, Hankemeier T, Kristal BS, van Ommen B, Pujos-Guillot E, Verheij, E, Wishart D, Wopereis S. Mass-spectrometry-based metabolomics: Limitations and recommendations for future progress with particular focus on nutrition research. *Metabolomics* 2009;5:435–58.

Schrimpe-Rutledge AC, Codreanu SG, Sherrod SD, McLean JA. Untargeted metabolomics strategies—challenges and emerging directions. *J Am Soc Mass Spectrom* 2016; 27:1897Y1905. DOI: 10.1007/s13361-016-1469-y.

Schromm AB, Howe J, Ulmer AJ, Wiesmüller KH, Seyberth T, Jung G, Rössle M, Koch MH, Gutsmann T, Brandenburg K. Physicochemical and biological analysis of synthetic bacterial lipopeptides: validity of the concept of endotoxic conformation. *J Biol Chem* 2007;282:11030-37.

Schymanski EL, Jeon J, Gulde R, Fenner K, Ruff M, Singer HP, Hollender J. Identifying small molecules via high resolution mass spectrometry: communicating confidence. *Environ Sci Technol* 2014;48(4):2097-8. doi: 10.1021/es5002105.

Sedghipour MR, Sadeghi-Bazargani H. Applicability of supervised discriminant analysis models to analyze astigmatism clinical trial data. *Clin Ophthalmol* 2012; 6: 1499-506. doi: 10.2147/OPTH.S34907.

Sellick CA, Hansen R, Stephens GM, Goodacre R, Dickson AJ. Metabolite extraction from suspension-cultured mammalian cells for global metabolite profiling. *Nat Protoc* 2011; 6:1241-9.

Serkova NJ, Standiford TJ, Stringer KA. The emerging field of quantitative blood metabolomics for biomarker discovery in critical illnesses. *Am J Respir Crit Care Med* 2011;184:647-55.

Shastri MD, Shukla SD, Chong WC, Dua K, Peterson GM, Patel RP, Hansbro PM, Eri R, O'Toole RF. Role of oxidative stress in the pathology and management of human tuberculosis. *Oxid Med Cell Longev* 2018; doi: 10.1155/2018/7695364.

Shi L, Salamon H, Eugenin EA, Pine R, Cooper A, Gennaro ML. Infection with *Mycobacterium tuberculosis* induces the warburg effect in mouse lungs. *Sci Rep* 2015;5:18176. doi: 10.1038/srep18176.

Shi L, Sohaskey CD, Kana BD, Dawes S, North RJ, Mizrahi V, Gennaro ML. Changes in energy metabolism of *Mycobacterium tuberculosis* in mouse lung and under in vitro conditions affecting aerobic respiration. *PNAS* 2005;102(43):15629–34.

Shiker MAK. Multivariate statistical analysis. *BJS* 2012;6(1):55-66.

Shimomura Y, Harris RA. Metabolism and physiological function of branched-chain amino acids: discussion of session 1. *J Nutr* 2006;136(1):232S–3S. doi.org/10.1093/jn/136.1.232S.

Shin JH, Yang JY, Jeon BY, Yoon YJ, Cho SN, Kang YH, Ryu DH, Hwang GS. (1)H NMR-based metabolomic profiling in mice infected with *Mycobacterium tuberculosis. J Proteome Res* 2011;10:2238-47.

Shin MH, Lee DY, Liu KH, Fiehn O, Kim KH. Evaluation of sampling and extraction methodologies for the global metabolic profiling of *Saccharophagus degradans*. *Anal Chem* 2010;82(15):6660-6. doi: 10.1021/ac1012656.

Shu MH, Appleton D, Zandi K, AbuBakar S. Anti-inflammatory, gastroprotective and anti-ulcerogenic effects of red algae *Gracilaria changii* (gracilariales, rhodophyta) extract. *BMC Complement Altern Med* 2013;13:61. doi:10.1186/1472-6882-13-61.

Skoog DA, Holler FJ, Crouch SR. *Principles of instrumental analysis.* 7th ed. USA: Cengage learning; 2018. pp. 726-45.

Slauch JM. How does the oxidative burst of macrophages kill bacteria? Still an open question. *Mol Microbiol* 2011;80(3):580–3. doi: 10.1111/j.1365-2958.2011.07612.x.

Sneddon J, Masuram S, Richert JC. Gas chromatography-mass spectrometry-basic principles, instrumentation and selected applications for detection of organic compounds. *Anal Lett* 2007;40:1003–12.

Snow NH, Sinex J, Danser M. Multiple dimensions of separations: SPME with GCxGC and GCxGC–TOF-MS. *LC GC Eur* 2010;23:260–267.

Sömjen D, Binderman I, Weisman Y. The effects of 24R,25-dihydroxycholecalciferol and of 1 alpha,25-dihydroxycholecalciferol on ornithine decarboxylase activity and on DNA synthesis in the epiphysis and diaphysis of rat bone and in the duodenum. *Biochem J* 1983;214(2):293–8. doi: 10.1042/bj2140293.

Song BJ, Akbar M, Abdelmegeed MA, Byun K, Lee B, Yoon SK, Hardwick JP. Mitochondrial dysfunction and tissue injury by alcohol, high fat, nonalcoholic substances and pathological conditions through post-translational protein modifications. *Redox Biol* 2014;3:109-23.

Song MG, Ryoo IG, Choi HY, Choi BH, Kim ST, Heo TH, Lee JY, Park PH, Kwak MK. NRF2 signaling negatively regulates phorbol-12-myristate-13-acetate (PMA)-induced differentiation of human monocytic U937 cells into pro-inflammatory macrophages. *PLoS ONE* 2015;10(7): e0134235. doi:10.1371/journal.pone.0134235.

Soto R, Perez-Herran E, Rodriguez B, Duma BM, Cacho-Izquierdo M, Mendoza-Losana A, Lelievre J, Aguirre DB, Ballell L, Cox LR, Alderwick LJ, Besra GS. Identification and characterization of aspartyl-tRNA synthetase inhibitors against *Mycobacterium tuberculosis* by an integrated whole-cell target-based approach. *Sci Rep* 2018;8:12664. doi: 10.1038/s41598-018-31157-3.

Soto-Ramirez MD, Aguilar-Ayala DA, Garcia-Morales L, Rodriguez-Peredo SM, Badillo-Lopez C, Rios-Muñiz DE, Meza-Segura MA, Rivera-Morales GY, Leon-Solis L, Cerna-Cortes JF, Rivera-Gutierrez S, Helguera-Repetto AC, Gonzalez-Y-Merchand JA. Cholesterol plays a larger role during *Mycobacterium tuberculosis in vitro* dormancy and reactivation than previously suspected. *Tuberculosis (Edinb)* 2017;103:1-9. doi: 10.1016/j.tube.2016.12.004.

Souberbielle JC. Epidemiology of vitamin-D deficiency. *Geriatr Psychol Neuropsychiatr Vieil* 2016;14:7–15.

Spanik I, Janacova A, Susterova Z, Jakubik T, Janoskova N, Novak P, Chlebo R. Characterisation of VOC composition of Slovak monofloral honeys by GCxGC–TOF-MS. *Chem Papers* 2012;67: DOI: 10.2478/s11696-012-0254-z.

Sprangers S, de Vries TJ, Everts V. Monocyte heterogeneity: consequences for monocyte-derived immune cells. *J Immunol Res* 2016;2016:1475435. doi: 10.1155/2016/1475435.

Steuer AE, Brockbals L, Kraemer T. Metabolomic strategies in biomarker research–new approach for indirect identification of drug consumption and sample manipulation in clinical and forensic toxicology? *Front Chem* 2019;7:319. doi: 10.3389/fchem.2019.00319.

Strefford JC, Foot NJ, Chaplin T, Neat MJ, Oliver RT, Young BD, Jones LK. The characterisation of the lymphoma cell line U937, using comparative genomic hybridisation and multi-plex FISH. *Cytogenet Cell Genet* 2001;94:9-14.

Subramani E, Jothiramajayam M, Dutta M, Chakravorty D, Joshi M, Srivastava S, Mukherjee A, DattaRay C, Chakravarty BN, Chaudhury K. NMR-based metabonomics for understanding the influence of dormant female genital tuberculosis on metabolism of the human endometrium. *Hum Reprod* 2016;31:854–65.

Sumner LW, Amberg A, Barrett D, Beale MH, Beger R, Daykin CA, Fan TWM, Fiehn O, Goodacre R, Griffin JL, Hankemeier T, Hardy N, Harnly J, Higashi R, Kopka J, Lane AN, Lindon JC, Marriott P, Nicholls AW, Reily MD, Thaden JJ, Viant MR. Proposed minimum reporting standards for chemical analysis Chemical Analysis Working Group (CAWG) Metabolomics Standards Initiative (MSI). *Metabolomics* 2007;3:211–21.

Sundstrom C, Nilsson K. Establishment and characterization of a human histiocytic lymphoma cell line (U-937). *Int J Cancer* 1976;17:565-77.

Talat N, Perry S, Parsonnet J, Dawood G, Hussain R. Vitamin D deficiency and tuberculosis progression. *Emerg Infect Dis* 2010;16:853–5.

Thacher TD, Clarcke BL. Vitamin D Insufficiency. *Mayo Clin Proc* 2011;86:50-60.

Thorn K. A quick guide to light microscopy in cell biology. *Mol Biol Cell* 2016;27(2):219-22. doi: 10.1091/mbc.E15-02-0088.

Tiwari S, van Tonder AJ, Vilchèze C, Mendes V, Thomas SE, Malek A, Chen B, Chen M, Kim J, Blundell TL, Parkhill J, Weinrick B, Berney M, Jacobs Jr WR. Arginine-deprivation-induced Oxidative Damage Sterilizes *Mycobacterium tuberculosis. Proc Natl Acad Sci U S A* 2018;115:9779-84.

Tortoli E. Clinical manifestations of nontuberculous mycobacteria infections. *Clin Microbiol Infect* 2009;15:906-10.

Tranchida PQ, Dugo P, Dugo G, Mondello L. Comprehensive two-dimensional chromatography in food analysis. *J Chromatogr A* 2004;1054:3-16.

Triba MN, Le Moyec L, Amathieu R, Goossens C, Bouchemal N, Nahon P, Rutledge DN, Savarin P. PLS/OPLS models in metabolomics: the impact of permutation of dataset rows on the k-fold cross-validation quality parameters. *Mol Biosyst* 2015;11:13-19.

Tripkovic L, Lambert H, Hart K, Smith CP, Bucca G, Penson S, Chope G, Hyppönen E, Berry J, Vieth R, Lanham-New S. Comparison of vitamin D_2 and vitamin D_3 supplementation in raising serum 25-hydroxyvitamin D status: a systematic review and meta-analysis. *Am J Clin Nutr* 2012;95:1357–64.

Trivedi DK, Iles RK. The application of SIMCA P+ in shotgun metabolomics analysis of ZIC®HILIC-MS spectra of human urine - Experience with the Shimadzu IT-TOF and profiling solutions data extraction software. *J Chromat Separation Techniq* 2012;3:6.

Trygg J, Holmes E, Lundstedt T. Chemometrics in metabonomics. *J Proteome Res* 2007;6:469–79.

Tumuluru JS, Sokhansanj S, Wright CT, Kremer T. GC analysis of volatiles and other products from biomass torrefaction process, in Mohd MA (ed.) *Advanced gas chromatography - progress in agricultural, biomedical and industrial applications*. Croatia: InTechOpen; 2012. pp. 211-34.

Tzoulaki I, Ebbels TMD, Valdes A, Elliott P, Ioannidis JPA. Design and analysis of metabolomics studies in epidemiologic research: a primer on -omic technologies. *Am J Epidemiol* 2014;180:129–39.

Ueno N, Wilson ME. Receptor-mediated phagocytosis of Leishmania: Implications for intracellular survival. *Trends Parasitol* 2012;28:335–44.

Urban PL. Quantitative mass spectrometry: an overview. *Philos Trans A Math Phys Eng Sci* 2016;374:20150382. doi: 10.1098/rsta.2015.0382.

Van de Vijver P, Vondenhoff, G. H., Kazakov, T. S., Semenova, E., Kuznedelov, K., Metlitskaya, van der Werf MJ, Ködmön C, Katalinić-Janković V, Kummik T, Soini H, Richter E, Papaventsis D, Tortoli E, Perrin M, van Soolingen D, Zolnir-Dovč M, Ostergaard Thomsen V. Inventory study of non-tuberculous mycobacteria in the European Union. *BMC Infect Dis* 2014;14:62. doi: 10.1186/1471-2334-14-62.

Vargason T, Howsmon DP, McGuinness DL, Hahn J. On the use of multivariate methods for analysis of data from biological networks. *Processes (Basel)* 2017;5(3):36. doi: 10.3390/pr5030036.

Venketaraman V, Dayaram YK, Amin AG, Ngo R, Green RM, Talaue MT, Mann J, Connell ND. Role of glutathione in macrophage control of mycobacteria. *Infect Immun* 2003;71(4):1864–71. doi: 10.1128/IAI.71.4.1864-1871.2003.

Venketaraman V, Millman A, Salman M, Swaminathan S, Goetz M, Lardizabal A, Hom D, Connell ND. Glutathione levels and immune responses in tuberculosis patients. *Microb Pathog* 2008;44(3):255-61. doi: 10.1016/j.micpath.2007.09.002.

Versaevel M, Grevesse T, Gabriele S. Spatial coordination between cell and nuclear shape within micropatterned endothelial cells. *Nat Commun* 2012;3:671.

Vinaixa M, Samino S, Saez I, Jordi D, Guinovart JJ, Yanes O. A guideline to univariate statistical analysis for lc/ms-based untargeted metabolomics-derived data. *Metabolites* 2012;2:775-95.

Viryasova GM, Golenkina EA, Tatarskii Jr VV, Galkin II, Sud'ina GF, Soshnikova NV. An optimized permeabilization step for flow cytometry analysis of nuclear proteins in myeloid differentiation of blood cells into neutrophils. *MethodsX* 2019;6:360–7. doi: 10.1016/j.mex.2019.02.011.

Vrieling F, Ronacher K, Kleynhans L, van den Akker E, Walzl G, Ottenhoff THM, Joosten SA. Patients with concurrent tuberculosis and diabetes have a pro-atherogenic plasma lipid profile. *EBioMedicine* 2018;32:192-200.

Wallner S, Schröder C, Leitão E, Berulava T, Haak C, Beißer D, Rahmann S, Richter AS, Manke T, Bönisch U, Arrigoni L, Fröhler S, Klironomos F, Chen W, Rajewsky N, Müller F, Ebert P, Lengauer T, Barann M, Rosenstiel P, Gasparoni G, Nordström K, Walter J, Brors B, Zipprich G, Felder B, Klein-Hitpass L, Attenberger C, Schmitz G, Horsthemke B. Epigenetic dynamics of monocyteto-macrophage differentiation. *Epigenetics Chromatin* 2016; 9:33. DOI 10.1186/s13072-016-0079-z.

Wanders RJA, Duran M, Loupatty FJ. Enzymology of the branched-chain amino acid oxidation disorders: the valine pathway. *J Inherit Metab Dis* 2012;35(1):5–12. doi: 10.1007/s10545-010-9236-x.

Warburg O. On the origin of cancer cells. *Science* 1956;123:309–14.

Watmuff B, Pouton CW, Haynes JM. In vitro maturation of dopaminergic neurons derived from mouse embryonic stem cells: implications for transplantation. *PLoS One* 2012;7(2):e31999. doi: 10.1371/journal.pone.0031999.

Weir GM, Karkada M, Hoskin D, Stanford MM, MacDonald L, Mansour M, Liwski RS. Combination of poly I:C and Pam3CSK4 enhances activation of B cells *in vitro* and boosts antibody responses to protein vaccines *in vivo. PLoS One* 2017; 12(6): e0180073. doi: 10.1371/journal.pone.0180073.

Wejse C, Gomes VF, Rabna P, Gustafson P, Aaby P, Lisse IM, Andersen PL, Glerup H, Sodemann M. Vitamin D as supplementary treatment for tuberculosis: a double-blind, randomized, placebo-controlled trial. *Am J Respir Crit Care Med* 2009;179:843-50.

Westad F, Marini F. Validation of chemometric models—a tutorial. *Anal Chim Acta* 2015;893:14–24. doi: 10.1016/j.aca.2015.06.056.

Westerhuis JA, Hoefsloot HCJ, Smit S, Vis DJ, Smilde AK, van Velzen EJJ, van Duijnhoven JPM, van Dorsten FA. Assessment of PLSDA cross validation. *Metabolomics* 2008;4:81–9.

Wiktor M, Weichert D, Howe N, Huang C-Y, Olieric V, Boland C, Bailey J, Vogeley L, Stansfeld PJ, Buddelmeijer N, Wang M, Caffrey M. Structural insights into the mechanism of the membrane integral N-acyltransferase step in bacterial lipoprotein synthesis. *Nat Commun* 2017;8:15952. DOI: 10.1038/ncomms15952.

Willard SS, Koochekpour S. Glutamate, Glutamate receptors, and downstream signalling pathways. *Int J Biol Sci* 2013;9(9):948-59. doi:10.7150/ijbs.6426.

Williams RJ. Biochemical Individuality. 1st ed. New York: John Wiley; 1956.

Wilson K, Walker J. *Principles and techniques of biochemistry and molecular biology*. 7th ed. United Kingdom: Cambridge University Press; 2010. pp. 536.

Wilson MB, Barnes BB, Boswell PG. What experimental factors influence the accuracy of retention projections in gas chromatography-mass spectrometry? *J Chromatogr A* 2014; 1373:179–89.

Wishart DS, Tzur D, Knox C, Eisner R, Guo AC, Young N, Cheng D, Jewell K, Arndt D, Sawhney S. HMDB: the human metabolome database. *Nucleic Acids* Res 2007;35:D521 6https://doi.org/10.1093/nar/gkl923.

World Health Organization. Global Tuberculosis Report 2018
https://apps.who.int/iris/bitstream/handle/10665/274453/9789241565646-eng.pdf

World Health Organization. Global Tuberculosis Report 2019
https://apps.who.int/iris/bitstream/handle/10665/329368/9789241565714-eng.pdf?ua=1

Worley B, Powers R. Multivariate Analysis in Metabolomics. *Curr Metabolomics* 2013;1:92–107.

Wu HX, Xiong XF, Zhu M, Wei J, Zhuo KQ, Cheng DY. Effects of vitamin D supplementation on the outcomes of patients with pulmonary tuberculosis: a systematic review and meta-analysis. *BMC Pulm Med* 2018;18:108. doi: 10.1186/s12890-018-0677-6.

Wu K, Feskanich D, Fuchs CS, Willett WC, Hollis BW, Giovannucci EL. A nested case–control study of plasma 25-hydroxyvitamin D concentrations and risk of colorectal cancer. *J Natl Cancer Inst* 2007;99:1120–9.

Wu Y, Gulbins E, Grassmé H. Crosstalk between sphingomyelinases and reactive oxygen species in mycobacterial infection. *Antioxid Redox Signal* 2018;28(10):935-48.

Wynn TA, Chawla A, Pollard JW. Macrophage biology in development, homeostasis and disease. *Nature* 2013;496:445-55.

Xi B, Gu H, Baniasadi H, Raftery D. Statistical Analysis and Modeling of Mass Spectrometry-Based Metabolomics Data. *Methods Mol Biol* 2014;1198:333–53.

Xue Y, Yun D, Esmon A, Zou P, Zuo S, Yu Y, He F, Yang P, Chen X. Proteomic dissection of agonist-specific TLR-mediated inflammatory responses on macrophages at subcellular resolution. *J Proteome Res* 2008;7:3180-93.

Yabsley W, Homer-Vanniasinkam S, Fisher J. Nuclear magnetic resonance spectroscopy in the detection and characterisation of cardiovascular disease: key studies. *ISRN* 2012; doi:10.5402/2012/784073.

Yanagisawa T, Sumida T, Ishii R, Takemoto C, Yokoyama S. A paralog of lysyl-tRNA synthetase aminoacylates a conserved lysine residue in translation elongation factor P. *Nat Struct Mol Biol* 2010;17:1136-43.

Yang CT, Cambier CJ, Davis JM, Hall CJ, Crosier PS, Ramakrishnan L. Neutrophils exert protection in the early tuberculous granuloma by oxidative killing of mycobacteria phagocytosed from infected macrophages. *Cell Host Microbe* 2012;12:301–12.

Yang L, Dai F, Tang L, Le Y, Yao W. Macrophage differentiation induced by PMA is mediated by activation of RhoA/ROCK signalling. *J Toxicol Sci* 2017;42:763-71.

Ye M, Zou H, Liu Z, Lei Z, Ni J. Study on open tubular capillary affinity liquid chromatography. *J Chromatogr Sci* 2000;38:517-20.

Yeom S, Javidi B, Watson E. Three-dimensional distortion-tolerant object recognition using photon-counting integral imaging. *Opt Express* 2007;15:1513-33.

Zamani F, Shahneh FZ, Aghebati-Maleki L, Baradaran B. Induction of CD14 expression and differentiation to monocytes or mature macrophages in promyelocytic cell lines: new approach. *Adv Pharm Bull* 2013;3:329-32.

Zaretsky I, Polonsky M, Shifrut E, Reich-Zeliger S, Antebi Y, Aidelberg G, Waysbort N, Friedman N. Monitoring the dynamics of primary T cell activation and differentiation using long term live cell imaging in microwell arrays. *Lab Chip* 2012;12(23):5007-15. doi: 10.1039/c2lc40808b.

Zhan X. Current status of two-dimensional gel electrophoresis and multi-dimensional liquid chromatography as proteomic separation techniques. *Ann Chromatogr Sep Tech* 2015;1:1009.

Zhang G, Zhang H, Liu Y, He Y, Wang W, Du Y, Yang C, Gao F. CD44 clustering is involved in monocyte differentiation. *Acta Biochim Biophys Sin (Shanghai)* 2014;46:540-7.

Zhang R, Naughton DP. Vitamin D in health and disease: current perspectives. *Nutr J* 2010; 9:65. doi: 10.1186/1475-2891-9-65.

Zhang S, Zeng X, Ren M, Mao X, Qiao S. Novel metabolic and physiological functions of branched chain amino acids: a review. *J Anim Sci Biotechnol* 2017;8:10. DOI 10.1186/s40104-016-0139-z.

Zhang W, Zhang N, Xie X, Guo J, Jin X, Xue F, Ding Z, Caoa Y. Toll-Like receptor 2 agonist Pam_3CSK_4 alleviates the pathology of leptospirosis in hamster. *Infect Immun* 2016;84:3350–7.

Zhao S, Fung-Leung WP, Bittner A, Ngo K, Liu X. Comparison of RNA-Seq and microarray in transcriptome profiling of activated T cells. *PLoS ONE* 2014;9:e78644. doi: 10.1371/journal.pone.0078644.

Zhou A, Ni J, Xu Z, Wang Y, Lu S, Sha W, Karakousis PC, Yao Y-F. Application of ^{1}H-NMR spectroscopy-based metabolomics to sera of tuberculosis patients. *J Proteome Res* 2013;12: doi: 10.1021/pr4007359.

Zhu H, Dai R, Zhou Y, Fu H, Meng Q. TLR2 ligand Pam_3CSK_4 regulates MMP-2/9 expression by MAPK/NF-κB signaling pathways in primary brain microvascular endothelial cells. *Neurochem Res* 2018;43:1897-904.

Zhu N, Lin Y, Li D, Gao N, Liu C, You X, Jiang J, Jiang W, Si S. Identification of an anti-TB compound targeting the tyrosyl-tRNA synthetase. *J Antimicrob Chemother* 2015;70(8):2287-94. doi: 10.1093/jac/dkv110.

Zia K, Siddiqui T, Ali S, Farooq I, Zafar MS, Khurshid Z. Nuclear magnetic resonance spectroscopy for medical and dental applications: A comprehensive review. *Eur J Dent* 2019; 13:124–28.

Zom GG, Willems MMJHP, Khan S, van der Sluis TC, Kleinovink JW, Camps MGM, van der Marel GA2, Filippov DV, Melief CJM, Ossendorp F. Novel TLR2-binding adjuvant induces enhanced T cell responses and tumor eradication. *J Immunother Cancer* 2018;6:146. doi: 10.1186/s40425-018-0455-2.

Zrostlıkova J. Hajslova J, Cajka T, Evaluation of two-dimensional gas chromatography-Time-Of-Flight mass spectrometry for the determination of multiple pesticide residues in fruit. *J Chromatogr A* 2003;1019:173-86.

Zumla A, Raviglione M, Hafner R, von Reyn CF. Current concepts tuberculosis. *N Engl J Med* 2013;368:745-55.

APPENDIX

The data presented in this chapter contains additional and complementary data that was not included in the main text. Raw data and any additional data which are not included in this chapter are available upon request from the Department of Biochemistry, University of Johannesburg.

1. Overlaid spectra ^{1}H NMR spectroscopy spectrum of metabolic profiling of U937 macrophages treated with Pam_3CSK_4, $1,25(OH)_2D_3$ and a combination of both Pam_3CSK_4 and $1,25(OH)_2D_3$ as well as control cells(untreated) – 16-hrs treatment.

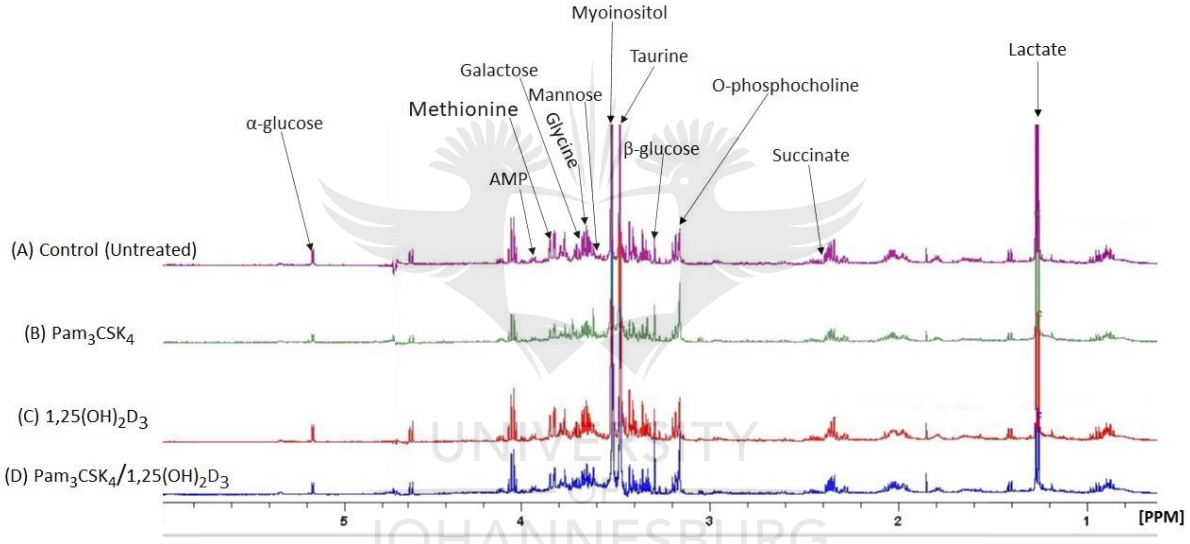

Figure A1: Overlaid ^{1}H NMR spectra acquired using a 500 MHz Bruker NMR spectrometer (16 h treatment). The spectra represent the metabolic profiling of (A) **control cells (untreated)**, (B) **Pam_3CSK_4 stimulated cells**, (C) **$1,25(OH)_2D_3$** treated cells and (D) **$Pam_3CSK_4/1,25(OH)_2D_3$ supplemented cells incubated for 16 hrs**. The labelled peaks are potential signatory metabolites identified from the Human Metabolome Database (HMDB) (http://www.hmdb.ca/) and relevant published literature (Govindaraju *et al*., 2000; Mickiewicz *et al*., 2014; Subramani *et al*., 2016). All spectra were referenced to TSP at δ 0.0 ppm and α-glucose at δ 5.53 ppm. $1,25(OH)_2D_3$: 1,25-dihydroxyvitamin D_3; AMP: Adenosine monophosphate.

2. Overlaid spectra ^{1}H NMR spectroscopy spectrum of metabolic profiling of U937 macrophages treated with Pam_3CSK_4, $1,25(OH)_2D_3$ and a combination of both Pam_3CSK_4 and $1,25(OH)_2D_3$ as well as control cells(untreated) – 24-hrs treatment.

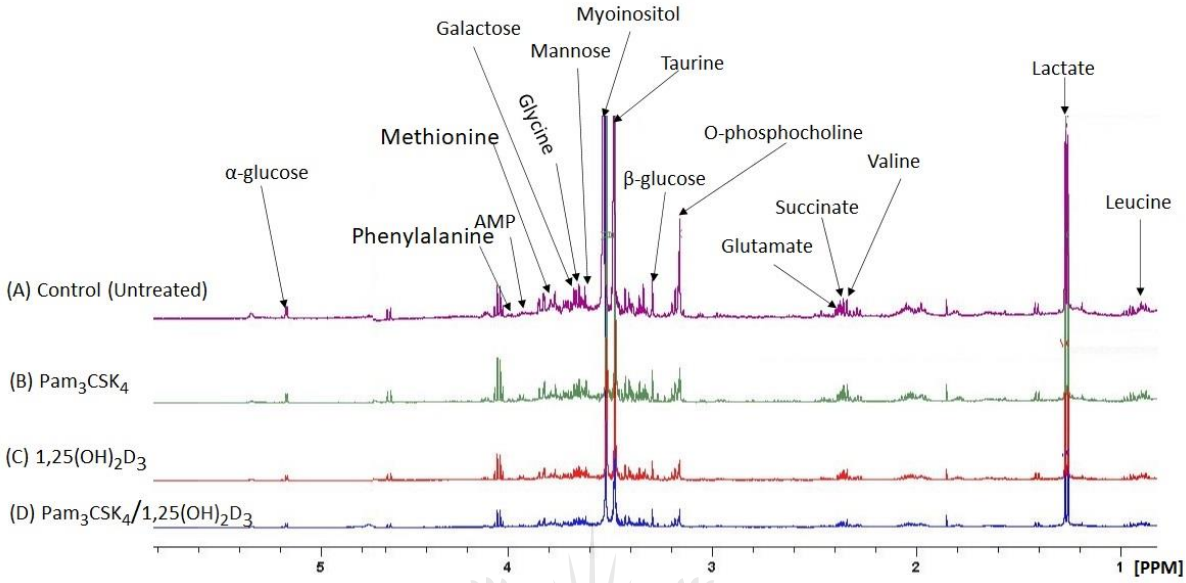

Figure A2: Overlaid ^{1}H NMR spectra acquired using a 500 MHz Bruker NMR spectrometer (24 hrs treatment). The spectra represent the metabolic profiling of (A) **control cells (untreated)**, (B) **Pam_3CSK_4 stimulated cells**, (C) **$1,25(OH)_2D_3$** treated cells and (D) **$Pam_3CSK_4/1,25(OH)_2D_3$ supplemented cells incubated for 24 hrs**. Potential signatory metabolites differentiating the study groups are shown as labelled peaks. These were identified from the Human Metabolome Database (HMDB) (http://www.hmdb.ca/) and relevant published literature (Govindaraju *et al*., 2000; Mickiewicz *et al*., 2014; Subramani *et al*., 2016). All spectra were referenced to TSP at δ 0.0 ppm and α-glucose at δ 5.53 ppm. $1,25(OH)_2D_3$: 1,25-dihydroxyvitamin D_3; AMP: Adenosine monophosphate.

3. Metabolic profiling of U937 treated with Pam_3CSK_4, $1,25(OH)_2D_3$ and $Pam_3CSK_4/1,25(OH)_2D_3$ –PCA modelling (16-hrs treatment).

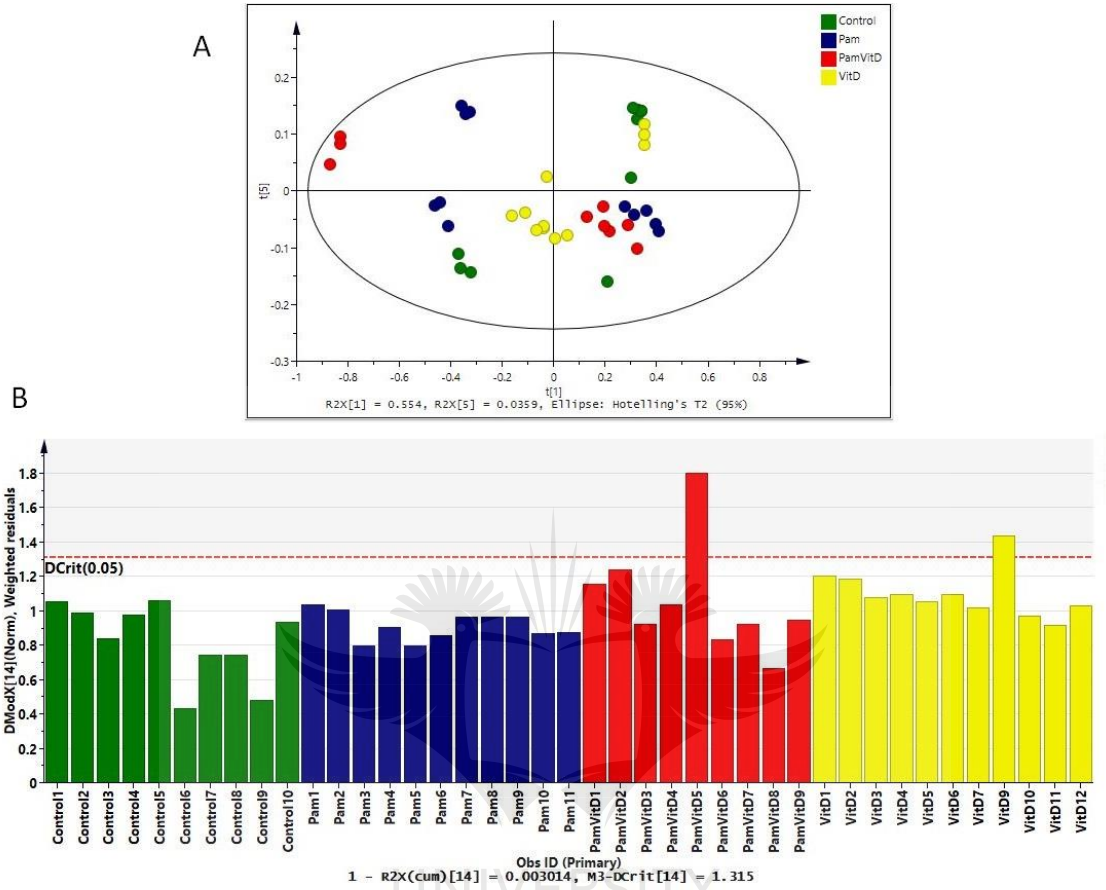

Figure A3: PCA modelling. (A) **PCA scores scatter plot** of control cells, Pam (Pam_3CSK_4), VitD ($1.25(OH)_2D_3$), and Pam_3CSK_4/Vit D ($Pam_3CSK_4/1.25(OH)_2D_3$) treated cells. The between-groups variation is explained by the y-axis and the within-group variation is explained by the x-axis (R^2= 0. 997, Q^2= 0. 95, components = 14). No strong outliers were detected using Hotelling's T^2 test at a 95% confidence level. (B) **DModX** shows two moderate outliers with DModX values greater than critical value, DCrit(0.05) (red dotted line). These outliers had no variable(s) with critical deviation from the rest of the dataset, hence they were retained.

4. Metabolic profiling of U937 treated with Pam_3CSK_4, $1,25(OH)_2D_3$ and Pam_3CSK_4/$1,25(OH)_2D_3$ – PCA modelling (24-hrs treatment).

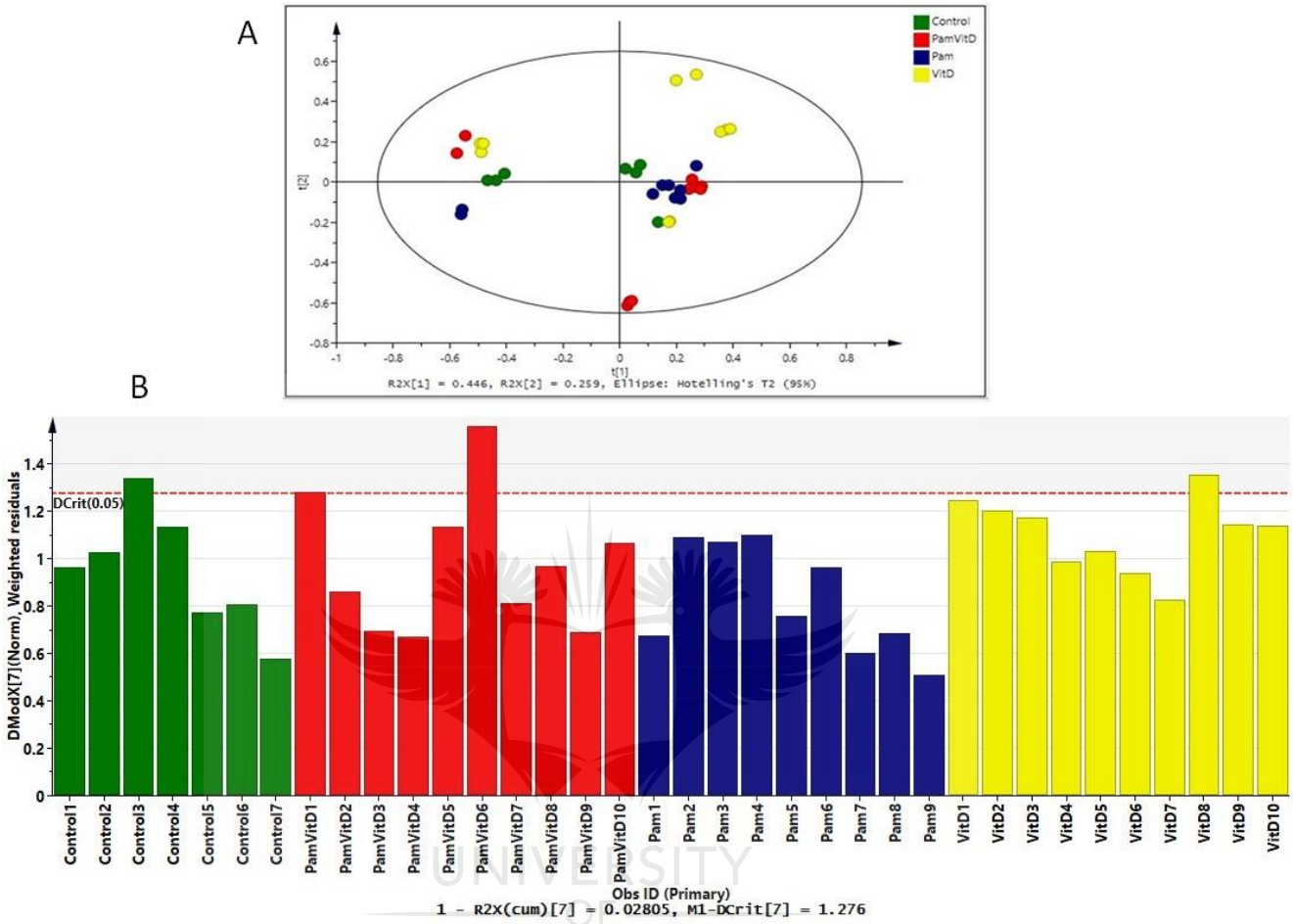

Figure A4: PCA modelling. (A) **PCA scores scatter plot** of Pam (Pam_3CSK_4), VitD ($1.25(OH)_2D_3$), and Pam_3CSK_4/Vit D (Pam_3CSK_4/$1.25(OH)_2D_3$) treated cells as well as the control cells. No strong outliers were detected according to Hotelling's T^2 test at a 95% confidence level. Moderate outliers were detected using **DModX** (B). These are observations with DModX values greater than critical value, DCrit(0.05) (red dotted line). (R^2= 0.972, Q^2= 0.863, components =7). Moderate outliers had no variable(s) with critical deviation from the rest of the dataset and therefore, they were retained.

5. Metabolic profiling of U937 treated with Pam_3CSK_4, $1,25(OH)_2D_3$ and Pam_3CSK_4/$1,25(OH)_2D_3$ – OPLS-DA modelling (16-hrs treatment).

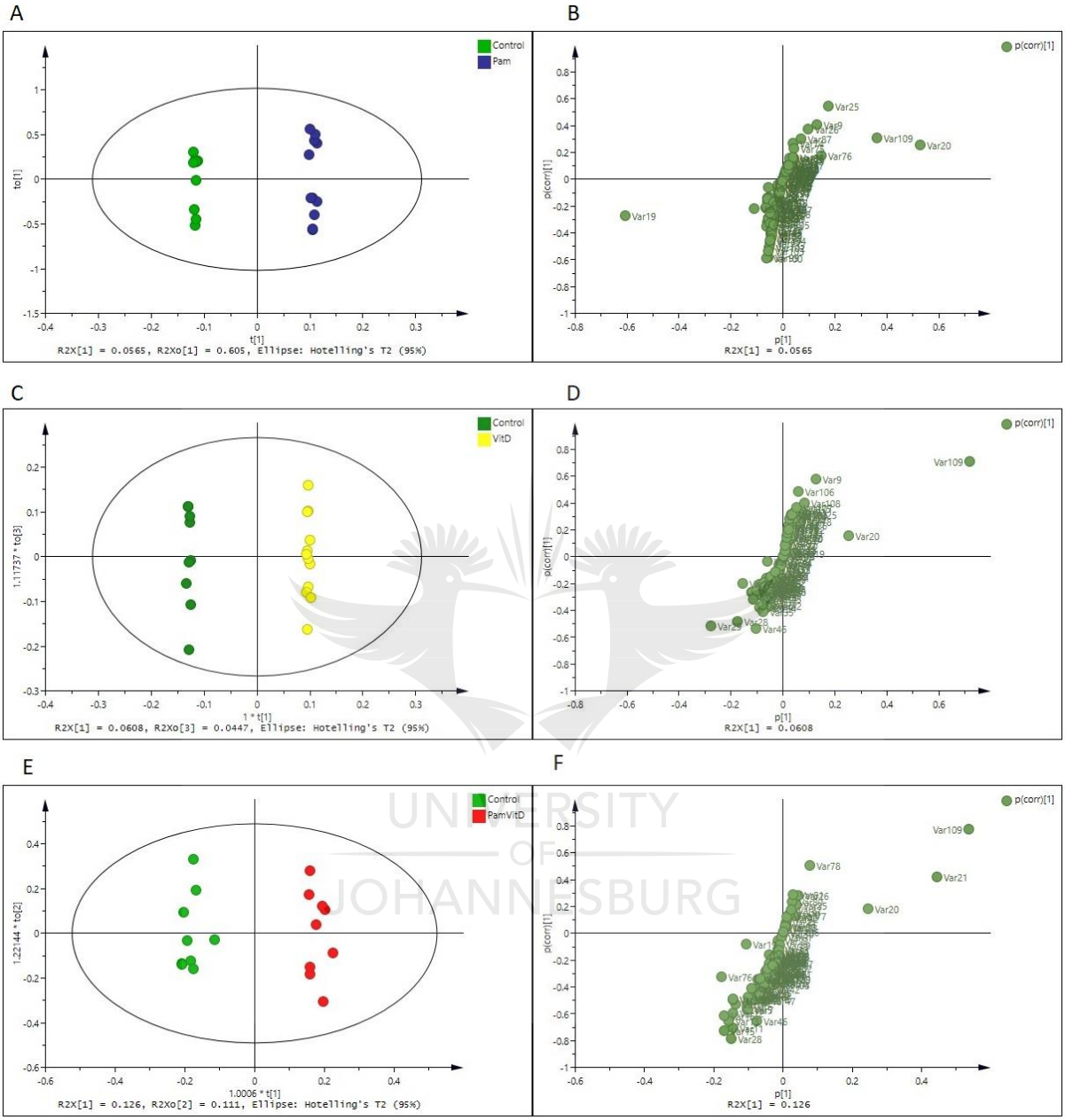

Figure A5: OPLS-DA modelling and variable selection. (A) An **OPLS-DA scores scatter plot** separating the control cells *vs*. Pam_3CSK_4 (Components: 1+8+0, R^2X= 0.995, R^2Y= 0.999, Q^2= 0.99, CV-ANOVA *p*-value = 9.31628×10^{-6}). The model displays the separation of the two classes in horizontal (t1) direction; and within-class variability is expressed in the vertical (to[1]) direction. (**B**) the **loading S-plot** displays discriminant variables – the variables that are situated in the extreme end of the S-plot are statistically relevant and represent prime candidates as discriminating variables. (C) An **OPLS-DA scores scatter plot** and (D) the **loading S-plot** of the control cells *vs*. $1,25(OH)_2D_3$. A clear separation can be seen between the two classes (Components: 1+8+0, R^2X = 0.992, R^2Y = 0.999, Q^2 = 0.983, CV-ANOVA *p*-value =5.90137×10^{-5}). (E) An **OPLS-DA scores scatter plot** and (F) the **loading S-plot** of the control cells *vs*. Pam_3CSK_4/$1,25(OH)_2D_3$ (Components:1+3+0, R^2X = 0.968, R^2Y = 0.98, Q^2 = 0.945, CV-ANOVA *p*-value =1.64464).

6. Metabolic profiling of U937 treated with Pam_3CSK_4, $1,25(OH)_2D_3$ and Pam_3CSK_4/$1,25(OH)_2D_3$ – OPLS-DA modelling (24-hrs treatment).

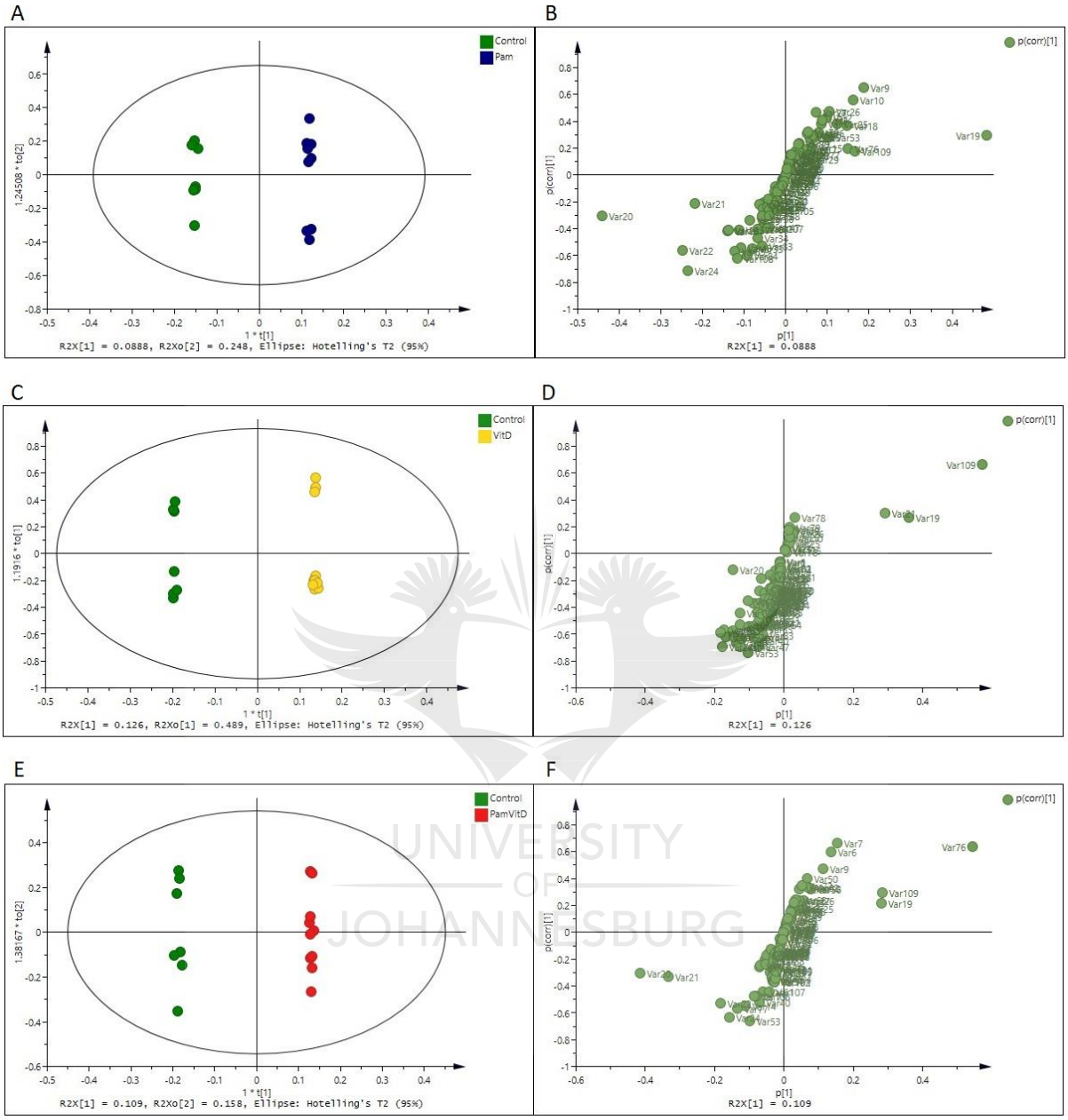

Figure A6: OPLS-DA modelling and variable selection. (A) An **OPLS-DA scores scatter plot** separating the control cells *vs*. Pam_3CSK_4 (Components: 1+6+0, R^2X= 0.994, R^2Y= 0.999, Q^2= 0.973, CV-ANOVA *p*-value =0.00251). The model displays the separation of the two classes in horizontal (t1) direction; and within-class variability is expressed in the vertical (to[1]) direction. (**B**) the **loading S-plot** showing the discriminant variables. Potential discriminating variables are situated in the extreme end of the S-plot. (C) An **OPLS-DA scores scatter plot** and (D) the **loading S-plot** of the control cells *vs*. $1,25(OH)_2D_3$. A clear separation can be seen between the two classes (Components: 1+8+0, R^2X = 0.997, R^2Y = 1, Q^2 = 0.99, CV-ANOVA *p*-value = 0.00196). (E) An **OPLS-DA scores scatter plot** and (F) the **loading S-plot** of the control cells *vs*. Pam_3CSK_4/$1,25(OH)_2D_3$ (Components: 1+6+0, R^2X = 0.987, R^2Y = 0.999, Q^2 = 0.975, CV-ANOVA *p*-value =0.00049).

7. Volcano plot showing significant, discriminatory metabolites between control cells *vs*. Pam_3CSK_4; and control cells *vs*. $Pam_3CSK_4/1.25(OH)_2D_3$ supplemented cells. The metabolic profiling was performed using GCxGC–TOFMS (12-hrs treatment).

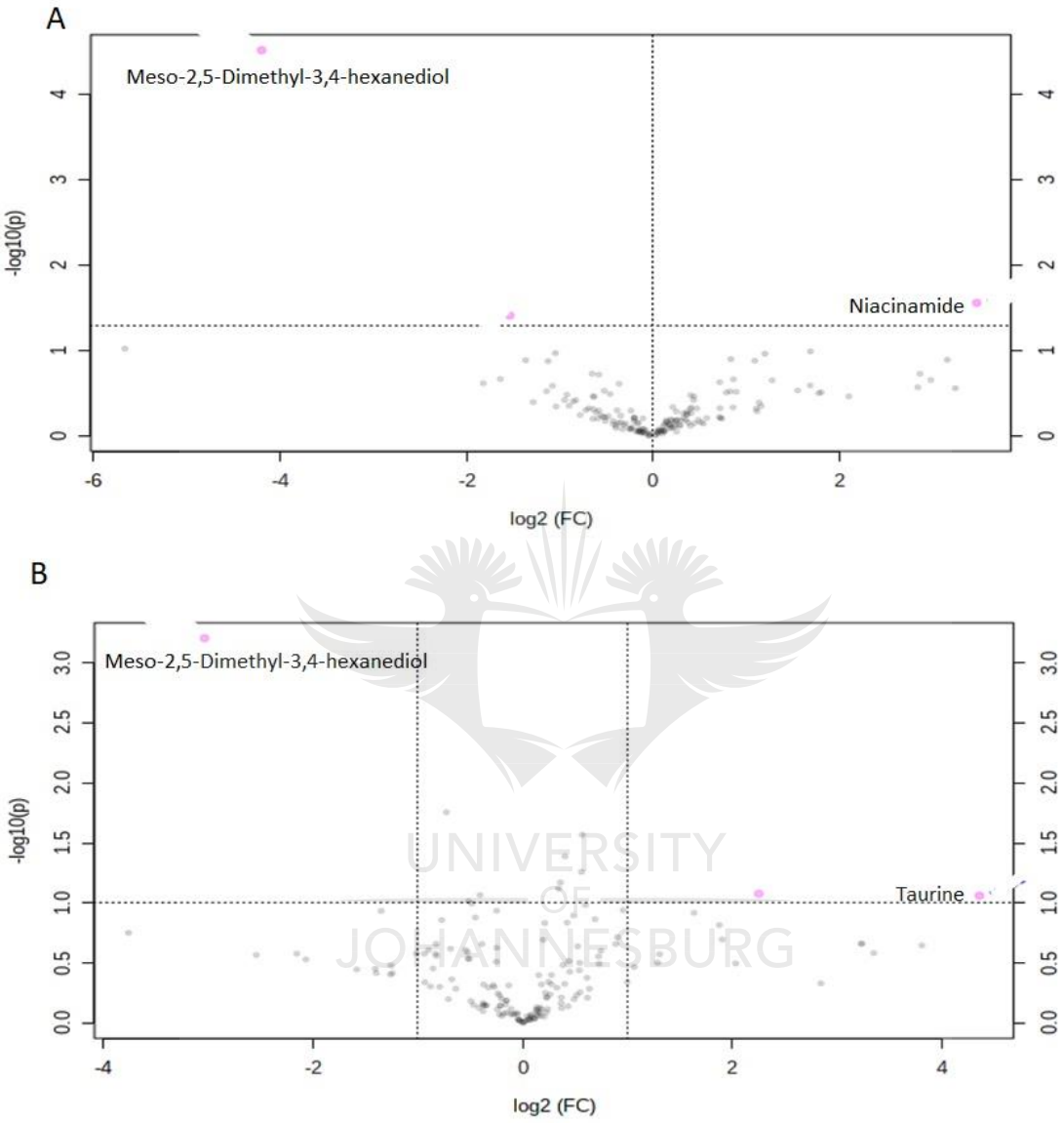

Figure A7: Volcano plot of significant metabolites. (A) Volcano plot of **control cells *vs*. Pam_3CSK_4** stimulated; and that of (B) **control cells *vs*. $Pam_3CSK_4/1.25(OH)_2D_3$** supplemented cells. Significant discriminatory variables (metabolites) are located away from the origin (0) of the plot. They are located towards the top left or the top right of the plot.

8. PCA modelling of GCxGC-TOFMS based metabolic profiling of control cells *vs*. Pam_3CSK_4; and control cells *vs*. Pam_3CSK_4/1.25$(OH)_2D_3$ supplemented cells (12-hrs treatment).

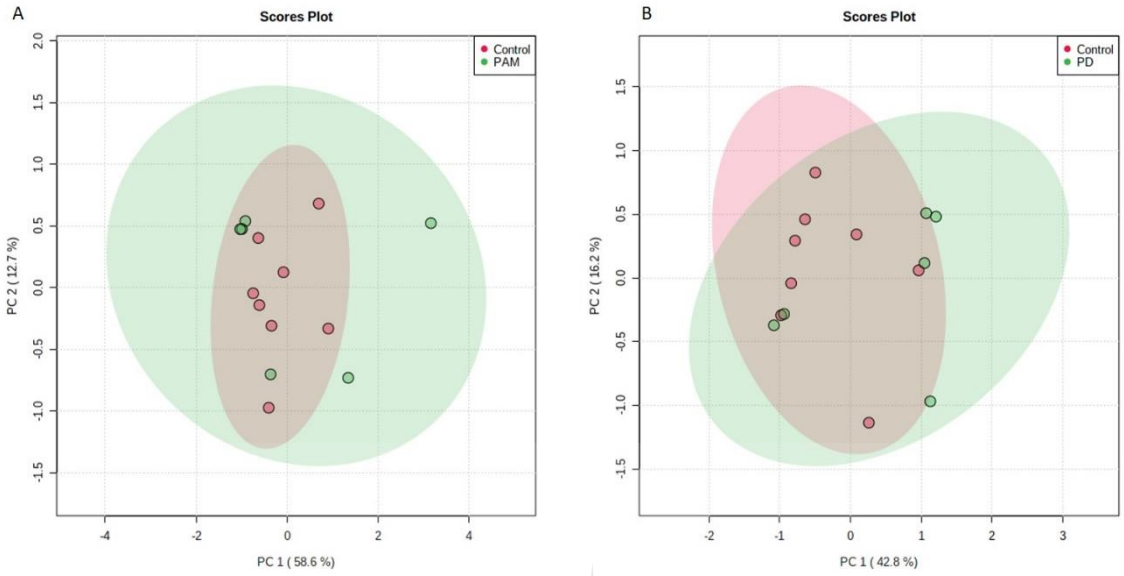

Figure A8: PCA modelling. PCA scores scatter plot of (A) **control *vs*. Pam_3CSK_4** stimulated cells; and (B) **control vs. Pam_3CSK_4/1.25$(OH)_2D_3$** supplemented cells. The within-group separation and between-groups separation is shown by the x-axis (PC1) and y-axis (PC2), respectively. Abbreviations: PC: Principal component.

9. PLS-DA modelling of control *vs*. Pam_3CSK_4 stimulated cells; and control cells vs. $Pam_3CSK_4/1.25(OH)_2D_3$ supplemented cells (12-hrs treatment).

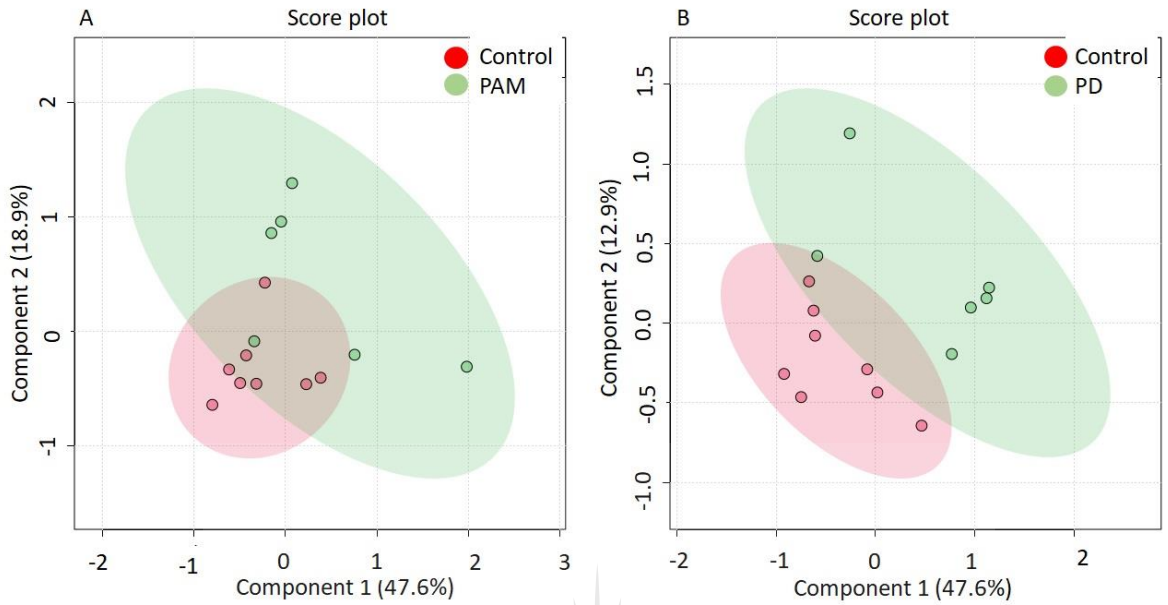

Figure A9: PLS-DA modelling. PLS-DA scores scatter plot separating (A) control *vs*. Pam_3CSK_4 stimulated cells; and (B) control *vs*. $Pam_3CSK_4/1,25(OH)_2D_3$ supplemented cells. Component 1 shows within-group separation and component 2 shows between-groups separation.

10. Selection of variables responsible for separation observed in PLS-DA score scatter plots generated from the GC-MS based metabolic profiling (12-hrs treatment).

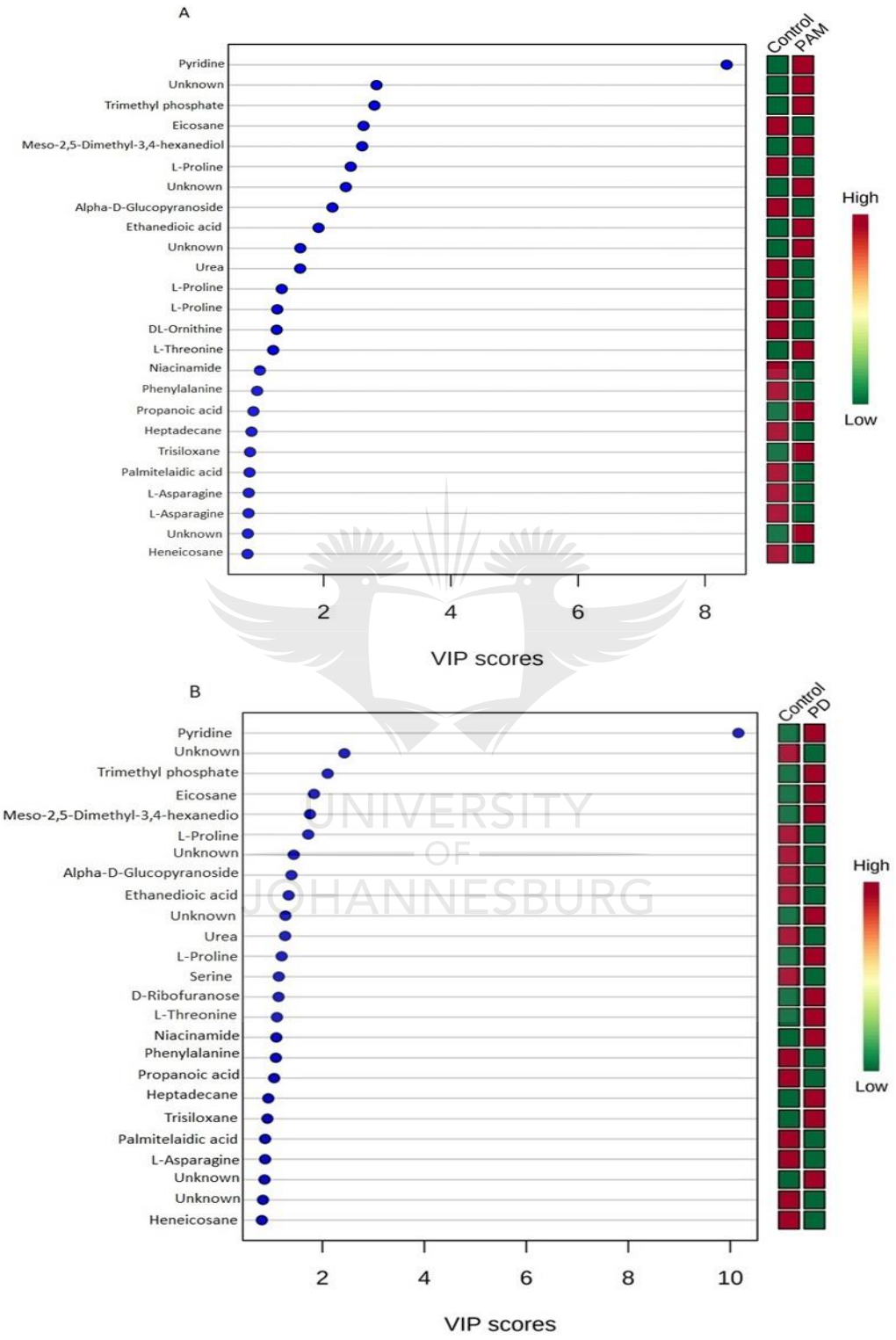

Figure A10: VIP scores. VIP scores showing potential signatory metabolites discriminating (A) **control cells *vs*. Pam_3CSK_4 stimulated** cells; and (B) **control cells vs. Pam_3CSK_4/1.25$(OH)_2D_3$** supplemented cells. Discriminatory metabolites have VIP > 1.

11. OPLS-DA modelling and variable selection of GC-MS based metabolic profiling (12-hrs treatment).

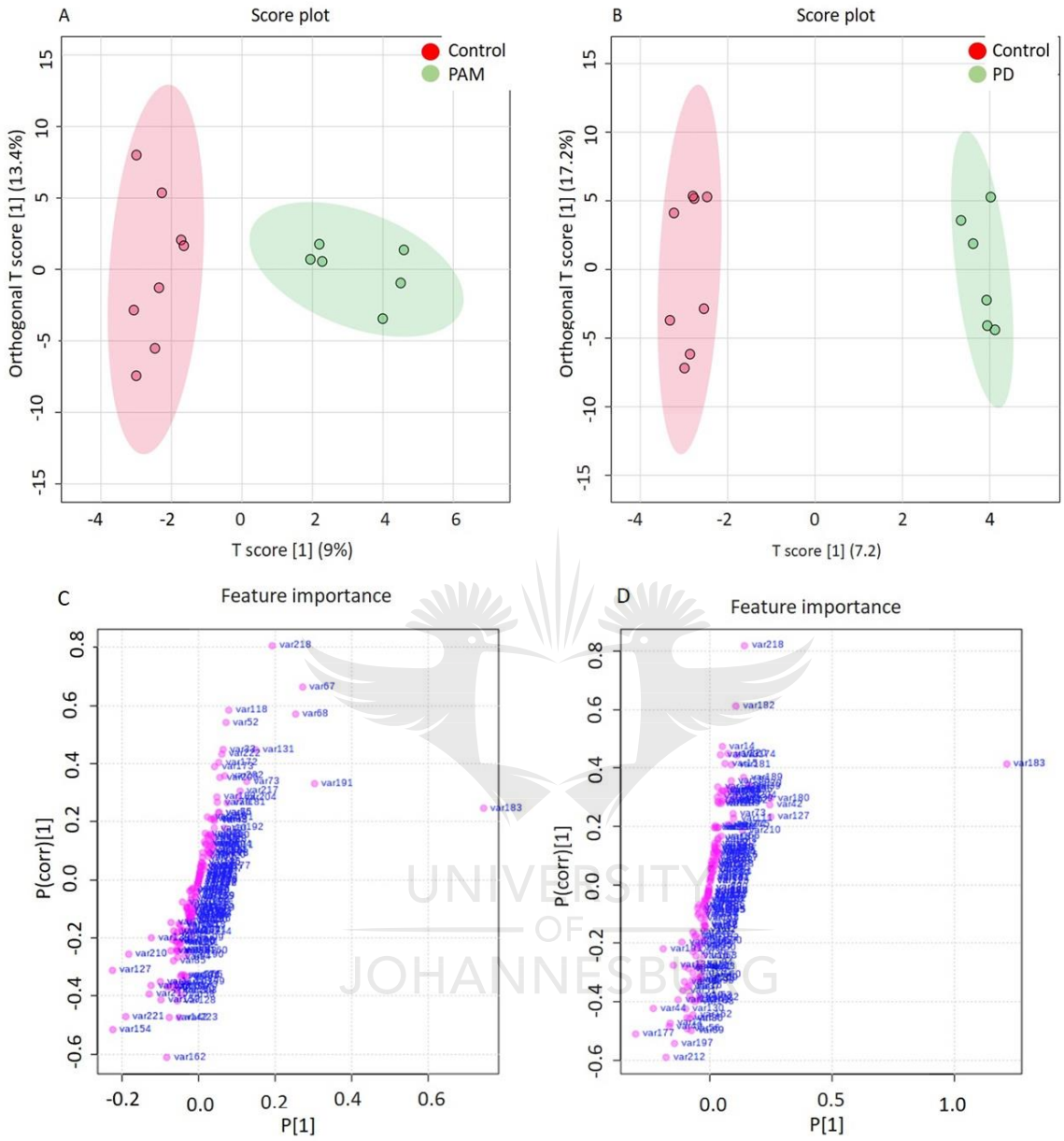

Figure A11: OPLS-DA modelling and variable selection. OPLS-DA scores scatter plot separating (A) **control cells *vs*. Pam_3CSK_4 stimulated cells** (Permutation analysis: Q^2 = -0.1, R^2Y=0.918); and (B) **control cells *vs*. Pam_3CSK_4/1,25$(OH)_2D_3$ supplemented cells** (Permutation analysis: Q^2 = -0.1, R^2Y=0.918). Discriminatory features responsible for the separation observed in the OPLS-DA scores scatter plots are shown in the loadings S-plots (C) **control cells *vs*. Pam_3CSK_4 stimulated cells** and (D) **control cells *vs*. Pam_3CSK_4/1,25$(OH)_2D_3$ supplemented** cells.

12. Metabolic pathway analysis

Table A1: Most significantly altered metabolic pathway in U937 macrophages treated with Pam_3CSK_4, $1,25(OH)_2D_3$ and a combination of both Pam_3CSK_4 and $1,25(OH)_2D_3$.

Metabolic Pathway	Total	Expected	Hits	Raw *p*-value	-log(p)	Holm adjust	FDR Impact	Impact
Aminoacyl-tRNA biosynthesis	48	0.84	8	6.62×10^{-7}	1.42×10^{1}	5.56×10^{-5}	5.56×10^{-5}	0.00
Arginine biosynthesis	14	0.24	4	6.51×10^{-5}	9.64	5.40×10^{-3}	1.89×10^{-3}	0.18
Galactose metabolism	27	0.47	5	6.76×10^{-5}	9.60	5.55×10^{-3}	1.89×10^{-3}	0.09
Valine, leucine and isoleucine biosynthesis	8	0.14	3	2.49×10^{-4}	8.30	2.02×10^{-2}	5.24×10^{-3}	0.00
Glutathione metabolism	28	0.49	4	1.13×10^{-3}	6.79	9.00×10^{-2}	1.89×10^{-2}	0.12